THESIS FOR THE DEGREE OF DOCTOR OF PHILOSOPHY

Aperiodic Array Synthesis for Telecommunications

CARLO BENCIVENNI

CHALMERS

Department of Electrical Engineering
CHALMERS UNIVERSITY OF TECHNOLOGY

Göteborg, Sweden 2017

Aperiodic Array Synthesis for Telecommunications

Carlo Bencivenni

Department of Electrical Engineering
Division of Communication and Antenna Systems, Antenna Group
Chalmers University of Technology
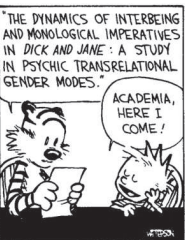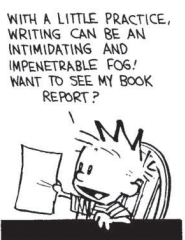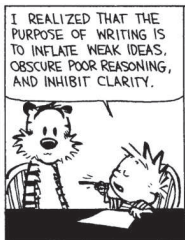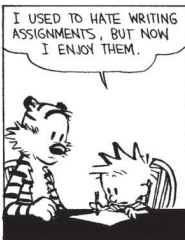SE–412 96 Göteborg
Sweden
Telephone: +46 (0)31 – 772 1000
Email: carlo.bencivenni@chalmers.se; cbencivenni@gmail.com

Alla mia famiglia

Abstract

Arrays of antennas offer important advantages over single-element antennas and are thus a key part of most advanced communication systems. The majority of current arrays are based on a classical regular layout, which offer simple design criteria despite some limitations. Aperiodic arrays can reduce the number of elements and improve the performance, however their design is far more challenging. This thesis focuses on the synthesis of aperiodic arrays, advancing the state-of-the-art of phased arrays and pioneering the application to Multiple-Input Multiple-Output (MIMO) systems.

In satellite communications (SATCOM), aperiodic sparse arrays have the potential for drastically reducing the costs of massive antennas. Most available synthesis methods are however either intractable, suboptimal or limited for such demanding scenarios. We propose a deterministic and efficient approach based on Compressive Sensing, capable of accounting for electromagnetic phenomena and complex specifications. Some of the key contributions include the extension to the design of multi-beam, modular, multi-element, reconfigurable and isophoric architectures.

The same approach is successfully applied to the design of compact arrays for Point-to-Point (PtP) backhauling. The aperiodicity is used here instead to reduce the side lobes and meet the target radiation envelope with high aperture efficiency. A dense, column arranged, slotted waveguide isophoric array has been successfully designed, manufactured and measured.

Line-of-Sight (LoS) MIMO can multiply the data rates of classical Single-Input Single-Output (SISO) backhauling systems, however it suffers from limited installation flexibility. We demonstrate how aperiodic arrays and their switched extensions can instead overcome this shortcoming. Since a small number of antennas are typically used, an exhaustive search is adopted for the synthesis.

Massive Multi-User (MU) MIMO is envisioned as a key technology for future 5G systems. Despite the prevailing understanding, we show how the MIMO performance is affected by the array layout. To exploit this, we propose a new hybrid statistical-density tapered synthesis approach. Results show a significant improvement in minimum power budget, capacity and amplifier efficiency, especially for massive and/or crowded systems.

Keywords: aperiodic array, maximally sparse array, compressive sensing, mutual coupling, density taper, SATCOM, PtP, LoS-MIMO, MU-MIMO.

Preface

This thesis is in partial fulfillment for the degree of Doctor of Philosophy at Chalmers University of Technology, Gothenburg, Sweden.

The work behind this thesis was carried out between June 2012 and May 2017 at the Antenna Systems Group, Division of Communication and Antenna Systems, Department of Electrical Engineering, Chalmers. Professor Marianna Ivashina has been both the examiner and main supervisor, and Associate Professor Rob Maaskant has been the co-supervisor.

This PhD project has been supported by the VINNOVA Excellence Research Centers Chase and ChaseOn, and embedded in two research projects, i.e. Next Generation Array Antennas (Chase, 2016) and Integrated Antenna Arrays (ChaseOn, 2017).

Acknowledgments

After months dedicated to complete this thesis, I am now left to write the final and most heartfelt part. This thesis concludes five years of work as a PhD student, but more importantly, it closes a chapter of my life. A journey rich with precious experiences and happy memories. Perhaps in fear of losing all this, I feel I now need to take the time to acknowledge the people that shared this moments. However, as I set to do so, I am sure I will be able to properly thank them all adequately.

First I have to thank my supervisor, Professor Marianna Ivashina, for giving me the opportunity to work on challenging and relevant research topics. I have to equally thank my co-supervisor, Associate Professor Rob Maaskant, for the time and dedication put into my work. I would also like to express my admiration for Professor Per-Simon Kildal for making the Antenna Group a thriving and friendly research environment. Your personality, enthusiasm and vision might be sadly lost, but will be long remembered by all of us.

I would like to acknowledge the CHASE center and our partners, Ericsson, RUAG and KTH, for supporting the project. In particular I would like to thank Dr. Johan Wettergren for the collaboration and hospitality in RUAG. Moreover, I would like to thank Prof. Lars Jonsson and Dr. Patrik Persson for their commitment to the success of the project. I would like also to recognize the Onsala Space Observatory, Dr. Miroslav Pantaleev and Dr. Tobia Carozzi for the collaboration related to my department work.

I would also like to recognize the researcher which I had the opportunity to collaborate with. Assistant Professor Andrés Alayón Glazunov, Adjunct Associate Professor Mikael Coldrey, Dr. Shi Lei and Dr. Theunis Beukman. It has bee a pleasure and honor to collaborate with such dedicated and professional people.

Thanks to all the colleagues of the Antenna Group for the friendly and enjoyable work environment. We might ironically refer to ourselves as the Antenna family, but we are indeed a sort of it. Thank you for the support, jokes and late evenings. We have been there for each other both in the happy and in the hard times, and this is what makes the difference. A particular

List of Publications

This thesis is based on the following appended papers:

Paper A
C. Bencivenni, M. Ivashina, R. Maaskant, and J. Wettergren, "Design of Maximally Sparse Arrays in the Presence of Mutual Coupling", in *IEEE Antennas and Wireless Propagation Letters*, Vol 14, pp. 159-162, 2015.

Paper B
C. Bencivenni, M. Ivashina, R. Maaskant, and J. Wettergren, "Synthesis of Maximally Sparse Arrays Using Compressive-Sensing and Full-Wave Analysis for Global Earth Coverage", in *IEEE Transactions on Antennas and Propagation*, Vol 64, no. 11, pp. 4872-4877, November 2016.

Paper C
S. Lei, **C. Bencivenni**, R. Maaskant, M. Ivashina, J. Wettergren and J. Pragt "Aperiodic Array of Uniformly-Excited Slotted Ridge Waveguide Antennas for Point-to-Point Communication at Ka-Band", to be submitted to *IEEE Transactions on Antennas and Propagation*.

Paper D
C. Bencivenni, M. Coldrey, R. Maaskant and M. Ivashina, "Aperiodic Switched Arrays for Line-of-Sight MIMO Backhauling", to be submitted to *IEEE Antennas and Wireless Propagation Letters*.

Paper E
C. Bencivenni, A. A. Glazunov, R. Maaskant and M. Ivashina, "Aperiodic Array Synthesis for Multi-User MIMO Applications", submitted to *IEEE Transactions on Antennas and Propagation*, March 2017.

Other related publications by the Author not included in this thesis:

[i] **C. Bencivenni**, M. Ivashina, and R. Maaskant, "A Simple Method for Optimal Antenna Array Thinning using a Broadside MaxGain Beamformer", *Eucap 2013, European Conference on Antennas and Propagation*, 8-12 April 2013, Gothenburg, Sweden.

[ii] R. Haas, M. Pantaleev, L. Helldner, B. Billade, M. Ivashina, O. Iupikov, **C. Bencivenni**, J. Yang, P. Kildal, T. Ekebrand, J. Jönsson, Y. Karandikar, and A. Emrich, "Broadband feeds for VGOS", *IVS 2014, International VLBI Service for Geodesy and Astrometry (IVS) General Meeting*, 2-7 March 2014, Shanghai, China.

[iii] **C. Bencivenni**, M. Ivashina, and R. Maaskant, "Aperiodic Array Antennas for Future Satellite Systems", *Swedish Microwave Days*, 11-12 March 2014, Gothenburg, Sweden.

[iv] M. Ivashina, T. Beukman, **C. Bencivenni**, O. Iupikov, R. Maaskant, P. Meyer, and M. Pantaleev, "Design of Wideband Quadruple-Ridged Flared Horn Feeds for Future Radio Telescopes", *Swedish Microwave Days*, 11-12 March 2014, Gothenburg, Sweden.

[v] R. Maaskant, **C. Bencivenni**, and M. Ivashina, "Characteristic Basis Function Analysis of Large Aperture-Fed Antenna Arrays", *Eucap 2014, European Conference on Antennas and Propagation*, 6-11 April 2014, The Hauge, Netherlands.

[vi] T. Beukman, M. Ivashina, R. Maaskant, P. Meyer, and **C. Bencivenni**, "A Quadraxial Feed for Ultra-Wide Bandwidth Quadruple-Ridged Flared Horn Antennas", *Eucap 2014, European Conference on Antennas and Propagation*, 6-11 April 2014, The Hague, Netherlands.

[vii] M. Ivashina, **C. Bencivenni**, O. Iupikov, and J. Yang "Optimization of the 0.35-1.05 GHz Quad-Ridged Flared Horn and Eleven Feeds for the Square Kilometer Array Baseline Design", *ICEAA 2014, International Conference on Electromagnetics in Advanced Applications*, 3-9 August 2014, Palm Beach, Aruba.

[viii] M. Ivashina, R. Bradley, R. Gawande, M. Pantaleev, B. Klein, J. Yang, and **C. Bencivenni**, "System noise performance of ultra-wideband feeds for future radio telescopes: Conical-Sinuous Antenna and Eleven Antenna", *URSI GASS 2014, General Assembly and Scientific Symposium of the International Union of Radio Science*, 16-23 August 2014, Beijing, China.

[ix] **C. Bencivenni**, M. Ivashina, and R. Maaskant, "Multi-element aperiodic array synthesis by Compressive Sensing", *ICEAA 2015, International Conference on Electromagnetics in Advanced Applications*, 7-11 September 2015, Turin, Italy.

[x] **C. Bencivenni**, M. Ivashina, and R. Maaskant, "Application of the Compressive-Sensing Approach to the Design of Sparse Arrays for SATCOM Applications", *Swedish Microwave Days*, 15-16 March 2016, Linköping, Sweden.

[xi] J. Wettergren, M. Svensson, and **C. Bencivenni**, "Footprint Sharing Sparse Arrays for 20 and 30 GHz", *Swedish Microwave Days*, 15-16 March 2016, Linköping, Sweden.

[xii] **C. Bencivenni**, M. Ivashina, and R. Maaskant, "Reconfigurable Aperiodic Array Synthesis", *Eucap 2016, European Conference on Antennas and Propagation*, 10-15 April 2016, Davos, Switzerland.

[xiii] **C. Bencivenni**, M. Ivashina, and R. Maaskant, "Synthesis of Circular Isophoric Sparse Array by Using Compressive Sensing", *APS/URSI 2016, IEEE International Symposium on Antennas and Propagation*, 6 June-1 July 2016, Fajardo, Puerto Rico.

[xiv] **C. Bencivenni**, A. A. Glazunov, R. Maaskant and M. Ivashina, "Effects of Regular and Aperiodic Array Layout in Multi-User MIMO Applications", to be presented at *APS/URSI 2017, IEEE International Symposium on Antennas and Propagation*, 9-14 July 2017, San Diego, California.

[xv] N. Amani, R. Maaskant, A. A. Glazunov, **C. Bencivenni** and M. Ivashina, "MIMO Channel Capacity Gains in mm-Wave LOS Systems with Irregular Sparse Array Antennas", to be presented at *ICEAA 2017, International Conference on Electromagnetics in Advanced Applications*, 11-15 September 2017, Verona, Italy.

[xvi] **C. Bencivenni**, A. A. Glazunov, R. Maaskant and M. Ivashina, "Aperiodic Array Synthesis for MIMO Applications", to be presented at *ICEAA 2017, International Conference on Electromagnetics in Advanced Applications*, 11-15 September 2017, Verona, Italy.

x

Acronyms

BS	Base Station
CS	Compressive Sensing
DRA	Direct Radiating Array
EEP	Embedded Element Pattern
EM	Electro Magnetic
FoV	Field of View
IEP	Isolated Element Pattern
LoS	Line-of-Sight
MC	Mutual Coupling
MoM	Method of Moments
MIMO	Multiple-Input Multiple-Output
MSA	Maximally Sparse Array
PtP	Point-to-Point
RIMP	Rich Isotropic MultiPath environment
SATCOM	Satellite Communications
SISO	Single-Input Single-Output
SLL	Side Lobe Level
SNR	Signal-to-Noise-Ratio
UE	User Equipment

Contents

Part I

Introductory Chapters

Chapter 1

Introduction

An array of antennas is a group of coordinated antennas designed to achieve improved performance and capabilities over a single-element antenna. Most notably, by deploying a number of antennas one can create directive and narrow beams or, in general, synthesize radiation patterns of arbitrary shape. Arrays also offer additional interesting capabilities such as electronic beam scanning, redundancy, power pooling and diversity.

These features are very attractive, especially for modern antenna systems, where reconfigurability and reliability are of key importance. However, the associated economic costs are often prohibitive, limiting full-fledged *active* arrays to few applications. Recent advances in manufacturing and solid state electronics have rendered the array architecture appealing to a number of new applications. Today, there is a great interest in advanced array systems where major attention is paid to the main cost drivers as well as several practical design considerations. The objective is then to minimize the total system cost, maximize the system performance and improve the overall maturity of array solutions in order to make them competitive against other well-established technologies.

This thesis attempts to address some of these aspects by exploiting aperiodic arrays and aims at improving the state-of-the-art synthesis techniques with the focus on minimizing the array cost and improving the antenna system performance. The work of this thesis is intended to be of general applicability, however particular attention has been given to satellite and mobile telecommunication applications. Accordingly, most of the results and design aspects discussed throughout this thesis are demonstrated for such scenarios. The choice of application is mainly motivated by the industrial partnership with RUAG Space AB and Ericsson AB.

In the following subsection a brief overview of the considered applications is given. In the remainder of this chapter the aims and the outline of the thesis are presented.
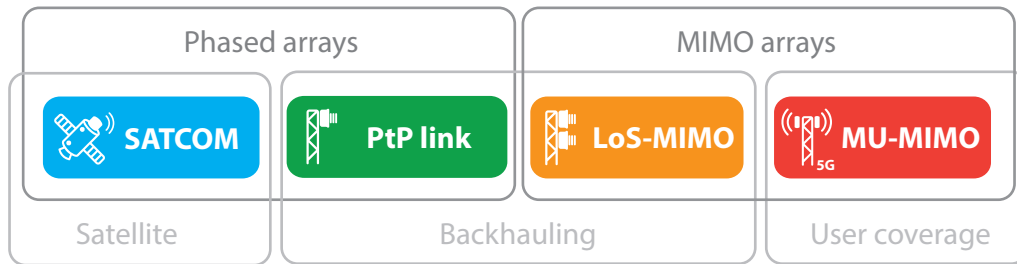
Figure 1.1: The four application scenarios considered.

1.1 Telecommunication Applications

One of the major application areas for antennas are telecommunications. However, the type, size and technologies adopted can vary considerably. We will focus on antennas that are part of the network infrastructure, either connecting parts of it (backhauling) or providing coverage to end users (base station). This implies that the antenna itself is stationary and of significant size, although the other link end(s) might not be. In this thesis we will discuss the following key application areas, as summarized in Figure 1.1:

- **Phased arrays for satellite communication:** Massive arrays with stringent mask requirements but limited field of view, where the number of antennas, and ultimately the cost, is critical.

- **Phased arrays for backhauling:** Compact dense arrays with standard radiation mask envelope, high aperture efficiency and moderate scanning capabilities.

- **MIMO arrays for Line-of-Sight backhauling:** Extremely sparse arrays for short-range channel multiplexing, typically limited by poor installation flexibility.

- **MIMO arrays for Multi-User coverage:** Moderate to massive sized arrays for multi-user cellular coverage, where capacity and link quality are paramount.

1.2 Aim of the Thesis

The aim of this thesis is to investigate the benefits of aperiodic arrays and propose effective synthesis methods for phased arrays and MIMO systems.

Aperiodic arrays have been long studied in phased array applications. We aim at developing a new deterministic synthesis method, capable of modeling realistic EM effects of complex antennas as well as satisfying

a number of requirements. The main objective of the proposed method is to overcome the limitations of current synthesis techniques, which are either computationally intractable or employ too simplistic antenna models and specifications. To this purpose, we propose a deterministic iterative hybrid approach based on Compressive Sensing (CS) theory and full-wave analysis. The problem is formulated in an iterative convex form which is solved efficiently and grants the flexibility to include additional specifications in a straightforward manner. Furthermore, we have extended the method to: i) multi-beam optimization for accurate beam scanning, ii) modularity for manufacturing cost reduction, iii) multi-element array for reduction of number of elements, iv) reconfigurable design for multi-service capabilities and v) isophoric design for maximum efficiency. Finally, with the objective of demonstrating the proposed methodology, we have designed a point-to-point backhauling antenna, which has been manufactured and measured successfully.

For MIMO systems for communication, where little to no work has been done on aperiodic arrays, we aim at investigating the potential benefits and propose effective synthesis methods. Against a common misconception, we aim at demonstrating that the array layout affects the performance of MIMO systems and motivating the advantage of aperiodic arrays. Two use cases are studied, each with a different objective. In the Line-of-Sight (LoS) MIMO case we aim at improving the installation flexibility of regular antennas, which is otherwise severely limited. In the Multi-User (MU) MIMO case we aim instead at improving the capacity, link quality and amplifier efficiency. To target these applications we employ an exhaustive search for the first case and develop a hybrid statistical-tapered approach for the second.

1.3 Thesis Outline

This thesis is divided into two main parts. The first part is organized in eight chapters and introduces the reader to the research topic and presents the main aspects of this work.

In Chapter 2 the reader is provided with a theoretical background on antennas and basic notions of the types of arrays. In Chapter 3 the problem of aperiodic array design is discussed together with earlier work on the topic. This clarifies the context of the present research, presents the proposed framework used in the following two chapters. In Chapter 4 satellite communication applications are considered. First a brief description of the specifications and challenges are given, then the key contributions are separately discussed. In Chapter 5 we describe a point-to-point backhauling antenna. The manufactured demonstrator is presented together with the

measured results. In Chapter 6 Line-of-Sight MIMO for backhauling appli-
cation is covered. Aperiodic array are demonstrated effective also for MIMO
systems. In Chapter 7 Multi-User MIMO applications are investigated. The
design is based on a statistical analysis that models Chapter 8 concludes
the first part of the thesis with a brief summary of the main contributions
and future work.

In the second part of the thesis, the author's most relevant contributions
to the literature are included in the form of appended papers. Additional
non-appended publications can be found as references in the section *List of
Publications.*

Chapter 2

Theoretical Background

An array of antennas is a set of antennas designed such that their combined signals have desired radiation characteristics [1, Chapter 10]. Arrays can appear in very different forms: from a simple slotted waveguide to a complex network of dish reflectors deployed over a large area. Despite the wide range of architectures, capabilities and specifications, the underlying operating principle is common.

Two main parts are identifiable in every array: the first is the antenna elements themselves, which are physically distributed over an area in order to realize an equivalent aperture distribution. The second part is the beamforming network, which is responsible for feeding or combining the elements' signals such as to obtain the desired beam characteristics. An array is referred to as *active* when each antenna has a dedicated transmit/receive module and *passive* when a feeding network is responsible of the distribution to/from a single common module [2, Section 1.2.2]. The first type is more powerful and flexible, however it is considerably more expensive.

This chapter introduces the theoretical basis of antenna arrays. The objective is to provide the reader with a basic understanding of the concepts, notation and terminology used throughout the thesis. First the analysis and design of classical regular arrays is presented. Then, aperiodic arrays are introduced as a superior, yet more challenging, architecture. The underlying working principle of phased array and Multiple-Input-Multiple-Output (MIMO) systems are also discussed.

2.1   Array of Antennas

Consider N antennas placed at the locations $\{\boldsymbol{r}_n\}_{n=1}^{N}$ and the set of respective embedded far-field vector element patterns $\{\boldsymbol{f}_n(\hat{\boldsymbol{r}})\}_{n=1}^{N}$, where the direction $\hat{\boldsymbol{r}}(\theta,\phi) = \sin(\theta)\cos(\phi)\hat{\boldsymbol{x}} + \sin(\theta)\sin(\phi)\hat{\boldsymbol{y}} + \cos(\theta)\hat{\boldsymbol{z}}$ (see also Fig. 2.1). The
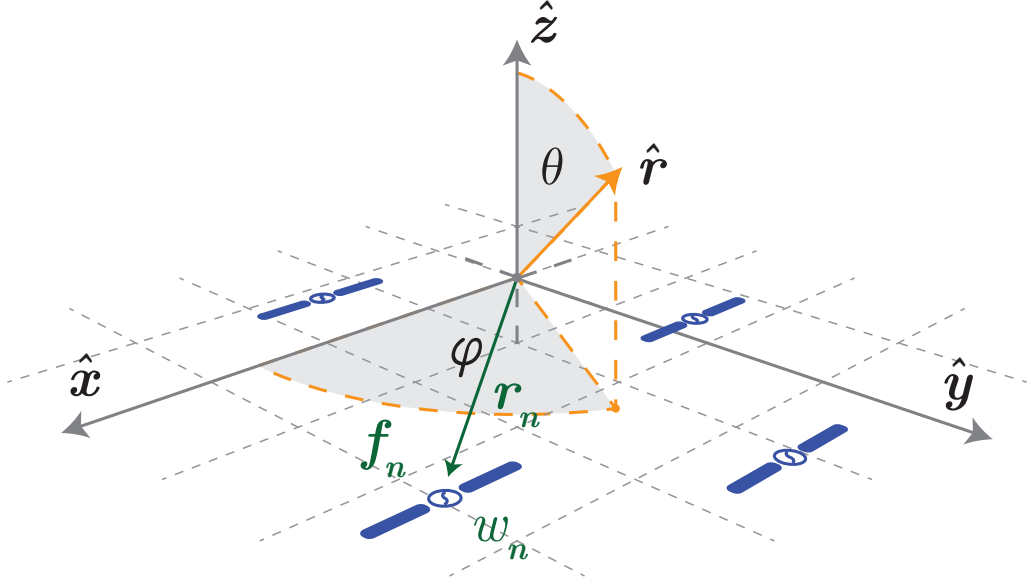
Figure 2.1: Illustration of a generic array layout; each antenna element is characterized by its position $\boldsymbol{r}_n$, embedded element pattern $\boldsymbol{f}_n$, and excitation coefficient w_n.

array far-field pattern can then be written as [1, Eq. (10.4)]

$$\boldsymbol{f}(\hat{\boldsymbol{r}}) = \sum_{n=1}^{N} w_n \boldsymbol{f}_n(\hat{\boldsymbol{r}}) \quad \text{with} \quad \boldsymbol{f}_n(\hat{\boldsymbol{r}}) = \boldsymbol{f}_n^o(\hat{\boldsymbol{r}}) e^{jk\boldsymbol{r}_n \cdot \hat{\boldsymbol{r}}}, \tag{2.1}$$

where w_n is the complex excitation coefficient of the nth element, and $k = 2\pi/\lambda$ is the wavenumber. Note that $\boldsymbol{f}_n$ includes the propagation phase delay with respect to $\boldsymbol{f}_n^o$, whose origin is on the element itself.

Now, for convenience, the vectorial form of the above expressions is also introduced. Let the N-dimensional excitation vector $\mathbf{w} = [w_1, w_2, \ldots, w_N]^T$, where ^{T} denotes the transpose, and let us expand the far-filed pattern into its co-polar and cross-polar components $\boldsymbol{f} = f_{\text{co}}\hat{\mathbf{co}} + f_{\text{xp}}\hat{\mathbf{xp}}$. Then Eq. (2.1) can be rewritten in the compact form

$$\boldsymbol{f}(\hat{\boldsymbol{r}}) = [\mathbf{w}^T \mathbf{f}_{\text{co}}(\hat{\boldsymbol{r}})]\hat{\mathbf{co}} + [\mathbf{w}^T \mathbf{f}_{\text{xp}}(\hat{\boldsymbol{r}})]\hat{\mathbf{xp}}, \tag{2.2}$$

where $\mathbf{f}_\nu = [f_{\nu,1}, \ldots f_{\nu,N}]^T$ is an N-element column vector with $\nu \in \{\text{co}, \text{xp}\}$.

With reference to Eq. (2.1), the resulting far-field pattern is determined by the element patterns, positions and excitation coefficients. The first two quantities are defined by the physical geometry of the array and therefore can not change after manufacturing. The excitation coefficients, on the other hand, can in principle be modified electronically, allowing to change the

array pattern without any mechanical movement, see Chapter 4.3 for further details.

Commonly arrays are assumed to have equal element patterns, i.e., all element patterns have the same shape and only differ by a phase and amplitude coefficient. Although this is generally not true due to mutual coupling, this assumption greatly simplifies the design and the analysis of the array. Under such condition, we can factorize the far-field in (2.1) as [1, Eq. (10.5),(10.6)]

$$\boldsymbol{f}(\hat{\boldsymbol{r}}) = \boldsymbol{f}_0^o(\hat{\boldsymbol{r}})F(\hat{\boldsymbol{r}}) \quad \text{with} \quad F(\hat{\boldsymbol{r}}) = \sum_{n=1}^{N} w_n e^{jk\boldsymbol{r}_n \cdot \hat{\boldsymbol{r}}}, \qquad (2.3)$$

where $F(\hat{\boldsymbol{r}})$ is the scalar Array Factor (AF) and $\boldsymbol{f}_0^o(\hat{\boldsymbol{r}})$ is the common vector element pattern centered at the origin. The envelope of the far-field pattern is defined by the element pattern. Once this is chosen, the design of the array reduces to the synthesis of the scalar AF. For the above expression to be valid, the common element pattern should be an acceptable approximation of the actual element patterns. This is true for single mode antennas, sufficiently large regular arrays and weakly coupled antennas, where the mutual coupling is included, approximated and ignored respectively.

2.2 Regular Arrays

Regular, uniform or equi-spaced arrays are the most widespread class of array layouts where the inter-element distance is constant [1, Section 10.1]. The environment for every element except for those near the periphery is identical and equal to that of an infinitely long regular array. For sufficiently large regular arrays, the common element pattern representation (which includes the mutual coupling) is accurate enough since the contribution of the edge elements is limited, thus Eq. (2.3) is valid.

Let us consider a regular linear array along the x-axis for simplicity as shown in Fig 2.2. Accordingly, the AF in (2.3) can the be written as

$$F(\theta) = \sum_{n=1}^{N} w_n e^{jk(n\Delta x)\sin\theta}. \qquad (2.4)$$

In a regular array, the layout is fully defined by the array aperture area A (or diameter D) and the inter-element spacing Δx, or likewise the number of elements N. The aperture area is directly related to the maximum array gain ($G = 4\pi A/\lambda^2$) or the corresponding minimum beamwidth ($\theta_{\mathrm{HPBW}} = \arcsin[0.2572\lambda/D]$). The inter-element spacing must be chosen small enough
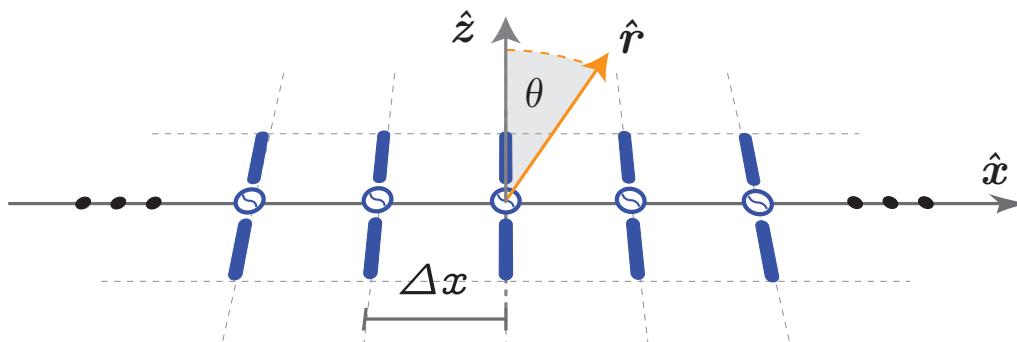
Figure 2.2: Illustration of a regular linear array; elements are placed along the x-axis with a constant inter-element distance Δx.

to guarantee the absence of grating lobes (see Section 3.2.1) in the visible range. Spacings from $\lambda/2$ to λ are needed to guarantee grating lobe-free regime, depending on the scanning requirements. Therefore, the layout of a regular array can be very easily obtained.

The remaining parameter, i.e., the element excitation, can be used to shape the radiation pattern, however at the expense of the aperture efficiency [3, Section 6.8]. Adopting the simple uniform excitation on all the elements gives maximum directivity but results in a first side lobe of -13.3dB. If a lower Side Lobe Level (SLL) is required, well-known closed-form solutions can instead be used to find the optimal excitation [2, Chapter 3]. Additionally, and as shown in Eq. (2.4), the far-field pattern and the element weights have a linear relationship, such that relatively straightforward beamforming algorithms can be applied to achieve desired patterns. Generally speaking, active arrays can adaptively change the excitations and thus the pattern while passive array have a fixed excitation that is assigned at design time.

2.3   Aperiodic Arrays

An array is said to be *aperiodic*, irregular or non-uniform when the inter-element distances or the antenna elements are not identical, see Fig. 2.1. Aperiodic arrays are sometimes also referred to incorrectly as *sparse* (vs *dense*), despite the fact that this term just indicates a large element spacing. This is because these indeed often adopt aperiodic layouts.

The aperiodic array can be interpreted as the most general array layout, where the additional degree of freedom given by the layout is exploited to optimize the array. Indeed, aperiodic arrays can offer superior characteristics compared to regular ones, by minimizing the number of elements, improving the radiation pattern and reducing the excitation tapering. Most notably,
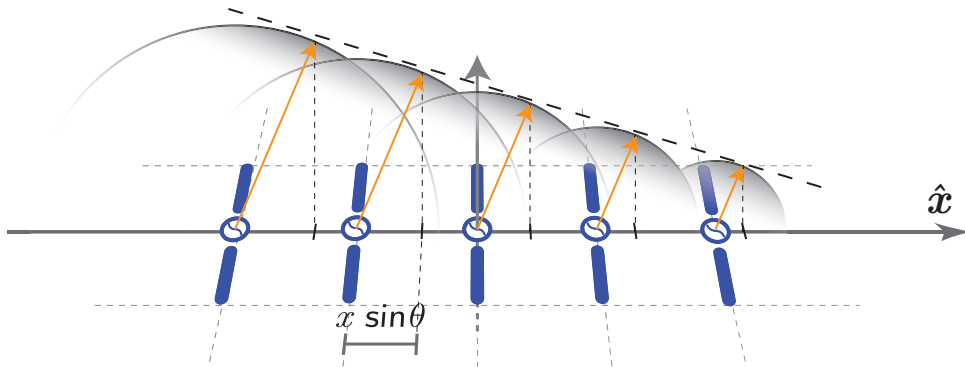
Figure 2.3: Illustration of a linear phased array.

aperiodic arrays exhibit pseudo-grating lobes and thus are highly preferred to regular arrays when very large spacing is required.

However, aperiodic arrays have a significantly more complex synthesis and design then regular array, thus limiting their adoption. Many approaches have been proposed for the synthesis of aperiodic arrays, from analytical methods to local refinement schemes. Unfortunately, the problem of synthesizing a Maximally Sparse Array (MSA), i.e. an array with the least number of elements, is very challenging, see Chapter 3. As expressed by (2.1), the relation between the array pattern and the element positions is an exponential function with a complex-valued argument, and therefore highly non-linear and oscillating. Additionally, the infinite array approach cannot be applied to aperiodic arrays, so most of the synthesis methods are limited to the case of isolated elements. The aperiodicity of the layout can also have considerable additional complexities for the design and manufacturing of the rest of the system. These include, for example, the feeding network (Section 5.3), the modularity (Section 4.2) and the thermal design.

2.4   Phased Arrays

Antenna arrays are referred to as *phased* when they provide electronic beam steering by excitation phase tuning [2, Section 1.2]. Electronic beam steering permits agile and reliable beam pointing for tracking users or scanning large sectors quickly. This functionality is not limited to active array only, passive can also realize this, for example, by frequency scanning or though additional components such as phase shifters.

Given an arbitrary excitation set $\{w_n\}$, the pattern can be translated to the direction $\hat{\boldsymbol{r}}_s$ by modifying the excitation phases according to the

expression $w_n^s = w_n e^{-jk\boldsymbol{r}_n \cdot \hat{\boldsymbol{r}}_s}$. Then, substituting in Eq. (2.3) gives

$$F^s(\hat{\boldsymbol{r}}) = \sum_{n=1}^{N} w_n^s e^{jk\boldsymbol{r}_n \cdot \hat{\boldsymbol{r}}} = \sum_{n=1}^{N} w_n e^{jk\boldsymbol{r}_n \cdot (\hat{\boldsymbol{r}} - \hat{\boldsymbol{r}}_s)} = \sum_{n=1}^{N} w_n e^{jk[x_n(u-u_s)+y_n(v-v_s)]} \quad (2.5)$$

where $u = \sin(\theta)\cos(\phi)$ and $v = \sin(\theta)\sin(\phi)$ are often referred to as sine or $u - v$ space. From the above expression it is clear that by linearly adjusting the element phases the pattern undergoes a translation in the $u - v$ space by the quantity (u_s, v_s). This is valid for the Array Factor, while the embedded element pattern is independent of the excitation.

2.5   MIMO Arrays

The capacity in bit/s/Hz of a classical, so-called, Single-Input-Single-Output (SISO) system according to the Shannon theorem is [4, Section 4.1]

$$C = \log_2 (1 + \text{SNR}) \quad (2.6)$$

where $\text{SNR} = E_r/N_0$ is the Signal-to-Noise Ratio, E_r is the received signal energy and N_0 is the noise energy. Increasing the transmitted power (and thus the SNR) increases the capacity. However, this tends to saturate due to the logarithmic dependence.

Since the pioneering work of Foschini and Gans in 1998 [5], Multiple-Input-Multiple-Output (MIMO) has become one of the most promising technology for high-bandwidth wireless communications. It can be thought as an array with advanced adaptive beamforming, capable of taking advantage of the complex surrounding environment. The MIMO architecture supports both diversity combining, for low signal levels, and spatial multiplexing, for higher SNR regimes. We will focus on multiplexing, i.e. the ability of creating multiple parallel data streams and thus increasing the capacity. It is however worth noticing that MIMO requires active arrays and signal processing capabilities. In a $N \times M$ narrowband flatfading MIMO system, see Fig. 2.4, the signal $\mathbf{y} \in \mathbb{C}^{M \times 1}$ received at the M antenna ports can be written as [6]

$$\mathbf{y} = \sqrt{\text{SNR}}\mathbf{H}\mathbf{x} + \mathbf{n}, \quad (2.7)$$

where $\mathbf{x} \in \mathbb{C}^{N \times 1}$ is the normalized signal at the N transmitting antennas, $\mathbf{H} \in \mathbb{C}^{M \times N}$ is the normalized channel matrix, $\mathbf{n} \in \mathbb{C}^{N \times 1} \sim \mathcal{CN}(0, \mathbf{I})$ is the zero-mean unit variance additive white gaussian noise and $\mathbf{I}$ is the identity matrix. The MIMO system employs coding to reconstruct the original signals from the received ones and the knowledge of the channel. Then, depending on the channel characteristics, it is possible to decouple the channels and transmit up to $\min(M, N)$ parallel streams.
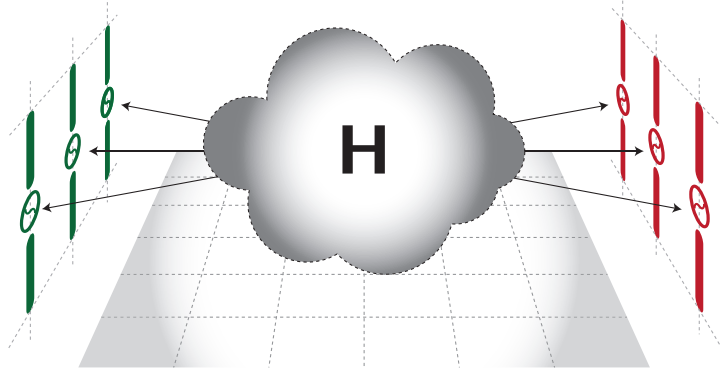
Figure 2.4: Illustration of a MIMO link.

The channel matrix $\mathbf{H}$ captures the instantaneous propagation conditions, which are highly volatile and dependent on the actual surrounding. It is however common to use simplified channel models, one is the popular Rician fading model [7]:

$$\mathbf{H} = \sqrt{\frac{K}{1+K}}\mathbf{H}_{\text{LoS}} + \sqrt{\frac{1}{1+K}}\mathbf{H}_{\text{NLoS}} \qquad (2.8)$$

where K is called the Rician factor, $\mathbf{H}_{\text{LoS}}|_{m,n} = \exp\left(j\frac{2\pi}{\lambda}r_{m,n}\right)$ is the Line-of-Sight (LoS) component and $\mathbf{H}_{\text{NLoS}} \sim \mathcal{CN}(0,\mathbf{I})$ is the scattered stochastic (thus varying) Non-Line-of-Sight (NLoS) component. For Rician factor $K = 0$, this coincide with the Rich Isotropic MultiPath channel (RIMP) or Rayleigh channel, where a large number of random and uniformly distributed waves illuminate the antenna [8]. For $K = \infty$, this coincide with pure undisturbed LoS propagation, as generally assumed in classic antenna analysis. Limited scattering (i.e. high Rician factor) is typically associated with poor multiplexing possibilities because it is the different reflected waves that enable the creation of separable channels. We will however discuss instances in which strong LoS condition support high multiplexing, i.e. when the antenna angular resolution is sufficient to separate the target antennas. This is indeed the case of well-separated terminals such as in multi-user coverage (Chapter 7), or very large antennas for backhauling (Chapter 6).

The capacity for a MIMO system without Channel State Information (CSI) at the transmitter, and thus equal power allocation, is [9]

$$C = \log_2 \det(\mathbf{I} + \frac{\text{SNR}}{N}\mathbf{H}\mathbf{H}^H) = \sum_{i=1}^{\min(M,N)} \log_2\left(1 + \frac{\text{SNR}}{N}\mu_i\right), \qquad (2.9)$$

where ^{H} is the Hermitian operator and μ_i are the eigenvlaues of the matrix $\mathbf{H}\mathbf{H}^H$ if $M \leq N$ and $\mathbf{H}^H\mathbf{H}$ if $M > N$. The latter expression shows how the

MIMO architecture created effectively $\min(M, N)$ parallel channels, each with a gain proportional to its eigenvalues. The desirable almost linear relationship of capacity and power can then be restored by dividing the power between the channels.

2.6 Summary and Conclusions

In this chapter, a theoretical background on antenna arrays is given. First, the basic terminology, classification and adopted notation are introduced to the reader. Regular arrays were then briefly presented to discuss classical design and assumptions. Aperiodic arrays were presented as a solution to further improve and optimize classical regular arrays. A short introduction to phased- and Multiple-Input-Multiple-Output-arrays (MIMO) was also given.

Regular arrays have simple and well-established design and analysis criteria, and are thus the most common architecture both for phased- and MIMO-systems. Aperiodic arrays, on the other hand, are attractive since they are potentially superior to the regular counterpart. Unfortunately, the synthesis of Maximally Sparse Arrays (MSA) (the array with the least number of antenna elements) is very challenging. Therefore, there is a strong interest in new effective aperiodic array synthesis techniques, which are flexible and mature, such as to be used for practical designs.

Chapter 3

Aperiodic Array Synthesis

Aperiodic arrays offer superior characteristics compared to regular arrays, however their design is far more challenging. In particular, the synthesis of a Maximally Sparse Array (MSA) is a complex problem, which has no direct solution due to its highly non-linear nature. Moreover, due to the huge dimensionality of the problem, an exhaustive search through all the possible array layouts is feasible only for the smallest arrays, see Chapter 6.

Several hybrid synthesis techniques have been proposed, ranging from analytical methods to general purpose global optimization [10]. However, they are typically restricted to simplified models and specifications or prohibitive computational requirements. We propose a synthesis framework based on Compressive Sensing (CS), a fast and flexible signal processing technique capable of maximizing the sparsity of the array. Moreover, we present a full-wave hybridization for modeling complex and realistic antennas, and thus overcoming the limitation of available methods. The developed framework is then applied and extended in Chapter 4 and 5.

In this chapter we discuss the problem of aperiodic array synthesis and present the core of the proposed method. First a brief overview of the literature on the topic is given, explaining the limitations of the state-of-the-art approaches. Subsequently the adopted CS approach is presented. The fullwave hybridization is presented then as a mean of including mutual coupling effects and accounting for complex and realistic antennas. Finally, conclusions are given. This chapter is based on Paper A.

3.1 Literature Review

Aperiodic array were first investigated by Unz [11], it was found that by tuning the element positions one is able to reduce the element number and/or SLL compared to classical regular arrays. A large number of techniques have

been proposed since. A brief review of some of the most popular ones and their major limitations are provided below.

Global optimization techniques

Global Optimization (GO) techniques, and more generally stochastic methods, are very popular in the design of aperiodic arrays. The first encouraging results were obtained in the 90s, when Haupt first applied GO methods to the synthesis of thinned arrays [12]. A number of techniques have been borrowed and refined from the mathematics science field, and subsequently been applied to the synthesis of aperiodic arrays. Some of the most popular GO methods are Genetic Algorithms [12], Particle Swarm [13], Ant Colony [14] and Invasive Weed Optimization [15]. GO techniques have been mostly applied to array thinning problems and in a few cases to aperiodic arrays too.

One of the most attractive aspects of GO methods is their flexibility. In general, it is possible to incorporate complex specifications in a heuristic fitness function. This allows to include various additional aspects of interest in virtue of the trial and error nature of the approach.

The major limitation of such methods is their high computational complexity. In most cases, only small to medium sized problems are tractable, but even these are often very time consuming to solve. For larger problems, their use is limited only to the refinement of an initial solution [16].

Analytical techniques

Several analytical techniques, and more generally, deterministic techniques, have been proposed for the synthesis of both sparse and thinned aperiodic arrays. In the 60s and 70s a large number of deterministic thinning algorithms were proposed [17–20]. However, due to the limited success in controlling the side lobes, some researchers conjectured that *cut-and-try random placement* is as effective as any deterministic placement algorithm could ever be [21].

Today, a number of effective deterministic techniques are available. Some worth mentioning are the Matrix Pencil Method [22], Almost Different Sets [23], the Auxiliary Array Factor [24], Poisson Sum Formula [25] and the Iterative Fourier Technique [26]. Another interesting and intuitively simple method interprets the aperiodic problem as the discrete approximation of an optimal contiguous aperture taper distribution. Elements are then placed with density proportional to a reference distribution, such as the standard Taylor's amplitude taper [27].

Analytical techniques can handle much larger problems and the solutions typically show a simpler relationship between the specifications and the

array design. The latter helps designers to have a better understanding of the relationship between the specifications and the solution, as opposed to global optimization methods. However, the major limitations are dictated by the rather simplified model and specifications they assume. Specifically, and in relation to the novel contribution discussed in this work, virtually no deterministic method accounts for mutual coupling effects or multiple assorted specifications.

3.2 Compressive Sensing Approach

Compressive Sensing (CS) is a signal processing technique designed for the efficient sampling and reconstruction of a continuous signal [28]. In fact, by exploiting the natural sparsity of a continuous signal it is possible to greatly reduce the number of samples required to reconstruct the signal compared to the classical Nyquist–Shannon sampling criterion.

A parallel can be drawn with the MSA synthesis problem in the antenna scenario. In the simplest form, the problem is that of minimizing the number of spatial samples (antenna elements) required to synthesize a desired radiation pattern [29]. The parallel between the two problems is further clarified by the relationship between the Fourier Transform of the (sampled) time signal in the signal processing case and the Array Factor (AF) of the (sampled) aperture field distribution in the array case.

The CS problem is then solved in an approximate form through an iterative weighted ℓ_1-norm minimization procedure [30]. This formulation allows for an efficient and deterministic solution by means of standard convex optimization algorithms. Furthermore, the algorithm is flexible enough to include additional constraints, provided they can be expressed, or be approximated, in a convex form (more details in Sec. 3.2.3).

In this section we briefly introduce the theoretical basis behind classical and CS sampling. Throughout this chapter the parallels between the signal processing and aperiodic array synthesis techniques are illustrated. The weighted iterative convex ℓ_1-norm optimization formulation is introduced afterwards. The method is demonstrated for the synthesis of small aperiodic arrays of isotropic radiators.

3.2.1 Nyquist Sampling and Grating Lobes

The Nyquist–Shannon sampling criterion guarantees lossless reconstruction of a continuous signal when uniformly sampling at twice the maximum frequency of the original signal. However, the theorem does not preclude the reconstruction in circumstances that do not meet the sampling criterion.
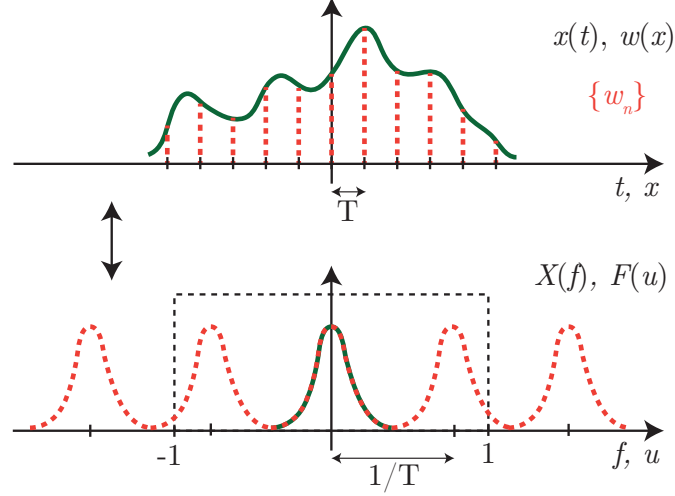
Figure 3.1: Illustration of the Nyquist sampling criterion/grating lobe free condition. In the time/space domain (top), the original continuous signal/aperture field distribution (in green) is sampled uniformly with T step (red). In the transformed frequency/array factor domain (bottom), the sampled signal (red) is a series of displaced replicas of the continuous signal (green) with period $1/T$. In arrays, the visible range is $u \in (-1, 1)$ (black).

Notice the parallel between the Discrete Time Fourier Transform (DTFT) and the AF expression (2.4):

$$X(f) = \sum_{n=-\infty}^{\infty} x(nT)e^{-j2\pi fTn} \longleftrightarrow F(u) = \sum_{n=1}^{N} w\left(n\frac{\Delta x}{\lambda}\right)e^{j2\pi u\frac{\Delta x}{\lambda}n}, \quad (3.1)$$

where in the equation on the left, $x(t)$ is the continuous signal sampled with the period T and $X(f)$ is the DTFT, periodic with period $1/T$; in the equation on the right, $w(x)$ is the aperture field distribution sampled at uniform distance $\Delta x/\lambda$ and $F(u)$ is the AF, periodic with period $\lambda/\Delta x$. The AF is a function of $u = \sin\theta$, thus the *visible range* extends between $u = \pm 1$ ($\theta = \pm 90^\circ$). When the inter-element distance $\Delta x > \lambda$, replicas of the main beam will be visible, as shown in Fig. 3.1. These new lobes, referred to as grating lobes, are highly undesired since they have the same amplitude of the main lobe (minus the attenuation effect due to the element pattern), thus compromising the directivity and dramatically increasing the SLL. When scanning up to the angle θ_s, the grating lobe free condition becomes roughly $\Delta x/\lambda \leq 1/(1 + |\cos\theta_s|)$ [1].

As a result, the appearance of grating lobes prevents us from increasing the inter-element distance and reducing the number of elements in a periodic layout. Since this effect is due to the adopted periodicity of the element
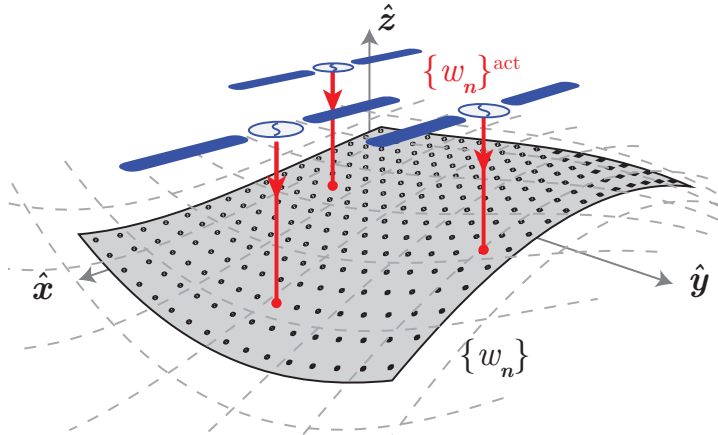
Figure 3.2: Illustration of a generic surface (gray) and its sampling (black dots). Between all the samples and the corresponding excitations $\{w_n\}$, only *active* samples (in red) are replaced by actual elements (in blue).

positions, choosing aperiodic layouts helps to reduce the effect of coherent field summation in unwanted directions.

3.2.2 Compressive Sensing Sampling

CS is a technique for minimizing the number of samples required to reconstruct a signal. Typically, signals are sampled according to the Nyquist criterion and are processed afterwards by a compression algorithm. CS, on the other hand, aims at directly minimizing the number of samples.

To find a minimal representation of the signal, CS relies on the solution of an under-determined system - a linear system of equations with more unknowns than equations. Under-determined systems have an infinite number of solutions. In order to choose one, additional constraints should be added. In compressive sensing the additional constraint is the sparsity condition which can be enforced by minimizing the number of non-zero components of the solution vector. In mathematical terms, the function returning the number of non-zero vector elements is the ℓ_0-norm.

In the array scenario, given an aperture sampling, the problem of designing a maximally sparse array is finding the excitation set $\{w_n\}$ with the minimum number of non-zero entries $\{w_n\}^{\mathrm{act}}$ while fulfilling certain pattern constraints, as shown in Fig. 3.2. Using the vector notation introduced in Eq. (2.2), the optimization problem can be stated as finding $\mathbf{w} \in \mathbb{C}^N$ such that [30]

$$\underset{\mathbf{w}\in\mathbb{C}^N}{\operatorname{argmin}} \ \|\mathbf{w}\|_{\ell_0}, \text{ subject to a \textit{set of constraints}.} \tag{3.2}$$

For pencil beam synthesis and for a beam with a maximum co-polar directivity in the scanning direction $\hat{\boldsymbol{r}}_s$ and a radiation mask M_ν on the ν component of the field, the set of constraints can be written as

$$\textit{set of constraints}: \begin{cases} f_{\text{co}}(\hat{\boldsymbol{r}}_{\text{s}}) = 1, \\ |f_\nu(\hat{\boldsymbol{r}})|^2 \leq M_\nu(\hat{\boldsymbol{r}}), \hat{\boldsymbol{r}} \in \text{mask}. \end{cases} \tag{3.3}$$

3.2.3 Iterative ℓ_1-norm Minimization

Unfortunately, Eq. (3.2) cannot be solved directly and finding a solution using a combinatorial search method is intractable, even for moderate array sizes [i]. Indeed, it can be shown that this problem is NP-hard [31]. NP-hard problems are the class of problems for whom just verifying a given solution hypothesis is already prohibitive. It follows that solving in a rigorous way the CS problem, i.e. actually finding *the* solution, is computationally infeasible.

To overcome this, approximate solution techniques are considered. In [30], the problem is relaxed and solved in a semi-analytical manner by approximating the ℓ_0-norm minimization through an iterative weighted ℓ_1-norm minimization procedure. One iteration of the algorithm reads [30]

$$\underset{\mathbf{w}^i \in \mathbb{C}^N}{\text{argmin}} \ \|\mathbf{Z}^i \mathbf{w}^i\|_{\ell_1}, \text{ subject to a \textit{set of constraints}} \tag{3.4}$$

where the mth element of the diagonal matrix $\mathbf{Z}^i$ is given by,

$$z_m^i = \frac{1}{|w_m^{(i-1)}| + \epsilon}. \tag{3.5}$$

The matrix $\mathbf{Z}^i$ is chosen to maximally enhance the sparsity of the solution $\mathbf{w}^i$; that is, redundant elements are progressively suppressed by magnifying their apparent contribution in the minimization process by an amount that is based on the previous solution $\mathbf{w}^{(i-1)}$. The parameter ϵ enables elements that are "turned off" to be engaged again later on during the iterative procedure. In practice, ϵ should be set slightly smaller than the smallest expected active excitation for an optimal convergence rate and stability. Typically, this numerically efficient procedure requires only few iterations for the excitation vector to converge.

Both the minimization problem and the set of constraints are formulated in a convex form, so that standard convex programming algorithm can be used to find a solution in a deterministic manner. For a convex problem the local minimum coincides with the global one, so that the solution is easily found.
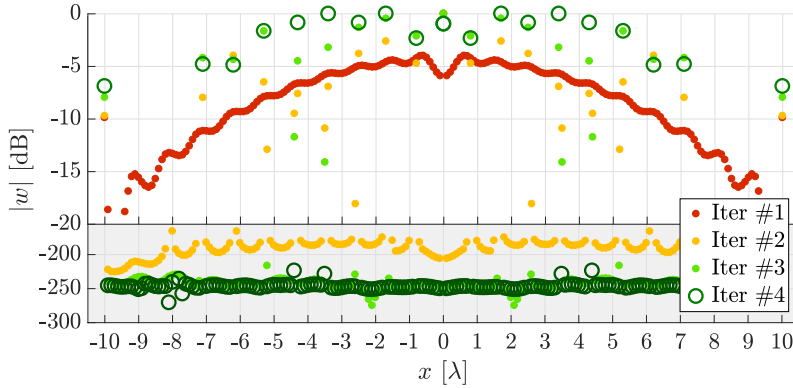
(a) Excitation coefficient magnitudes.
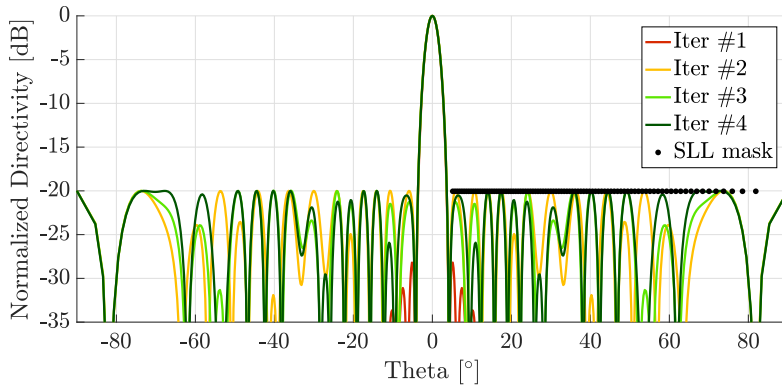
(b) Far-field radiation patterns.

Figure 3.3: Evolution of the array solution for subsequent iterations.

3.2.4 Results

The CS approach is here demonstrated in the synthesis of a linear symmetric array. To further illustrate the behavior of the method, the evolution of the synthesis process is examined. The chosen array is a linear array of isotropic radiators with an aperture diameter $d = 20\lambda$ and -20 dB SLL.

The aperture is first sampled finely so as to emulate a quasi-continuous element positioning (typical step size is $\Delta d = \lambda/100$, although here $\lambda/10$ is preferred for graphical reasons), and phase-shifted versions of the element patterns are assumed. The ℓ_1-norm minimization is then iterated until convergence of **w** occurs, yielding the optimal array layout. Although the optimization solution includes all the possible element positions, it is straightforward to identify active elements by a threshold level on the excitation magnitudes. Typically, inactive elements have normalized magnitudes in the order of -200 dB, the distinction is clear and their removal from the actual array has no practical impact on the final pattern. In Fig. 3.3(a)

19

the evolution of the element weights is shown, while the corresponding far-field patterns are illustrated in Fig. 3.3(b). In just 4 iterations, starting from a quasi-continuous element distribution, the algorithm selects only 17 active elements and the corresponding weights that guarantee the far-field requirements. The remaining elements have weights between -200 dB and -300 dB in magnitude and will therefore not have a noticeable effect on the far-field pattern when removed.

3.3   Antenna Mutual Coupling

The antenna radiation characteristics are strongly influenced by the immediate surroundings, in particular by conducting bodies. In an array, the proximity between antenna elements can strongly affect their far-field patterns and impedance characteristics. This effect, known as Mutual Coupling (MC), is often undesired but can also be exploited to improve directivity and bandwidth.

As discussed in Chapter 2, in array analysis and design, it is common to assume *identical* element pattern shapes. This approximation is appropriate for weakly coupled antennas (where MC can be ignored) and large regular arrays (where the majority of the elements experience identical MC effects).

In aperiodic arrays, the irregular structure and the dense element clusters complicate the modeling, as the element patterns can be very different from one another. The complexity of the MC effects and the lack of simple mathematical models require us to perform a time-consuming full-wave analysis. As a consequence, designing aperiodic arrays with MC included is practically impossible with analytic methods as well as computationally intractable for global optimization methods. For this reason, aperiodic array synthesis methods typically assume isolated element patterns, although such approximation may not always be accurate. Very recently, [32] and [33] have proposed two alternative methods to include MC.

The herein proposed CS method has been extended for the inclusion of MC effects in the synthesis of aperiodic arrays through an iterative full-wave analysis. The array is first designed by assuming Isolated Element Patterns (IEP), i.e., without MC effects, and simulated by the Method of Moment (MoM) analysis to evaluate the effects of MC. The array is then iteratively refined using the Embedded Element Patterns (EEP) that include the MC effects, until convergence is reached. The algorithm typically converges in few iterations making it numerically efficient.

In this section we describe the basic theory on MC effects and its inclusion in the array synthesis algorithm. Results are shown for the synthesis of a linear array of highly coupled dipole antenna elements.
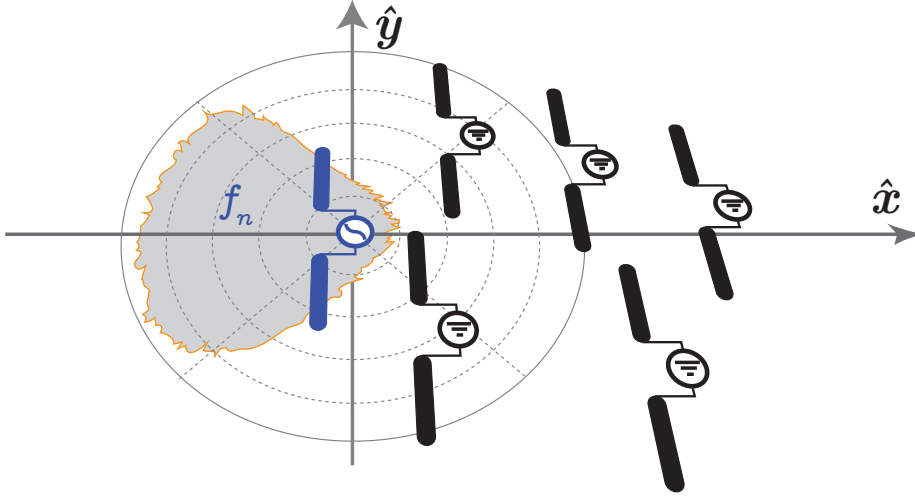
Figure 3.4: Illustration of the Embedded Element Pattern: the EEP $\boldsymbol{f}_n(\hat{\boldsymbol{r}})$ (gray) is defined when the element n is excited (blue) and the rest are passively terminated on a matched load (black).

3.3.1 Embedded Element Pattern

Antennas are typically characterized in free space, i.e., in *isolation* from any other body, and are described by the IEP. Once an antenna element is placed inside an array, the proximity to other elements will influence its behavior due to MC. Exciting one antenna induces currents on nearby elements which can re-radiate and subsequently couple to other antennas. This gives rise to two effects: (i) a change in the total pattern due to radiating currents induced on the other antennas; (ii) a change in the antenna impedance due to the induced current at the antenna ports. These effects are dependent on the element excitations, or in the case of phased arrays, on the scanning direction. In practice, the magnitude of such effects is strongly affected by the element directivity and spacing. Due to a lack of simple mathematical models, it is in general impossible to predict MC a priori.

A common approximation to the analysis of MC effects is the *isolated element approach* [1], where the shape of the electric current is assumed to be identical for all elements. This is valid only for single mode antennas, where the geometry of the antenna element supports only one current mode. For example, in the specific case of a minimum scattering antenna (e.g. half-wave dipoles), the neighboring antennas are effectively invisible when open-circuited. As a result, when the antennas are terminated, the resulting pattern of one excited antenna can be expressed as the sum of the identical patterns of all elements multiplied by their corresponding induced currents. The inclusion of the MC effects therefore reduces to find the induced currents

on neighbouring elements when one is excited, which can be done through the antenna input impedance matrix. The impendence matrix can be obtained by means of a full-wave analysis and can be used directly to compensate for MC effects [34].

The approach adopted here is the more general *embedded element approach* [35]. The EEP is defined as the element pattern when one element is excited and the rest of the elements are passively terminated by a matched load, see Fig. 3.4. When this representation is adopted, Eq. (2.1) is valid since the MC effects are incorporated in the EEP definition. Additionally, this definition is not limited to single mode antennas. The excitation coefficients $\{w_n\}$ represent the incident voltage excitation and the scan impedance can be calculated from the N-port S-parameters.

It is pointed out that changing the element positions would modify the resulting mutual impedance and EEPs. Hence, regardless of the representation, the MC must be recalculated for a specific array layout.

3.3.2 Fast Array Simulation by CBFM

A full-wave analysis of electrically large structures is often resource demanding, which renders the analysis of arrays of complex antennas impractical. The MoM is a popular numerical method based on an integral formulation of the Maxwell equations. In MoM, the unknown current distribution $\boldsymbol{J}$ is discretized by dividing the antenna surface in N_J appropriately sized facets (the mesh) supporting the current basis functions as

$$\boldsymbol{J}(\boldsymbol{r}) = \sum_{n=1}^{N_\mathrm{J}} I_n \boldsymbol{J}_n(\boldsymbol{r}), \tag{3.6}$$

where $\boldsymbol{J}_n$ and I_n are the nth basis function and its unknown expansion coefficient, respectively. The unknown currents at the N_J basis function supports are solved by testing the boundary conditions using N_J test weight functions leading to a system of linear equations of the form

$$\mathbf{ZI} = \mathbf{V}, \tag{3.7}$$

where $\mathbf{I}$ is the vector of unknown expansion coefficients for the current, while $\mathbf{Z}$ and $\mathbf{V}$ are the moment matrix and excitation vector, respectively.

With reference to (3.7), storing the moment matrix requires $O(N_J^2)$ memory, while performing the matrix inversion requires $O(N_J^3)$ solve time. As an example, a single pipe horn element (Section 4.1) requires about 9000 Rao-Wilton-Glisson basis functions [v]. Consequently, only arrays of very few of these elements can be simulated in practice by standard MoM

methods on regular computing platforms, while the desired array sizes that we need to consider can be in order of hundreds of elements.

The Characteristic Basis Function Method (CBFM) is a macro domain basis function method that greatly reduces the numerical complexity of the antenna array analysis [36]. The method first analyzes the characteristic behavior of the single antenna, then maps the local basis functions to a restricted set of characteristic vasis functions on the whole antenna. The method compresses the number of unknowns that need to be solved for in (3.7) by assuming that only a reduced set of current distributions are sufficient to accurately represent the actual current distribution. The total current can therefore be represented as

$$\boldsymbol{J}(\boldsymbol{r}) = \sum_{c=1}^{N_{\mathrm{CBF}}} I_c^{\mathrm{CBF}} \boldsymbol{J}_c^{\mathrm{CBF}}(\boldsymbol{r}) \quad \text{with} \quad \boldsymbol{J}_{p,s}^{\mathrm{CBF}} = \sum_{n=1}^{N_{\mathrm{p}}} I_{n,p,s} \boldsymbol{J}_{n,p}(\boldsymbol{r}), \qquad (3.8)$$

where $\boldsymbol{J}_{p,s}^{\mathrm{CBF}}$ is the sth CBF of the pth antenna. Eq. (3.7) can then be rewritten in terms of the above unknown CBF coefficients. Typically, starting from a very large number of local basis function, only a very reduced set of CBFs is sufficient for the accurate representation of the current distributions on the elements, therefore resulting in a very large compression (typically a factor 100 in the number of unknowns) of the linear system of equations.

3.3.3 Inclusion of Mutual Coupling Effects

The proposed synthesis method involves two subsequent steps, as shown in Fig. 3.5. First, the MSA is designed in the *absence* of MC effects as in the previous section and in accordance with other aperiodic synthesis methods. For this *initial*, uncoupled array design, phase-shifted versions of the EM-simulated IEP are assumed. The ℓ_1-norm minimization is invoked and the active elements are identified by thresholding on the excitation magnitudes.

In the second step, an iterative, full-wave optimization is performed where the ℓ_1-norm minimization approach is hybridized by a full-wave EM analysis. First, we perform a full-wave analysis of the active elements of the initial array layout to estimate the MC effects as well as to obtain the EEPs of the active elements. The isolated element patterns for the active element are then replaced by the simulated EEPs. The element patterns of the inactive elements are estimated by assuming a phase-shifted version of their nearest simulated EEP[1]. With this new set of EEPs, the ℓ_1-norm minimization

---

[1]If needed, more sophisticated pattern interpolation techniques can be used to better estimate the embedded element patterns of inactive elements.
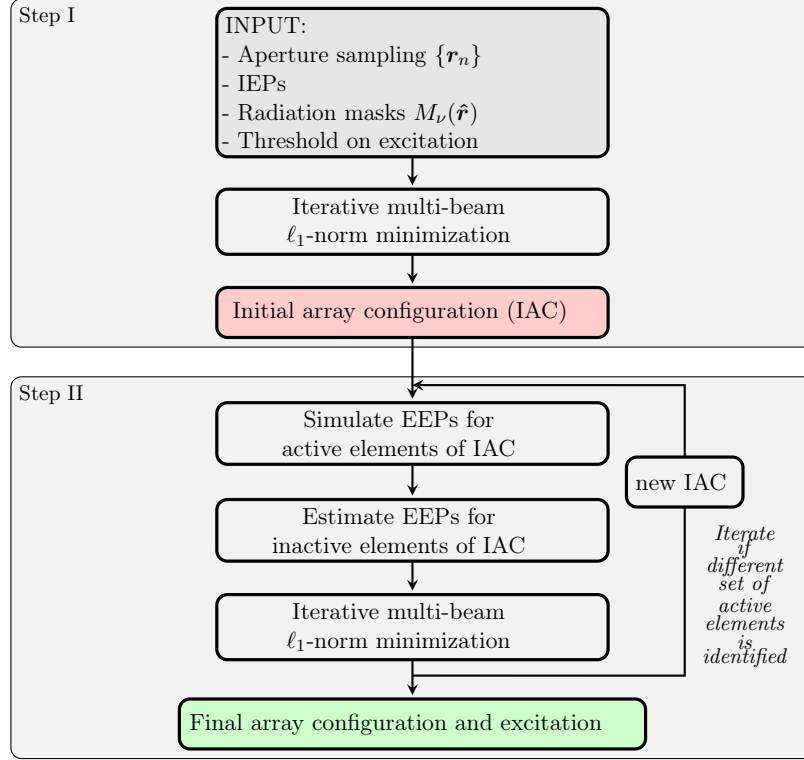
Figure 3.5: Block diagram of the proposed optimization approach, where IEP and EEP denote the isolated and embedded element patterns, respectively.

algorithm is invoked again to obtain a new array layout. This procedure is repeated until the convergence criterion is satisfied, i.e., the state of active and inactive elements remains the same between two subsequent iterations. Typically, few MoM-ℓ_1 iterations are needed to reach convergence; for the MoM analysis, the full-wave in-house developed CAESAR solver is used [37]. Including the coupling effects in the synthesis phase not only allows us to correct for the associated degradations, but also to exploit such effects to improve the array design.

3.3.4 Results

The validity of the above extended method has been demonstrated in the synthesis of a small symmetric linear aperiodic array of parallel of $\lambda/2$ resonant dipoles. We consider the problem of designing a broadside array of aperture size $d = 10\lambda$. The chosen SLL mask has the main lobe confined in the $|\theta| \leq 5.5°$ ($|u| \leq 0.0965$) region and a SLL of -22 dB. These specifications are chosen to be similar to those frequently used when benchmarking array

synthesis algorithm, although a slightly more stringent SLL with respect to the typical -20 dB has been chosen to compensate for the slightly higher element directivity with respect to the commonly employed isotropic radiator. Furthermore, since we consider a broadside scanned array of identical antenna elements, a symmetric array layout will be synthesized.

As discussed, the array is first optimized assuming isolated element patterns. This initial design is then simulated by a full-wave analysis to asses the coupling effects. Fig. 3.6(a) shows the meshed model. The resulting normalized directivity when including MC effects, shown in Fig. 3.6(b), registers a SLL degradation of about 7 dB in proximity of the main lobe. Fig. 3.6(c) shows the IEP and EEPs for the positive x-positioned elements only. The negative x-positioned elements are omitted due to the symmetry.

Starting from this initial design, the algorithm proceeds to re-optimize the array excitations and layout for the updated set of EEPs. The evolution of the positive elements for each MoM-ℓ_1 iteration is summarized in Table 3.1. Fig. 3.7(a) shows the corresponding array patterns for each iteration. The initial and final element positions and weight magnitudes are shown in Fig. 3.7(b), where one can observe how the central and dense part of the array layout changes upon introducing MC effects. The array layout converges in just 3 iterations, reduces the elements from 16 to 12 and corrects the SLL, while the broadside directivity is barely compromised.

3.4 Summary and Conclusions

In this chapter we have introduced the problem of aperiodic array synthesis and presented the proposed synthesis framework. First, a brief overview of the literature and the current limitations is given. The Compressive Sensing (CS) approach is then described and applied to synthesize a Maximally Sparse Array antenna (MSA). The method is then extended to include Mutual Coupling (MC) effects by adopting an iterative refinement approach involving rigorous Electro Magnetic (EM) simulations.

The proposed CS based framework has several interesting characteristics. The convex formulation allows for the problem to be solved in an efficient and deterministic manner. Additionally, it is flexible and can be extended by additional constraints, when these are expressed in a convex form. The full-wave hybridization allows for the inclusion of mutual coupling directly in the design process. The method converges in few iterations with a limited computational burden. In the following two chapters the proposed method is used for the design of actual antennas.
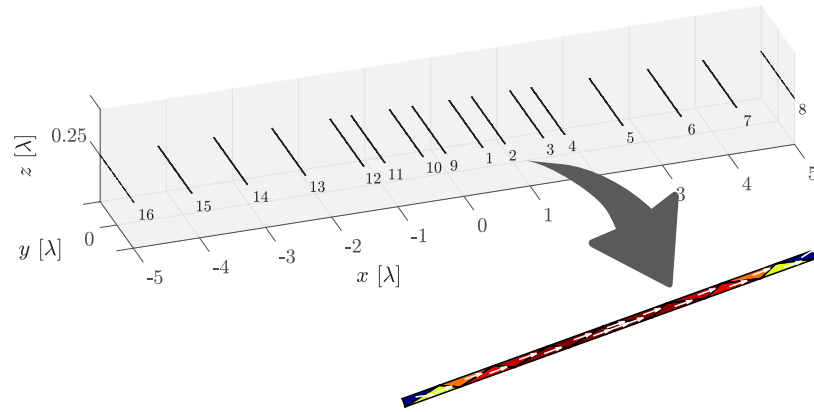
(a) Meshed geometry and detail of the current distribution on one element.
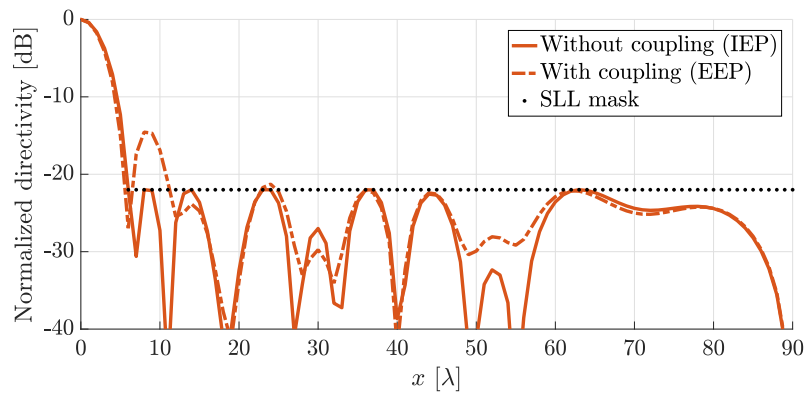
(b) Effect of MC on the array directivity for the IAC.
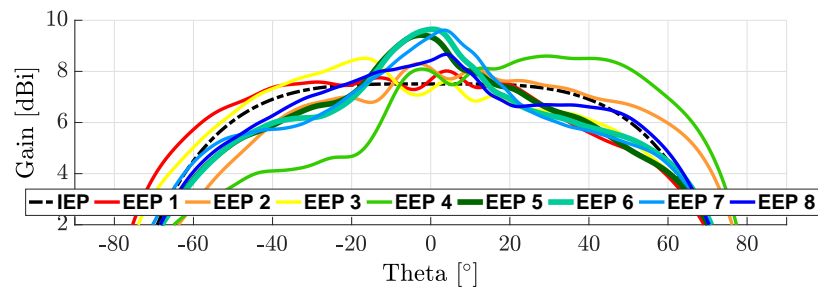
(c) Isolated and embedded element patterns (75Ω matched).

Figure 3.6: Initial array design (IAC) and effect of mutual coupling.
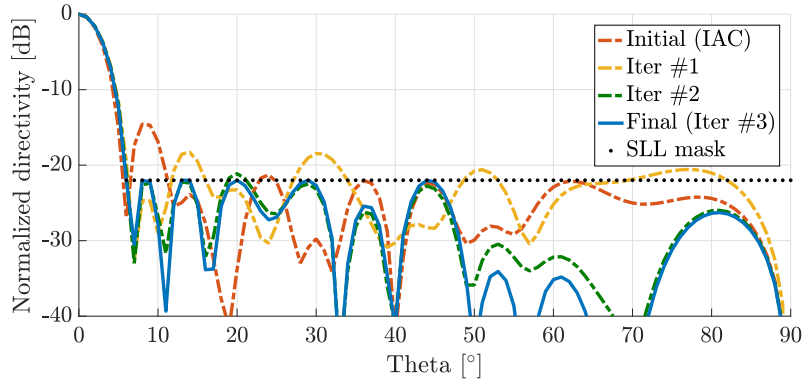
(a) Normalized array directivity in the presence of MC for subsequent iterations.
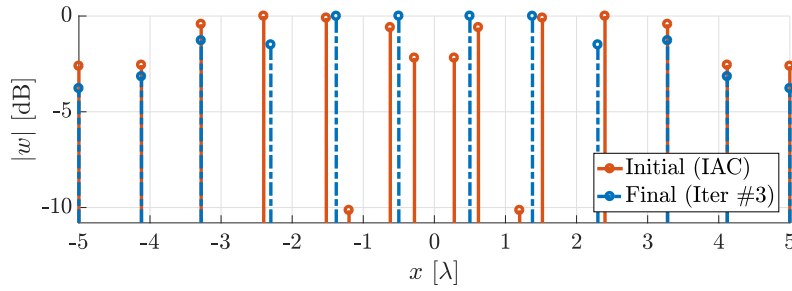
(b) Active elements positions and weight magnitudes of initial and final array.

Figure 3.7: Evolution of the array solution including MC.

Iteration	1	2	3	4	5	6	7	8
● Initial (IAC)	0.28	0.62	1.2	1.52	2.4	3.28	4.12	5
● Iter#1		0.5		1.38	2.4	3.28	4.12	5
● Iter#2		0.5		1.38	2.3	3.28	4.12	5
● Final (Iter#3)		0.5		1.38	2.3	3.28	4.12	5

Table 3.1: Element positions in wavelengths for each iteration

Chapter 4

Satellite Communications

One of the foreseen applications for the next generation array antennas are Satellite Communications (SATCOM) [38]. In such a scenario, the onboard antennas are designed to provide connectivity (Internet, TV and radio) to terminals located on the ground, see Fig. 4.1.

Current satellite systems typically deploy large reflectors with cluster feeds in a *one feed per beam* configuration. The increasing complexity due to multi-beam, multi-channel, dual-polarization and reconfigurability capabilities make such systems challenging in their design. A common view is that active arrays, also referred to as Direct Radiating Arrays (DRA:s), have the potential to handle such challenges and will have a leading role [39]. However, as of today, DRA:s are very expensive, mostly due to the high number of elements and associated electronic components. Aperiodic array can drastically reduce the associated costs and are thus a candidate technology for next generation array antennas. However, several design aspects need to be investigated first.

In this chapter we introduce the considered application scenario, the specification and challenges. Subsequently we will focus on a series of aspects that have been investigated, such as mutual coupling, multi-beam optimization, modular layout, multi-element array, reconfigurability, and isophoric layout. Conclusion will also be presented. This chapter is based on Paper B and, partially, on [iii], [ix], [x], [xi], [xii], and [xiii].

4.1   Application Scenario

An example of two dense DRA:s of patch excited antennas for Medium Earth Orbit (MEO) communication at S-band are shown in Fig. 4.2. Geostationary Earth Orbit (GEO) antennas at K-band have about the same physical dimensions but larger electrical dimensions. Densely filled arrays for such
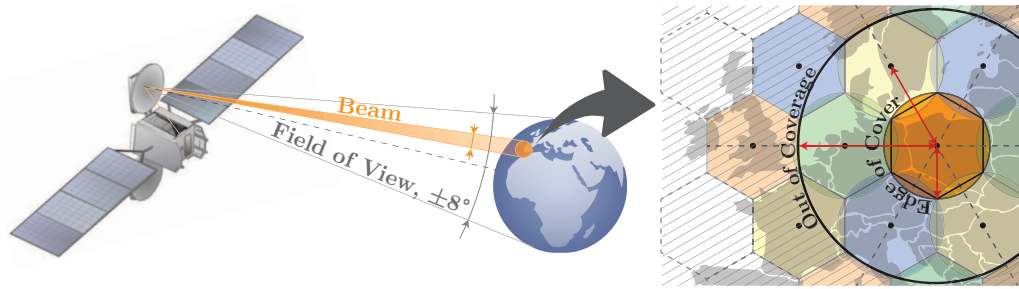
Figure 4.1: Illustration of a typical multi-spot GEO SATCOM scenario. The satellite illuminates Earth by means of beams (left). A hexagonal cell division with a 4-band reuse scheme (shown in color) is adopted (right).

applications are estimated to require a number of elements in the order of a thousand. Hence, there exists a strong interest in investigating new ways to design such arrays and to minimize the number of elements. For GEO satellites, the Earth is observable within an angular range of $\pm 8°$, often referred as Field of View (FoV), c.f. Fig. 4.1. Radiation outside this, i.e., towards open Space, is lost power. However this is of minor concern since it does not lead to interference or a significant noise. To increase the system communication capacity, multi-beam strategies are employed. In a multi-beam spot configuration, pencil beams of about $0.5°$ to $1°$ in beamwidth provide a cellular-like hexagonal grid coverage with a 4-band frequency reuse scheme to isolate adjacent beams. To obtain such narrow beams, massive aperture diameters of about 100λ are required.

The most challenging aspect of these systems is to synthesize narrow beams with stringent interference levels over the entire FoV, see Fig. 4.1. The Edge of Coverage (EoC) of a beam is defined as the largest angular distance belonging to a cell (and beam): for a hexagonal grid this corresponds to the

Table 4.1: Specifications for the considered SATCOM application

Array type	Planar, dual polarized at K-band
Antenna Element type	Corrugated pipe horn by RUAG
Field of View (FoV)	$\pm 8°$
Beam arrangement	Multi-spot, 4-band hexagonal grid
Interbeam distance	$1.06°$
Edge of Coverage (EoC) angle	$0.61°$
Out of Coverage (OoC) angle	$0.795°$
Max. SLL in the OoC region	-25 dB

Figure 4.2: Two dense DRA:s of patch-excited antennas for MEO communication at S-band. For GEO applications, an order of a thousands elements is expected.
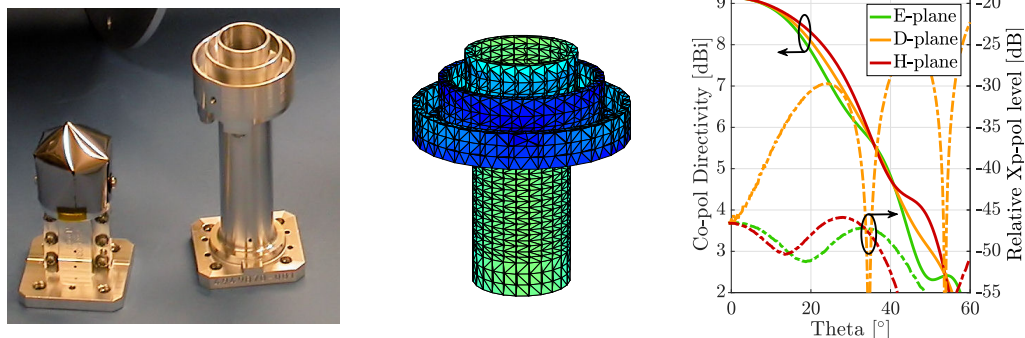
Figure 4.3: Corrugated pipe horn antenna element as designed by RUAG: manufactured (left), meshed MoM model and current distribution when excited by an internal monople (center), isolated element pattern (right).

inter-beam distance divided by $\sqrt{3}$. Within this angular range, a maximum roll-off gain at the EoC is generally required so as to guarantee appropriate connectivity over the entire cell. The Out of Coverage (OoC) is the angular distance where the first iso-frequency interfering beam appears: for a 4-band system this amounts to 1.5 inter-beams. To respect the iso-frequency interference limits, very stringent Side Lobe Levels (SLLs) are required from the OoC to the FoV angle. Accordingly, the required radiation profile of the beam, called radiation mask, describes a minimum gain from broadside to EoC and a maximum SLL from the OoC to the edge of the FoV.

The considered case study is a K-band GEO SATCOM application, c.f. Table 4.1. Accordingly, beams should be optimized for an OoC angle of $\pm 0.795°$ and a maximum SLL of -25 dB. The array element type has been provided by RUAG Space AB [40] and is shown in Fig. 4.3. The array element is a circular corrugated pipe horn with an aperture diameter of 1.5λ. Over the FoV this element has a virtually constant directivity of about 9 dBi and a relative cross-polarization level in the order of -35 dB in the diagonal plane, see Fig. 4.3 (right).

The very large array sizes and strict SLL specifications required in SATCOM applications make them very challenging in their design and therefore represents an interesting test case for the method presented in this thesis.

4.2 Modular Layout

Minimizing the number of elements is of key importance and is thus at the core of our approach. However, this may not always be the only aspect to

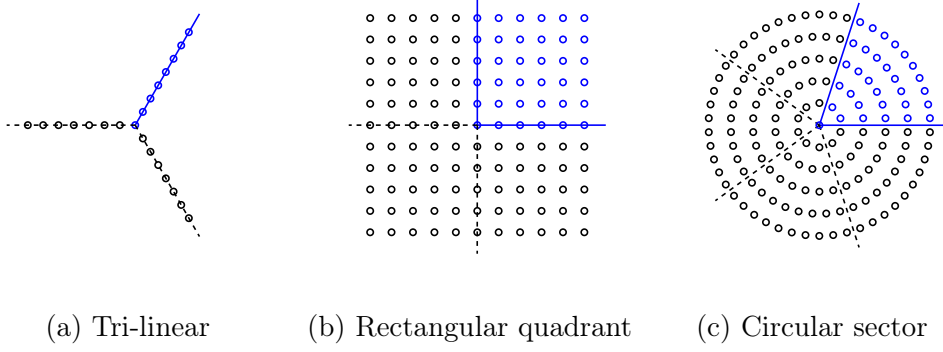(a) Tri-linear   (b) Rectangular quadrant   (c) Circular sector

Figure 4.4: Examples of array layout symmetries, base elements in blue.

consider when trying to reduce the array complexity – and thus the associated cost. Layout and excitation symmetries, especially in large and complex arrays such as DRA:s, can be very beneficial in reducing the manufacturing costs [41]. In fact, component reuse and modular designs enable simpler and more economical solutions. Additionally, one can substantially simplify other aspects including the beamforming network and the thermal design [42]. For these reasons it is of great interest for designers to have the ability to impose and evaluate different types of layouts in order to find the most appropriate one for the specific application at hand.

A geometry is said to be *symmetric* if it is invariant to some geometrical transformation, such as rotation, reflection or translation, as shown in Fig. 4.4 as an example. Probably the most simple example of a symmetric layout is a linear array of identical elements. In such array, the elements are positioned symmetrically with respect to the center and excited in a conjugate symmetric way. The principle of combining the base (positive-x) element and the symmetrical (negative-x) element can be applied to an arbitrary array layout and set of element patterns. For the case of a vectorial far-field pattern, Eq. (2.1) can be expanded as,

$$
\begin{aligned}
\boldsymbol{f}(\hat{\boldsymbol{r}}) = \ & \{w_{1,1}\boldsymbol{f}_{1,1}(\hat{\boldsymbol{r}}) + w_{1,2}\boldsymbol{f}_{1,2}(\hat{\boldsymbol{r}}) + ...\}+ \\
& \{w_{2,1}\boldsymbol{f}_{2,1}(\hat{\boldsymbol{r}}) + w_{2,2}\boldsymbol{f}_{2,2}(\hat{\boldsymbol{r}}) + ...\} + ... \\
= \ & w_1\{\tfrac{w_{1,1}}{w_1}\boldsymbol{f}_{1,1}(\hat{\boldsymbol{r}}) + \tfrac{w_{1,2}}{w_1}\boldsymbol{f}_{1,2}(\hat{\boldsymbol{r}}) + ...\}+ \\
& w_2\{\tfrac{w_{2,1}}{w_2}\boldsymbol{f}_{2,1}(\hat{\boldsymbol{r}}) + \tfrac{w_{2,2}}{w_2}\boldsymbol{f}_{2,2}(\hat{\boldsymbol{r}}) + ...\} + ... \\
= \ & w_1\boldsymbol{f}_1(\hat{\boldsymbol{r}}) + w_2\boldsymbol{f}_2(\hat{\boldsymbol{r}}) + ...
\end{aligned}
\tag{4.1}
$$

where $w_{n,s}$ and $\boldsymbol{f}_{n,s}$ are the excitation coefficient and far-field pattern of element n and symmetry region s, respectively, while w_n and $\boldsymbol{f}_n$ are the base excitation coefficient and equivalent far-field pattern obtained by summing the far-field pattern of the symmetric elements of n. That is, for the base
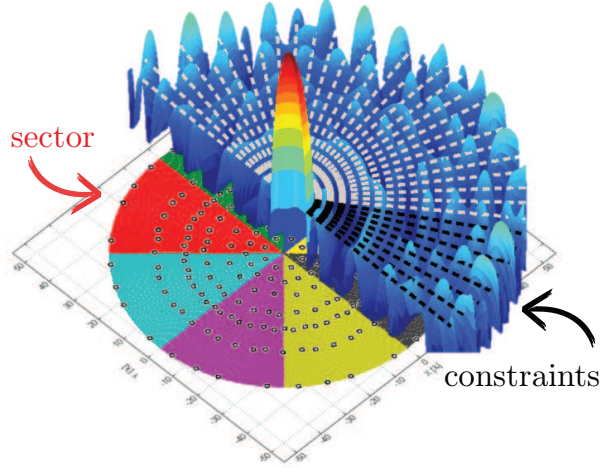
Figure 4.5: Array layout and far-field constraints for an 8-fold rotational symmetry. Only one sector of the aperture and of the pattern are considered.

element n with $N_{\text{sym}}(n)$ symmetrical elements and for a scanned beam p, the associated pattern can be written as

$$\boldsymbol{f}^p(\hat{\boldsymbol{r}}) = \sum_{n=1}^{N} w_n \boldsymbol{f}_n^p(\hat{\boldsymbol{r}}) \quad \text{with} \quad \boldsymbol{f}_n^p(\hat{\boldsymbol{r}}) = \sum_{s=1}^{N_{\text{sym}}(n)} \boldsymbol{f}_{n,s}(\hat{\boldsymbol{r}}) e^{-jk\Phi_{n,s}^p}. \qquad (4.2)$$

Additionally, since the base element n represents now a collection of $N_{\text{sym}}(n)$ elements, its weight should be corrected for in the MSA optimization. Accordingly, in the iterative ℓ_1-norm minimization, Eq. (3.5) becomes:

$$z_m^i = \frac{1}{\sum_{s=1}^{N_{\text{sym}}(m)} |w_m^{(i-1)}| + \epsilon} = \frac{1}{N_{\text{sym}}(m)|w_m^{(i-1)}| + \epsilon}. \qquad (4.3)$$

This general formulation can be applied to a very large number of symmetry types. Fig. 4.4 shows some examples including a linear, rectangular and circular sector. Additionally, composition of different symmetries and pre-imposed amplitude taper can also be modeled, although this has not been investigated in this thesis.

The effects of symmetries on the array design is applied to the SATCOM case-study. Since for such a scenario the specifications are for a rotationally symmetric beam (ϕ-invariant), the natural choice of the layout is rotationally symmetric as well. For such type of symmetry the circular layout is divided in N_{sym} (i.e., order of symmetry) identical sectors, as shown in Fig. 4.5 for an 8-fold symmetry. As discussed, only the base sector is considered during the sparsification phase, while the rest of the array is obtained by rotation. Additionally, since the symmetry is also found in the radiation pattern, only
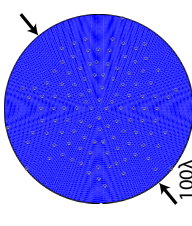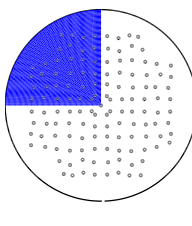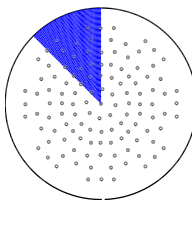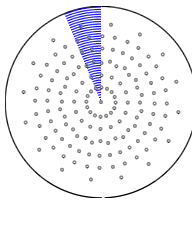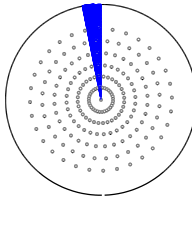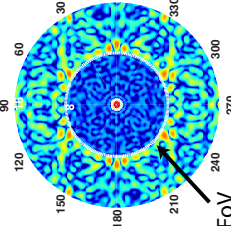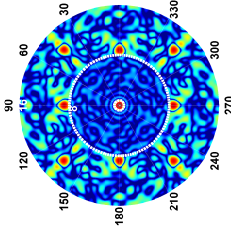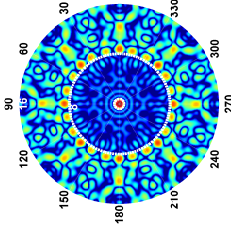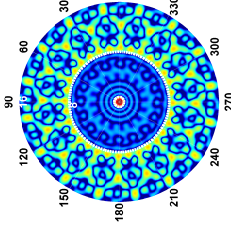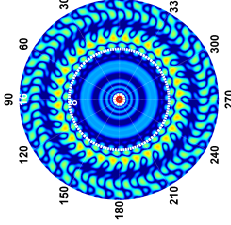
Symmetry order	none (reference)	4	8	16	32
Array layout					
Broadside beam pattern					
Element #	$N^{\{\mathrm{ref}\}} = 116$	$N^{\{\mathrm{ref}\}} + 17$ (15%)	$N^{\{\mathrm{ref}\}} + 5$ (4%)	$N^{\{\mathrm{ref}\}} + 29$ (25%)	$N^{\{\mathrm{ref}\}} + 80$ (69%)
Directivity	$D^{\{\mathrm{ref}\}} = 29.19\mathrm{dBi}$	$D^{\{\mathrm{ref}\}} + 0.3\mathrm{dB}$	$D^{\{\mathrm{ref}\}} + 0.1\mathrm{dB}$	$D^{\{\mathrm{ref}\}} + 0.4\mathrm{dB}$	$D^{\{\mathrm{ref}\}} + 0.9\mathrm{dB}$
Design time	$t^{\{\mathrm{ref}\}} = 48\mathrm{h}36\mathrm{m}$	$t^{\{\mathrm{ref}\}}/16$	$t^{\{\mathrm{ref}\}}/64$	$t^{\{\mathrm{ref}\}}/256$	$t^{\{\mathrm{ref}\}}/4096$

Table 4.2: Array layout for increasing rotational symmetry orders

one sector of the pattern needs to be considered. As a consequence, the synthesis problem size reduces like $1/N_{\text{sym}}$ both in terms of the problem unknowns as well as the number of constraints.

To study the effects of imposing symmetries, the array has been optimized for a 4-, 8-, 16- and 32-fold symmetry as well as without imposing any symmetry. Table 4.2 summarize the resulting layouts and far-field patterns, the number of elements, directivities and the total design times.

From the layout figures an increase in the regularity of the array and of the patterns is clearly visible. On the other hand, as the array modularity increases, so does the number of elements. The number of elements grows from 116 without symmetry to 193 for a 32-fold symmetry, an increase of about 2% per order of symmetry. The 8-fold case experiences a lower increase in the number of elements than expected (less than the 4-fold case). This is conjectured to be due to the approximated nature of the ℓ_1-norm minimization. Additionally, an increase in number of elements leads to an increased directivity, since the aperture filling and efficiency are higher for densely populated arrays. As discussed, the design time is also reduced proportional to $1/N_{\text{sym}}^2$ due to the reduction both in the solution and constraint spaces.

4.3 Multi-beam Optimization

In phase scanned arrays, multi-beam capabilities are obtained by phase control only, see Section 2.4. The array is designed for a specific beam shape, commonly a pencil beam, which can be re-directed (scanned) by changing the element excitation phases. Since the amplitudes are kept constant, only a time delay (or phase shifter) is needed at each element. Phased arrays can benefit significantly from cost reduction, beamforming network simplification, and a constant amplifier efficiency.

Phased arrays are typically designed for a single direction (broadside) and ideal scanning by phase shifting is assumed. Since the entire radiation pattern translates with the main beam, enlarged radiation masks are commonly used to prevent the appearance of side lobes, which before were outside the visible region. In practice however, there are a number of non-idealities that can lead to severe beam deformation when scanning [2]: i) phase scanning is a translation in the $u - v$ space, but this is not a linear relationship to the $\theta - \phi$ space, thus the main beam widens when scanned; ii) the element pattern, and in general the equivalent aperture, changes with the scan angle, thus the main beam loses directivity while the side lobes increase; iii) mutual coupling effects typically increase when scanning, since neighboring elements are more strongly excited, thus scanned beam can be degraded;
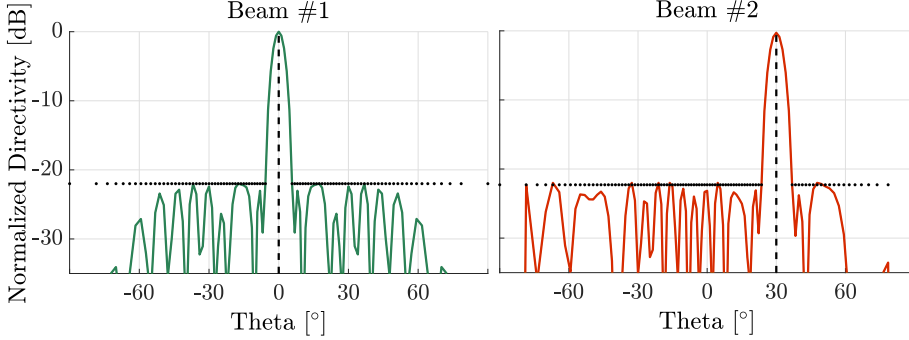
Figure 4.6: Illustration of multi-beam optimization: the array is simultaneously optimized for broadside (beam #1) and scanned (beam #2) directions.

iv) often phased shifter are used instead of time delays, this results in *beam squint*, i.e., scanned beams that deviate from the intended direction when changing frequency; and v) time delay or phase control is typically realized in a quantized way, resulting in phase discretization error and typically increasing the SLL. Additionally, the layout in aperiodic arrays is specifically designed to suppress radiation in unwanted directions, therefore scanning can pose additional difficulties. For these reasons it is desirable to include beam scanning effects in the design of phased arrays and cope with them in the best possible way.

The proposed method overcomes the limitations of conventional phase scanning approaches by optimizing the array for multi-beam applications. In phased arrays, the excitation coefficients and the expression for the pattern [Eq. (2.1)] can be defined in the general form

$$\boldsymbol{f}^p(\hat{\boldsymbol{r}}) = \sum_{n=1}^{N} w_n^p \boldsymbol{f}_n(\hat{\boldsymbol{r}}) \quad \text{with} \quad w_n^p = w_n e^{j\Phi_n^p}, \tag{4.4}$$

where Φ_n^p is the phase shift at element n for beam p.

For linear phase shift scanning in the direction of $\hat{\boldsymbol{r}}_p$, the corresponding phase shift term is $\Phi_n^p = -k\boldsymbol{r}_n \cdot \hat{\boldsymbol{r}}_p$. However, quantized phase shifters and non-linear frequency response can affect such values. To account for this, the phase shift can be modified to model such effects, e.g. by appropriate phase rounding for quantized phase shifters.

For P focused beam patterns scanning in the directions $\{\hat{\boldsymbol{r}}_p\}_{p=1}^P$ and prescribed radiation masks $\{M_\nu^p(\hat{\boldsymbol{r}})\}_{p=1}^P$ for the polarization component ν (see Fig. 4.6), the algorithm in (3.4) is modified to read

$$\operatorname*{argmin}_{\boldsymbol{w}^i \in \mathbb{C}^N} \|\boldsymbol{Z}^i \boldsymbol{w}^i\|_{\ell_1}, \text{ subject to } \begin{cases} f_{\text{co}}^p(\hat{\boldsymbol{r}}_{\text{p}}) = 1, & p = 1 \\ |f_\nu^p(\hat{\boldsymbol{r}})|^2 \le M_\nu^p(\hat{\boldsymbol{r}}), & p = 1, ..., P \end{cases}. \tag{4.5}$$

(a) Reference approach

(b) Proposed multi-beam approach: not accounting for phase shifter quantization

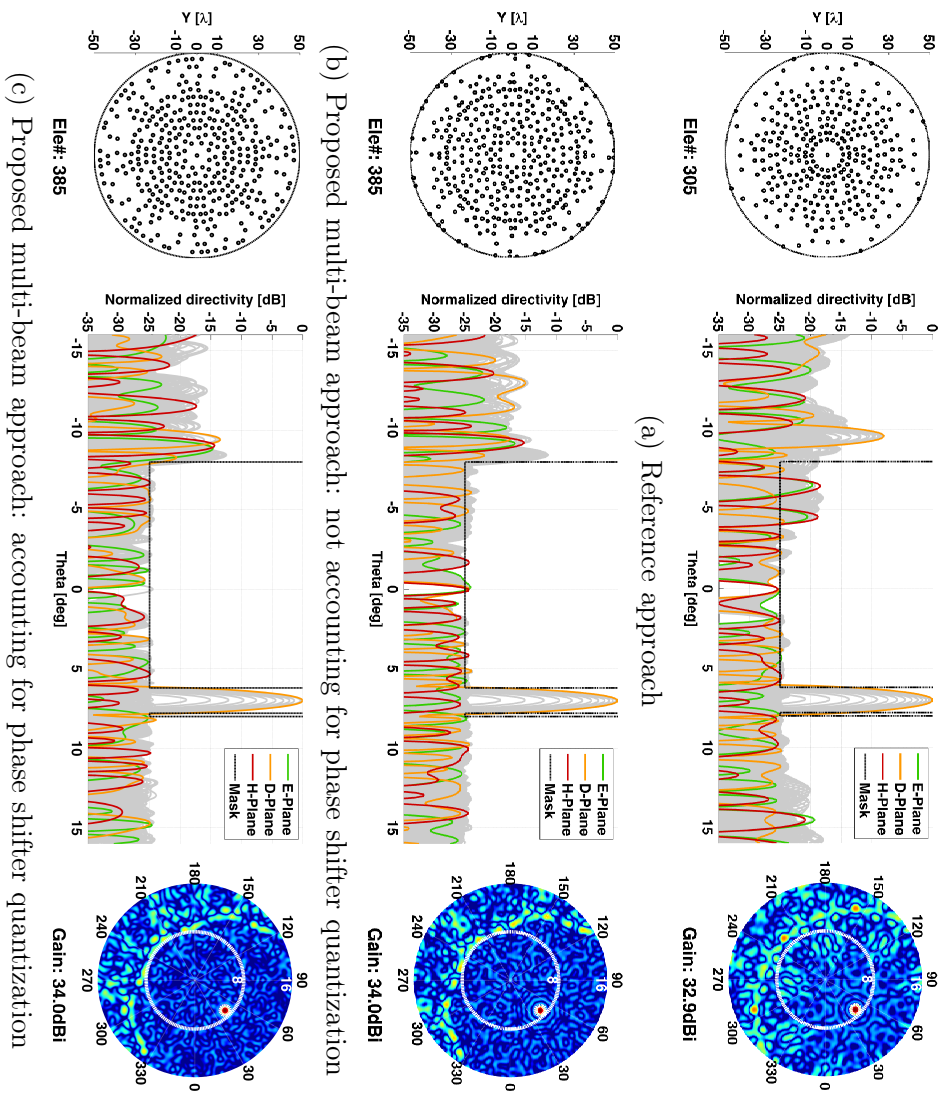(c) Proposed multi-beam approach: accounting for phase shifter quantization

Figure 4.7: Array layout and corresponding co-pol radiation pattern when scanning at $(\theta, \phi) = (8, 45)°$

The method optimizes the array layout and the complex excitations $\{w_n\}$ when an arbitrary number of scanned beams is considered simultaneously. This formulation allows to include any source causing beam degradation that can be modeled.

The proposed multi-beam optimization approach is demonstrated for the given SATCOM scenario, with an 8-fold symmetry and a 10° phase shifter quantization. The layout and farfield pattern for the worst-case scanning situation, i.e, when the scan angle corresponds to the edge of the FoV in the diagonal plane are shown in Fig. 4.7. The reference approach is the classical design methodology, where a SLL mask suppression region twice larger than the FoV (±16°) is chosen to guarantee the desired SLL when scanning within ±8°. The resulting array is unsuitable for scanning to such large angles, as the 18.2 dB peak side lobe level in Fig. 4.7(a) largely exceeds the required -25 dB level within the FoV. In Fig. 4.7(b), the proposed multi beam approach is applied without however including for the phase shifter quantization in the optimization phase. The array has maximum relative SLL increase of 2.3 dB. Finally, the multi beam approach is tested with the inclusion of the phase quantization, Fig. 4.7(c), with a SLL error or less then 0.7 dB.

This performance improvement is owing to the fact that the pattern mask constraints for both the broadside and the outermost scanned beams were imposed, albeit at the cost of an increased number of elements. We have found that this two-beam optimization procedure is adequate choice to achieve the desired accuracy and keep the optimization time to minimum (due to the increased number of constraints) relate to the single beam optimization case.

4.4 Mutual Coupling Effects

We consider the inclusion of mutual coupling effects for a SATCOM application scenario: the considered design is an 8-fold symmetric array optimized for full multi-beam applications, as discussed in Section 4.3 and 4.2. The resulting array is a large planar array of 385 horn type antennas, its CBFM-model is shown in Fig. 4.8(left). The minimum inter-element distance varies between 2λ to 6.7λ with dense element clusters as well as sparsely spaced elements, therefore MC effects as well as strong variations between the element patterns are expected. As shown in Fig. 4.8(right), the EEPs exhibit a strong oscillating behaviour around the IEP (bold lines). The co-polarization component shows a ripple of about ±2 dB and the cross-polarization about ±20 dB around the IEP.

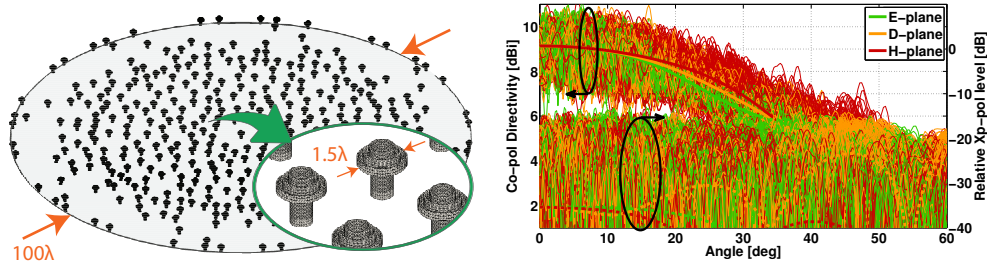The total array patterns in the D-plane are shown in Fig. 4.9. The

Figure 4.8: Array full-wave meshed model comprising 385 pipe horn antenna elements (left) and respective embedded element patters (right).
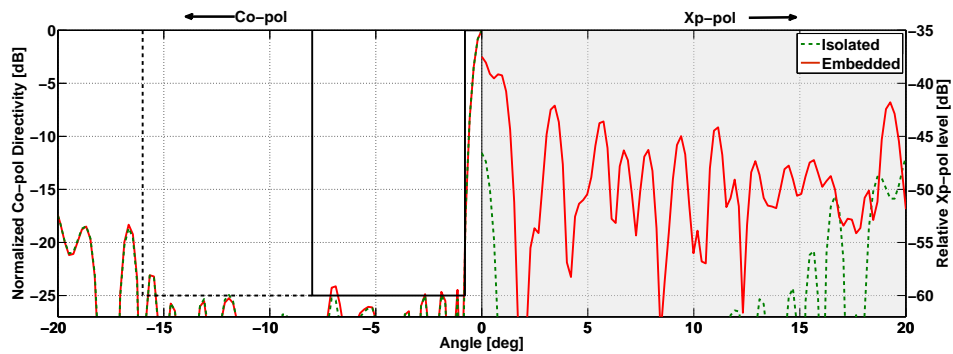
Figure 4.9: Far-field pattern without mutual coupling (isolated element pattern) and after full-wave analysis (embedded element patterns).

pattern computed from the initially assumed IEPs are compared to the MoM-simulated EEPs. The co-polarization component (left) has an increase in the SLL of about 1 dB both in the close proximity of the main beam as well as for far-off scanned beams. The cross-polarization pattern (right) is affected with an increase of about 10 dB in the broadside direction and around 30 dB over the rest of the FoV.

It is worth noticing that, despite the strong distortion of the EEPs, the effects on the total co-polar pattern are limited. As a result, the algorithm corrects for this distortion with just two additional iterations and without significantly modifying the array layout. On the other hand, the cross-polarization pattern modeled through the EM-analysis shows much higher levels than those predicted during the optimization procedure when ignoring MC effects, but are still acceptable for the chosen scenario. For applications that are more susceptible to cross-polarization variations or high cross-polarization levels it is recommended to include the cross-polar mask constraint levels in the optimization process.

Figure 4.10: Illustration of the UCAs of radii 1, 1.5 and 2λ (from light to dark blue) and the effect of their pattern on the array broadside (green) and scanned beam (red).
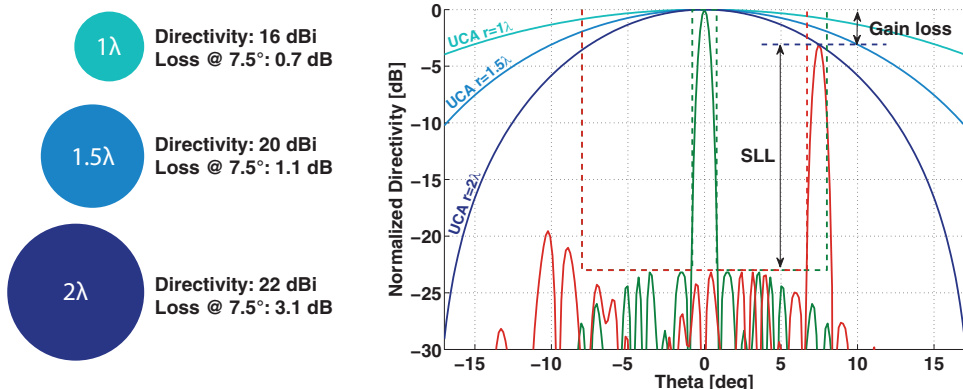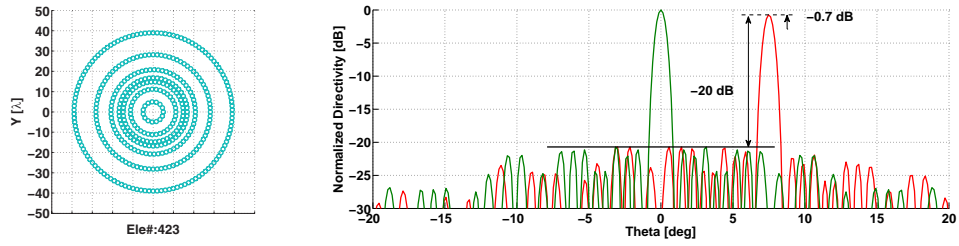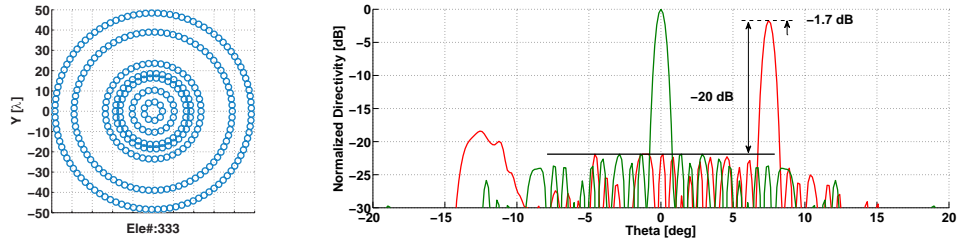
4.5 Multi-element Array

Using multiple element types can be an effective approach to reduce the number of elements, improve the aperture filling and decrease the excitation tapering. Moreover, as highlighted in Eq. 2.3, the element pattern defines the envelope of the array pattern and thus strongly affects the final performance. The ideal element pattern would be constant within the FoV, to minimize scan losses, and zero outside, to naturally suppress the radiation in undesired directions and thus minimizing the number of elements. Although it is possible to design an element with similar proprieties, this is always connected to an increased complexity and decreased directivity [43]. Moreover, there is always a tradeoff between the directivity and the scan loss. Instead, a combination of different elements can also help this.

Following the presented CS approach, including multiple elements at the same time can be simply achieved by sampling the array aperture multiple times, once for every considered antenna type [ix]. It is also possible to only sample certain specific regions for a given element type. In this way, one can enforce the layout to consist of rings with increasingly larger elements, for instance, thus controlling the distribution of the elements on the aperture.

We will consider the same SATCOM scenario as before. However we will assume here a circular array and a SLL mask of -20dB instead. The multiple elements that we are considering are Uniform Circular Apertures (UCA) of radii 1, 1.5 and 2λ. As summarized in Fig 4.10, larger UCAs have higher directivity and loss at the edge of coverage. Note that the SLL mask is defined with respect to the least directive beam, i.e. the far-off beam, pointing at $\theta_m = 7.5°$. Accordingly, as larger elements have higher gain

(a) Single element: only UCAs of radius 1λ.

(b) Single element: only UCAs of radius 1.5λ.
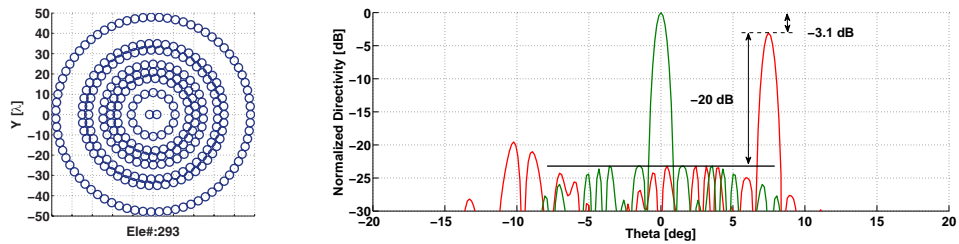
(c) Single element: only UCAs of radius 2λ.
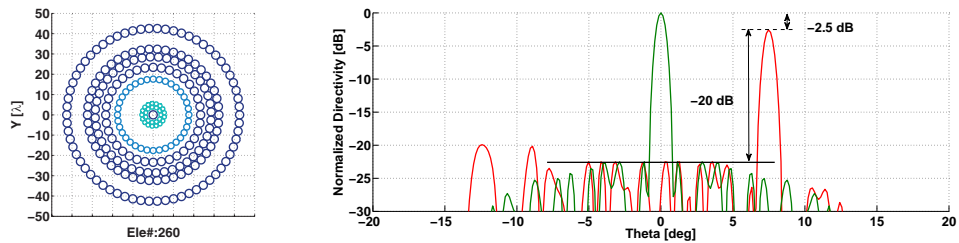
(d) Multi-element: mix of UCAs of radii 1, 1.5 and 2λ.

Figure 4.11: Array layout and radiation pattern for different UCAs.

loss when scanning, they also cause stricter relative SLL for the main beam. Four array designs are presented together with their layout and beams, as shown in Fig. 4.11. The first three arrays (Fig. 4.11a-c) all employ a single element type, a UCA, of progressively increasing size. As expected, the number of elements progressively decreases from 423 to 333 to 293 elements, however the loss connected to the far-off beam increases, from 0.7 to 1.7 to 3.1dB. Finally, the multi-element array, deploying all the the three previous elements, is shown in Fig. 4.11(d). The proposed array further reduces the
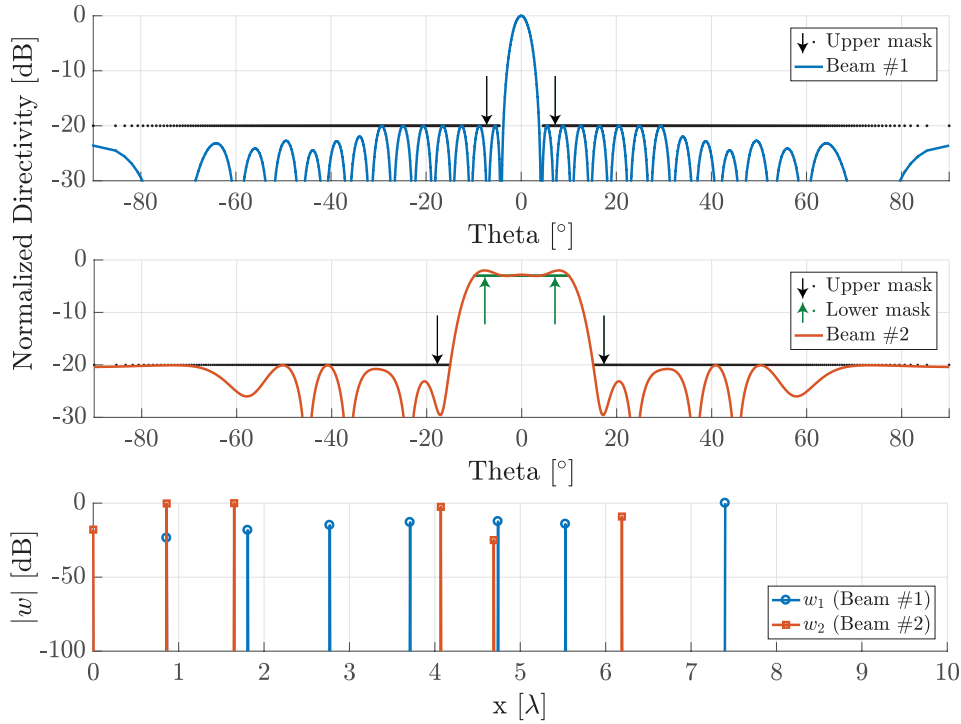
Figure 4.12: Farfield patterns and excitations of two separate arrays.

number of elements to 260 while improving the scan loss to 2.5dB.

4.6 Reconfigurable Array

It can be desirable to design an array capable of switching between different beamshapes, a so-called *reconfigurable* array. For example, in some SATCOM applications multiple services might be required, such as high data rate multi-spot coverage, as previously discussed, together with low rate broadcasting, or regional/linguistic coverage. Aperiodic arrays are typically designed for one beam only and their layout is connected to that beam. Unlike regular arrays which have strong adapting capabilities, aperiodic arrays may exhibit less flexibility due to the reduced number of elements. Thus the problem of designing aperiodic arrays capable of switching between a set of beams arises.

Let us consider the case of a circular ring array of maximum radius 10λ and two desired radiation patterns, a pencil beam and a flat top one, with a SLL of 20dB, as shown in Fig. 4.12. We could approach the problem by designing two separate arrays, one for each beam and then find a design that best approximates both. However, as shown, it is not clear what would

43
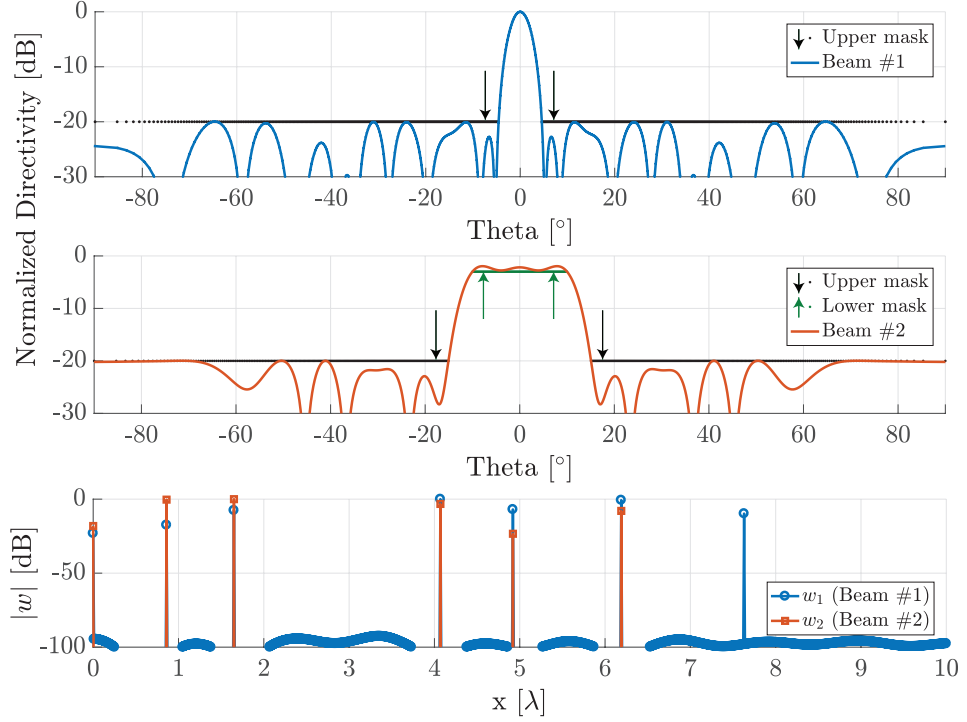
Figure 4.13: Farfield patterns and excitations of a reconfigurable array.

be the layout best accommodating both beams, which elements should be merged, which should be adjusted in position. Moreover, such approach would lead certainty to a suboptimal solution.

The proposed solution to extend the analysis to multibeam arrays is the introduction of multiple excitation coefficients and their respective radiation pattern constraint [xii]. Additionally, the formulation is modified to encourage a common element position for all beams while preserving the convexity of the problem. Let us consider $b = 1, \ldots, B$ shaped beams and their respective excitation coefficients $\mathbf{w}_b$, then the synthesis problem can be written as:

$$\underset{\mathbf{w}^i \in \mathbb{C}^N}{\operatorname{argmin}} \max \left\{ \|\mathbf{Z}_1^i \mathbf{w}_1^i\|_{\ell_1}, \|\mathbf{Z}_2^i \mathbf{w}_2^i\|_{\ell_1}, ..., \|\mathbf{Z}_B^i \mathbf{w}_B^i\|_{\ell_1} \right\} \qquad (4.6a)$$

$$\text{subject to} \begin{cases} f^b(\hat{\boldsymbol{r}}_0) = 1, & \text{normalize} & (4.6b) \\ |f^b(\hat{\boldsymbol{r}})|^2 \leq M^b(\hat{\boldsymbol{r}}), & \text{upper mask} & (4.6c) \\ 2\Re(f^b(\hat{\boldsymbol{r}})) \geq L^b(\hat{\boldsymbol{r}}), & \text{lower mask} & (4.6d) \\ |f^b(\hat{\boldsymbol{r}}) - F^b(\hat{\boldsymbol{r}})|^2 \leq \delta, & \text{ref. pattern} & (4.6e) \end{cases}$$

$$b = 1, \ldots, B$$

where constraint (4.6b) is the normalized broadside directivity, M^b in (4.6c) is the maximum radiation mask, L^b in (4.6d) is the minimum radiation mask (valid for symmetric conjugate arrays only) and F^b in (4.6e) is a reference pattern. Note that in the formulation, independent excitations in amplitude and phase are allowed for each beam. However, the objective of the minimization is to minimize the total number of elements. As a results the approach promotes element sharing, however there is no hard constraint that an antenna should be used by one, multiple or all elements either.

Considering the previous scenario (i.e. Fig. 4.12) we apply the proposed approach. As shown in Fig. 4.13, the new array exhibits a much more effective layout. A total of 7 distinct rings are synthesized, where all but the last are shared between both arrays.

4.7 Isophoric Array

As previously discussed, a large number of different excitation levels can lead to an increase in the complexity and thus the cost of the array. In fact, in practice, the solid state amplifiers connected to each antenna port operate at maximum efficiency when close to saturation, a critical condition when transmitting. To guarantee this for each of the antennas it is then required to design and manufacture an amplifier for each of the excitation levels. This can clearly imply a considerable burden for the design. Moreover, a non-uniform excitation always leads to a decrease in aperture efficiency, which might not be desired. In Section 4.2 this aspect has been partially addressed by exploiting symmetries. In this way the maximum number of distinct amplitude levels is limited by the number of elements in the base sector: thus higher symmetry order will lead to fewer excitation levels and different amplifiers. It might be desired to design an array with the minimum number of excitation levels, i.e., one single. This type of array is referred to as *isophoric*.

Unfortunately, despite the flexibility, the adopted CS approach does not allow for an straightforward extension to include of the isophoric constraint. We thus adopt a two step hybrid approach partially based on the current framework and partially relying on the density taper approach [xiii].

The first step involves the application of the usual CS synthesis approach, however this time continuous circular rings are synthesized instead. The scalar far-field pattern of an array of R continuous rings in the direction θ can be written as

$$f(\theta) = \sum_{r=1}^{R} w_r J_0(ka_r \sin\theta),$$ (4.7)

45

where w_r and a_r are the excitation coefficient and radius of ring r, respectively, and J_0 is the zeroth order Bessel function. Note how this is ϕ invariant, since each continuous ring is rotationally symmetric. As usual, the CS approach can then be applied to $\mathbf{w} = [w_1, w_2, \ldots, w_R]^T$ in order to obtain the set of locations and excitations for the MSA. Note that at this stage the array is idealized by continuous rings, each with a different excitation, thus not isophoric.

The second step is the conversion of the continuous rings in discrete isophoric ring array. It can be shown that the pattern from an array of rings of uniformly elements, can be written as:

$$F(\theta, \phi) = \sum_{r=1}^{R} W_r N_r \sum_{t=-\infty}^{\infty} J_{tN_r}(ka_r \sin\theta)e^{jtN_r(\pi/2-\phi)}, \qquad (4.8)$$

where N_r and W_r are the number of elements and the prescribed excitation level of ring r respectively. Let us focus for a moment only on the zeroth order term of Eq.(4.8). Then the two equations are approximately equivalent when the product of number of ring elements and excitation is chosen proportional to the original continuous ring amplitude, i.e. $W_r N_r \propto w_r$. Moreover, since we are interested in isophoric arrays, $\{W_r = 1\}_{r=1}^{R}$, this simplifies to $N_r \propto w_r$. Thus, given an arbitrary total number of elements N, the number of elements per ring can be obtained as [44]

$$N_r = \left\lfloor \left(N - \sum_{l=1}^{l<r} N_l \right) \frac{|w_r|}{\sum_{m=r}^{K} |w_m|} \right\rfloor, \quad r = 1...R \qquad (4.9)$$

where $\lfloor \bullet \rfloor$ indicates the floor function. One then needs to sweep the total number of elements and select the array layout with the appropriate number of elements. Note however that the higher order terms of Eq.(4.8) are negligible only if $\sin\theta \ll N_r/ka_r$, which in general demands a very large number of elements. In practice, this is not the case, especially for large angles and large rings, thus a certain amount of deviation from the desired pattern is expected.

The approach is demonstrated in the synthesis of an isophoric circular array with a SLL of -25dB for $\theta > 3.45°$. The choice of scenario is motivated by the availability of reference density taper solutions. In [45] and [44] a reference Taylor distribution with radius $R = 10\lambda$ is used. Instead we have been however capable of satisfying the same radiation mask with a reduced aperture radius of $R = 9.1\lambda$. In Fig. 4.14(left) the initial continuous ring array's far-field pattern and excitation amplitudes are shown as obtained by the CS approach. Fig. 4.14(right) shows the resulting peak side lobe (over every ϕ cut) versus the total number of elements, following (4.9). As
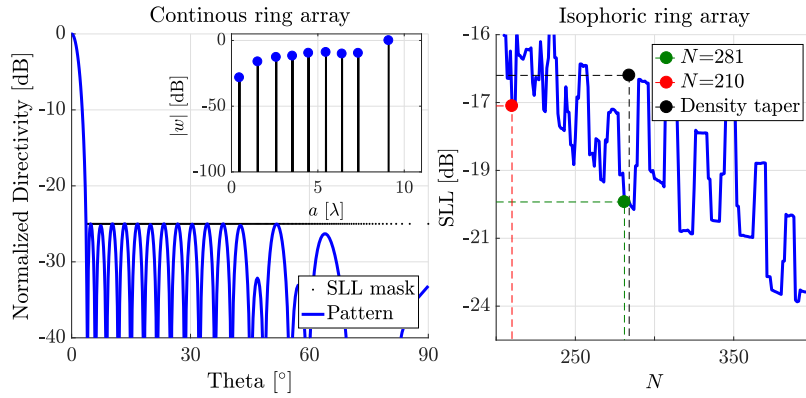
Figure 4.14: Continuous ring array pattern and layout (left) and relative SLL error of isophoric array as a function of number of elements (right).
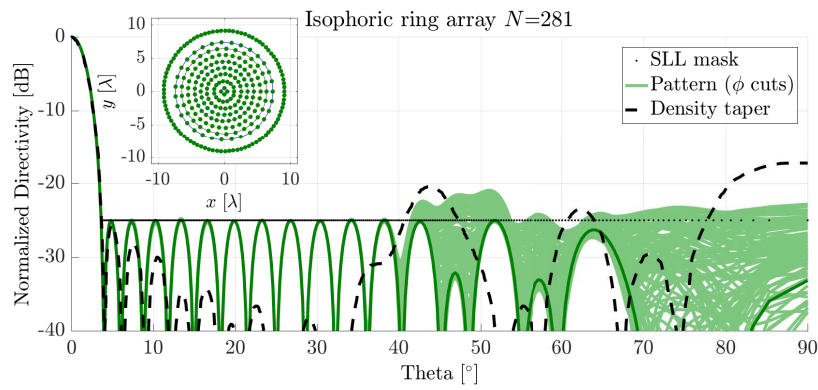

Figure 4.15: Radiation pattern and array layout (inset) for $N = 281$
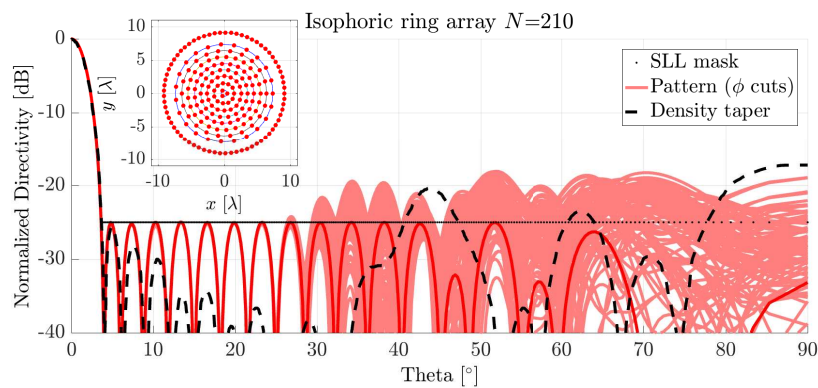
Figure 4.16: Radiation pattern and array layout (inset) for $N = 210$.

47

expected, the SLL decreases progressively with the number of elements. However a rather strong oscillatory behavior (caused by the higher order terms) is also present. From Fig. 4.14(right) two designs (green and red) are picked and compared to [45] (black). The green-line design, shown in Fig. 4.15, has approximately the same number of elements as that in [45] (281 and 286), but exhibits better performance in the peak side lobe (-21db against -17dB) as well as total radiated power above the target level. The red-line design, shown in Fig. 4.16, has a similar peak SLL (-18dB and -17dB) with a significantly reduced number of elements (210 against 286).

4.8   Summary and Conclusions

In this chapter we have investigated the design of aperiodic arrays for Satellite Communications (SATCOM) applications. First, we have introduced the specifications and why aperiodic array synthesis for SATCOM applications is a challenging task. We have then considered and studied the effects of a number of aspects, including: i) simplified modular design, ii) accurate multibeam optimization, iii) realistic mutual coupling effects, iv) multipurpose reconfigurable arrays, and v) power efficient isophoric array.

Aperiodic arrays are shown to be capable of severely reducing the number of elements, from more than one thousand to a few hundreds. The proposed method is shown to be capable of synthesizing massive arrays of complex antennas. Moreover, the flexibility of the Compressive Sensing (CS) approach has been shown to be very useful in including several different design aspects.

Chapter 5

Point-to-Point Backhaul

Microwave radio links are an efficient solution for connecting parts of the network, when a cabled installation is either impractical or too expensive. The expected increase in deployed base stations will heavily depend on such types of links [46]. Therefore, Point-to-Point (PtP) backhauling links will be a key component in modern network infrastructure.

To reach the required high-end performance, highly directional antennas with low interference are used [47]. These requirements are typically and effectively met with reflector antennas. However, antenna arrays offer low profiles and easier scanning capabilities, though meeting the strict interference levels is a challenging task. Moreover, at mm-wave frequencies, planar technologies such as microstrip antennas are popular suffer from high losses [48]. We propose an aperiodic slotted waveguide antenna array with improved side lobes and high efficiency. The antenna is realized by milling three layers of aluminum and bonding them together by vacuum brazing. Results show wide bandwidth, high aperture efficiency and patterns compliant with regulations in all planes.

In this chapter we present the design of an aperiodic isophoric array for PtP communication at Ka-band. First we introduce the application scenario and the requirements. Then we discuss the aperiodic array layout adopted for this application and the designed antenna and feeding network is presented. Finally, measured results are presented. This chapter is based on Paper C, where the design and manufacturing has mainly been followed by visiting researcher Dr. Shi Lei.

5.1 Application Scenario

Backhauling systems are used for high capacity, highly reliable and spectrally efficient links. This is achieved by using microwave frequencies and
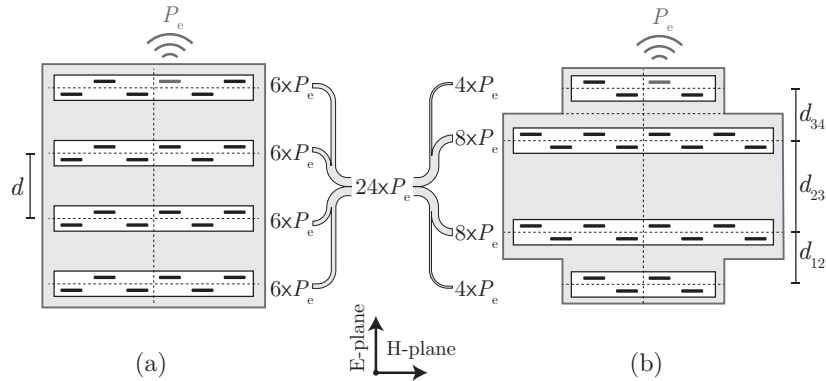
Figure 5.1: Illustration and comparison of (a) a regular and (b) an aperiodic isophoric waveguide array. Note that the aperiodic array has different spacing d_k and power P_k per waveguide, where P_e is the power per slot.

highly directive antennas with strict interference limits. Standardization organizations mandate the specifications that antennas must fulfill. The European Telecommunications Standards Institute (ETSI) identifies four classes of Radiation Pattern Envelops (RPE), depending on the interference risk in the network [49]. In the following we will focus on ETSI class II specifications.

At mm-wave frequencies, standard planar technologies are not suitable due to high losses. Instead, alternative architectures have been proposed, such as Substrate Integrated Waveguides (SIW) [50, 51] and gap waveguides [52]. We have adopted a classical standard metal hollow waveguide architecture [53–58]. To meet the RPE requirements, amplitude tapering is typically adopted [57, 59, 60], at the cost of reduced efficiency, see Section 2.2. Another common solution is tilting of the array, which however increases the cross polarization [48]. Tilting is possible since the RPE is defined only for the main plane, and a rotation will move the major side lobes to a diagonal plane.

We propose instead an aperiodic isophoric dense layout, capable of meeting the RPE in all planes while keeping high efficiency. To exploit a simpler slotted waveguide architecture we have opted for a column arranged layout, as illustrated in Fig. 5.1. A set of waveguides are positioned side-by-side with an aperiodic spacing and different number of slots. The aperiodicy is only along the E-plane, while every slotted waveguide has a regular layout and acts as a subarray. Note that the feed network must be designed to provide in-phase and appropriate power at each waveguide. This is done to compensate for the different spacing and number of slots per subarray.
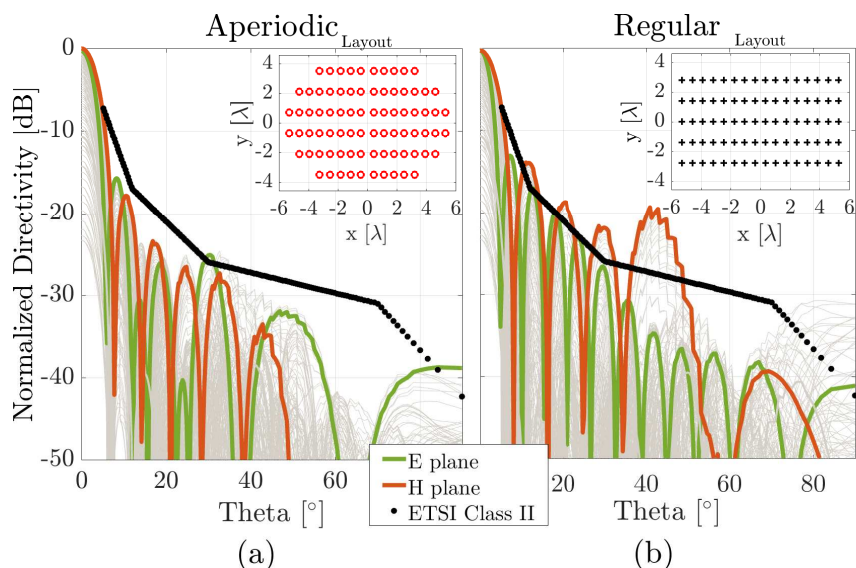
Figure 5.2: Far-field patterns and layout for (a) the aperiodic array and (b) a comparable regular array. Each antenna position represents a two slots. The spacings are $d_x = 0.45\lambda_0 \sim 0.72\lambda_0$ for the aperiodic and $d_x = 0.7\lambda_0$ for the regular, while for both $d_y = 0.5\lambda_0$.

5.2 Antenna Layout

The array layout has been optimized for the target specifications, while keeping practical design aspects in consideration. In order to obtain a high efficiency compact array we have used the synthesis procedure presented in Section 4.7. Since we aim at designing a column arranged layout, instead of the original circular one [xiii], we have adapted the procedure. The two step procedure requires: i) synthesis of an aperiodic tapered linear aperiodic array by CS for the target mask and adopted slot elements, ii) transformation to an aperiodic isophoric array by placing a subarray of equispaced slots in number proportional to the original element amplitude. Moreover, in order to simplify the design of the rest of the antenna, a number of practical constraints have been added. These include: E- and H-plane symmetry, 2^n number of columns, minimum inter-column spacing, maximum number of elements per column and an even number of slots per column. The target radiation mask is the ETSI class II RPE with a 2dB error margin and a scanning range of $\pm 15°$ in the azimuth plane.

The optimized layout and the radiation pattern for every ϕ-cut are shown in Fig. 5.2(a). The total number of slots is 160, organized in 16 columns. Three types of columns (Type I, II and III) are identified depending on the number of slots contained, 12, 8 and 4 respectively, see Fig. 5.3. An
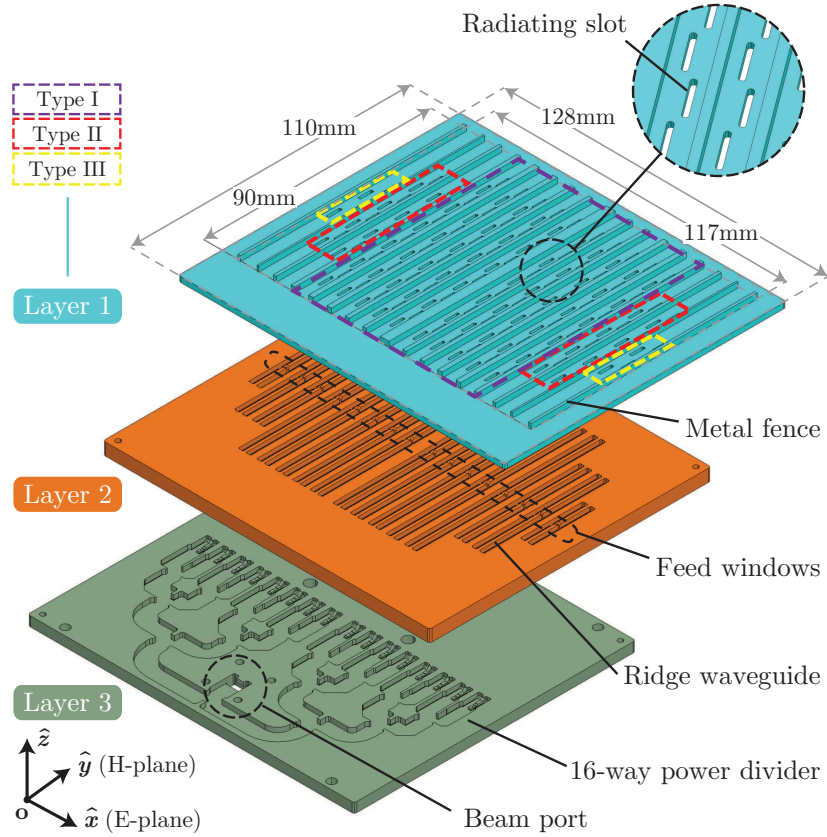
Figure 5.3: Exploded view of the proposed antenna: (i) Layer 1 (blue) is the radiation layer, with slots and metal fences; (ii) Layer 2 (orange) is the column feeding layer, with 16 ridged waveguides; (iii) Layer 3 (green) is the distribution layer, with the corporate feed network.

equivalent regular array with the same number of elements and aperture is shown for comparison in Fig. 5.2(b).

5.3   Antenna Design

Based on the aperiodic layout, the rest of the antenna, including the feeding network, has been designed. An exploded view of the complete antenna is shown in Fig. 5.3. The antenna is realized by milling three layers of aluminum and subsequently bonding them by vacuum brazing. The structure has a total outline of $128{\times}110\text{mm}^2$ and a thickness of 10.7mm. The top layer is the radiating plate and contains the slots organized in columns and separated by metal fences. The intermediate layer hosts the ridge waveguides, which are fed at the center by a feeding window, and used to excite the column subarray. The corporate feed network is realized betweeen the middle and
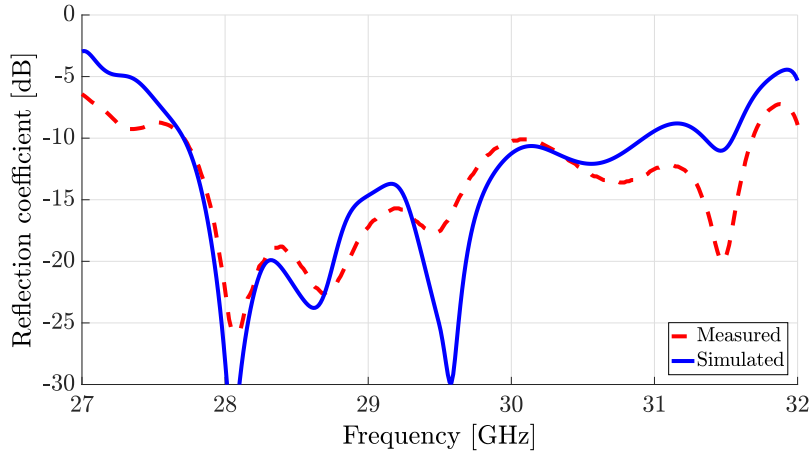
Figure 5.4: Simulated and measured reflection coefficients.

the bottom layer. The input port is a standard WR-28 waveguide port located at the bottom of the antenna.

Each column in the design is a slotted waveguide, which acts as a subarray. A ridge slotted waveguide has been used to broaden the bandwidth and reduce the column width to better accommodate the aperiodic spacing. The waveguide and slots dimensions have been designed according to [61] and then the three column types have been optimized for wideband matching. Each column is fed from the center by a dual ridged feed window embedded with a balanced power divider. Below this, a double ridge stepped transition is used to change to a rectangular waveguide, as used in the rest of the feed network.

The feed network distribute the signal from the input port to each of the column ports. A corporate feed network architecture is used to provide the appropriate power and phase distribution over a wide band. The power division ratio of each of the 15 power dividers is calculated according to the number of slots per waveguide, resulting in four type of power dividers [62]. Moreover, the feeding network layout is designed to provide in-phase excitation despite non-equal port positions. This is achieved by adjusting the power divider position such as to guarantee identical path lengths for all branches.

5.4 Results

The antenna has been manufactured and tested in an anechoic chamber. The simulated and measured reflection coefficients show good agreement, Fig. 5.4. The impedance bandwidth is about 12% (28.0GHz∼31.5GHz) for
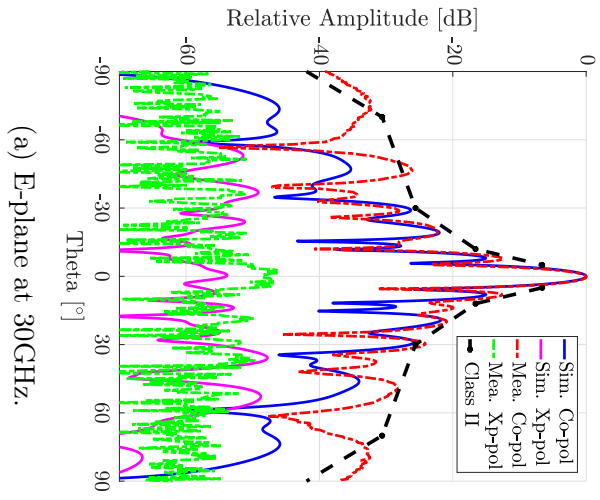
(a) E-plane at 30GHz.
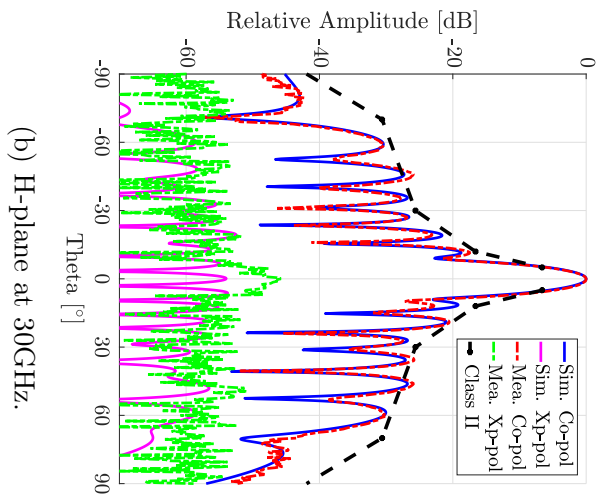
(b) H-plane at 30GHz.
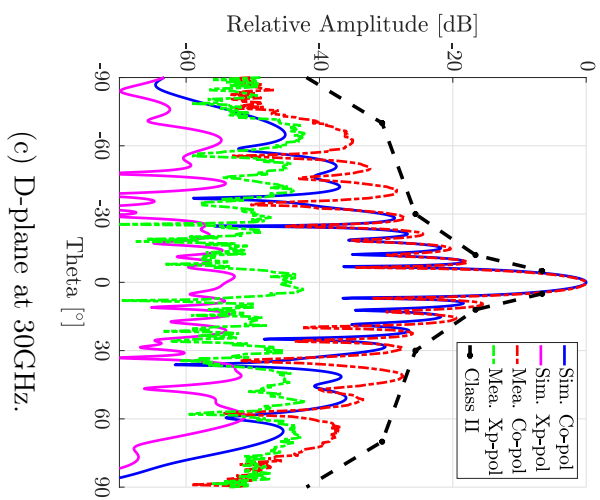
(c) D-plane at 30GHz.

Figure 5.5: Simulated and measured co- and cross-polar farfield radiation patterns and RPE.
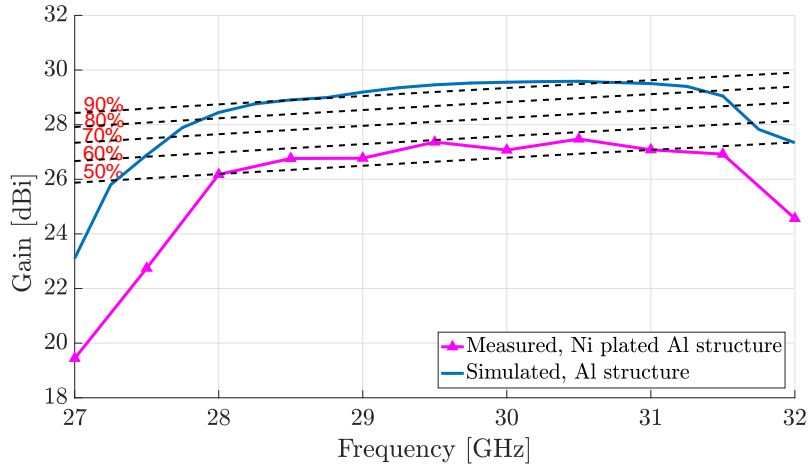
Figure 5.6: Simulated and measured gains and relative efficiency.

a return loss better then 10dB.

The farfield pattern in the three principal planes (E-, H- and D-plane) are shown in Fig. 5.5 at 30GHz. Measured and simulated results show good agreement and meet the ETSI Class II RPE in every plane cut. The measured cross-polar levels are better then -45dB over the frequency band.

The measured and simulated gain and efficiency are shown in Fig. 5.6. The simulated is better than 28.5dBi over the frequency range from 28.0GHz to 31.0GHz. The efficiency calculated with respect to the active aperture is better than 80% over the bandwidth and exceeds 90% at 30GHz. The measured gain is about 2.2dB lower than the simulated one, which is believed to be due to the ohmic losses introduced by the plating. While simulations are presented for a complete aluminum structure, the measured prototype had a nickel plating applied, which allows easier brazing with tin. Nickel has significant losses at Ka band, which has been confirmed in simulations. An entirely aluminum prototype is currently under manufacture. Measurement results will then be updated.

5.5 Summary and Conclusions

In this chapter we have presented a dense aperiodic array for PtP communication at Ka-band. First, we have introduced the application scenario and the key specifications. Then we have proposed an isophoric column-arranged aperiodic array with reduced side lobes and high efficiency. The manufactured slotted waveguide array antenna and the feeding network design is briefly discussed. Finally, simulated and measured results are presented.

The dense isophoric aperiodic array is capable of meeting ETSI class II

specifications in the entire space with high efficiency. In contrast with the previous chapter, the aperiodicity is used here to meet the RPE instead of minimizing the number of elements. The adopted column-arranged layout adapts to an easier implementation with the well-established slotted waveguide architecture. The corporate feed network is designed to provide appropriate power and phase distribution over a wide band, compensating for the different number of slots and positions of each column. The antenna is milled in three layers of aluminum, then bonded by vacuum brazing. Measurements show a 12% impedance bandwidth (28-31.5GHz). The simulated gain is better then 28.5dB and the efficiency is above 80% (>90% at 30GHz). Radiation patterns are compliant with ETSI class II requirements in all plane cuts.

Chapter 6

Line-of-Sight MIMO Backhaul

The fast-paced growth in mobile connectivity poses new challenges to the current wireless network infrastructures [63]. New technological solutions are needed both in the systems that provide coverage to the end user (Chapter 7), as well in their interconnections that support such demands (Chapter 5).

One of the proposed solutions for increasing the capacity of current backhauling systems is to adopt the Multiple-Input-Multiple-Output (MIMO) architecture [64], see Section 2.5. However, these systems are typically deployed in a Line-of-Sight (LoS) environment and thus must rely on near-field propagation to support multiplexing. Besides the relative short maximum distances, LoS-MIMO systems are characterized by poor installation flexibility [65]. Aperiodic arrays can substantially improve the minimum capacity for a wide range of distances and thus enable flexible and readily deployable units. Moreover, the aperiodic switched array is proposed as a simple extension to further improve the capacity. Due to the typically small number of antennas employed, an exhaustive search has been adopted in the synthesis. Instead of sophisticated synthesis methods, a simple exhaustive search has been adopted due to the small number of antennas employed.

In this chapter we introduce the underlying principle of LoS-MIMO backhauling, its specifications, and the limitations of current regular arrays. After providing an intuitive reason why regular arrays have such limitation, we show how aperiodic arrays can improve this. We then present results demonstrating the benefits of aperiodic arrays and the aperiodic switched concept. Finally, conclusions are given. This chapter is based on Paper D.

6.1 Application Scenario

As discussed in Section 2.5, the performance of MIMO systems typically depends on the surrounding scattering environment and their ability to create
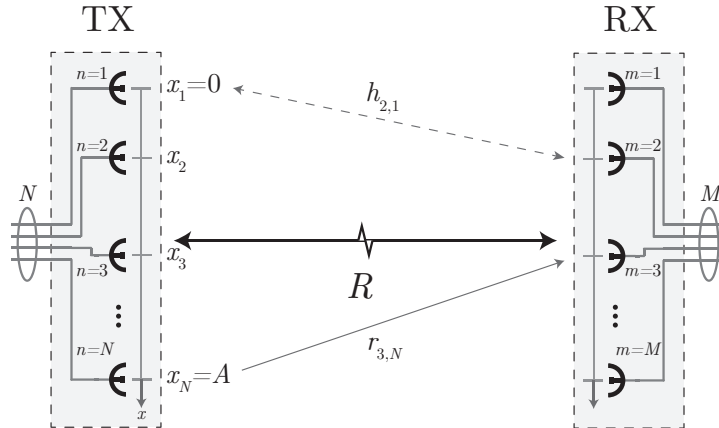
Figure 6.1: Illustration of a 4×4 line-of-sight MIMO link.

uncorrelated channels and enable multiplexing. In backhauling applications however, alternative mechanisms are needed, because what is typically experienced is LoS propagation instead, i.e., $K = \infty$ in Eq. (2.8). It is a known fact that in far-field LoS it is not possible to obtain MIMO capabilities excepts for dual polarization [66]. However, in the (non-reactive) near-field or Fresnel region, i.e. for $R < 2D^2/\lambda$, it is possible to obtain orthogonal channels. That is, for relatively small distances, the path length differences between each pair of transmit and receive antennas are not negligible and can be exploited to create independent channels. Therefore, to cover any practical distance, electrically massive apertures and thus large inter-element spacings are needed. This, in turn, requires very high frequencies to maintain practical antenna dimensions. In line with the current trend towards dense micro-cells, we will consider the scenario of a short-range urban backhauling. We thus consider a four element linear array operating at mm-wave frequencies with an aperture size of about one meter and a *hop length* (link distance) of few hundreds meters.

From Eq. (2.9), it can be shown that the maximum capacity is obtained when all the channel eigenvalues are equal [67]. This condition corresponds to the capacity of N identical SISO channels. For unbalanced eigenvalues the capacity decreases, the minimum of which being equivalent to that of one single SISO channel. To measure how far the actual channel is from this ideal state, the condition number $\kappa = \mu_{\max}/\mu_{\min}$ is often used. For $\kappa = 1$ the channels are perfectly balanced while for larger values the capacity decreases ($\kappa = 10$ being often considered the highest acceptable value). We will here instead present the actual capacity as this gives a better understanding of the actual data rate. To do so, we will assume a SNR of 30dB, in line with typical power levels in backhauling applications [68].
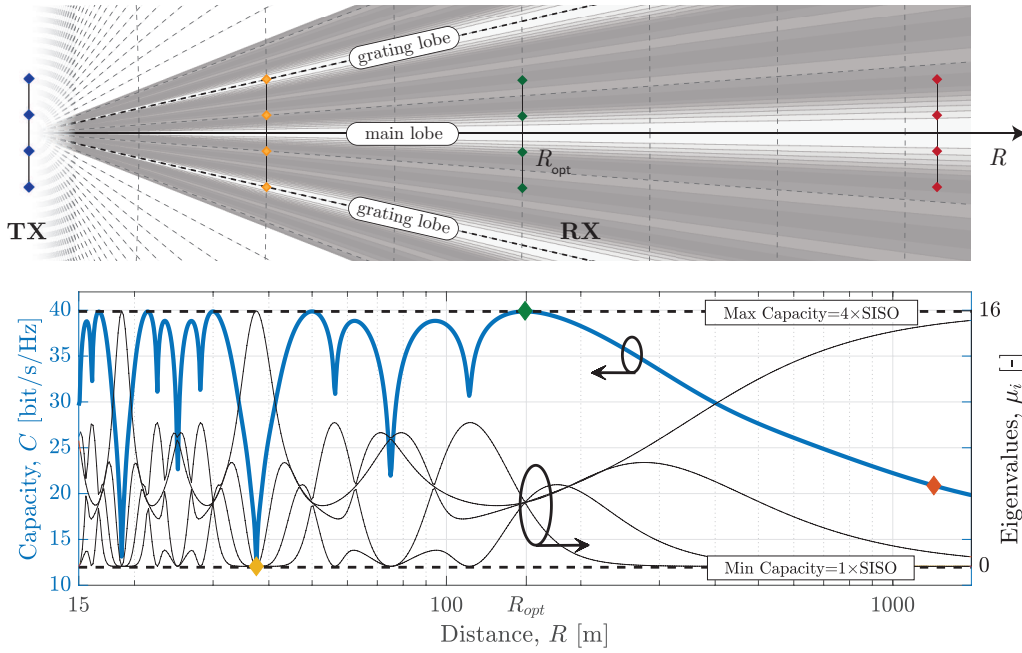
Figure 6.2: Effect of the distance between the terminals R on: (top) the geometry and (bottom) the capacity and eigenvalues, for a LoS-MIMO regular array.

6.2 Hop Length

Consider a link between two identical regular arrays. It can be shown analytically that the following relation holds for a LoS-MIMO link [69]

$$d = \sqrt{\frac{R_{\text{opt}}\lambda}{N}}, \tag{6.1}$$

where d is the inter-element spacing, R_{opt} is the optimal hop length, also known as Rayleight distance, and N is the number of elements per antenna. That is, the Rayleigh distance is the largest separation at which the antennas experience perfectly uncorrelated channels and thus maximum capacity. Note that the capacity in this case exceeds that in the scattering environment, since fading channels do not have identical eigenvalues. According to the above relation and the target application scenario, we have chosen to study a 4×4 system with a frequency of 80GHz and an inter element spacing of $d = 100\lambda$. This results in an aperture of $A = 1.125$m and an optimal link distance of $R_{\text{opt}} = 150$m. However we are interested in deploying the designed antenna in a range of distances $R \in [15, 200]$m, thus we need to consider what happens to the capacity when Eq. (6.1) is not satisfied.

The channel capacity and eigenvalues of a conventional regular array as a function of the hop distance are shown in Fig. 6.2(bottom). As desired, the

a) Regular   b) Aperiodic   c) Aperiodic switched
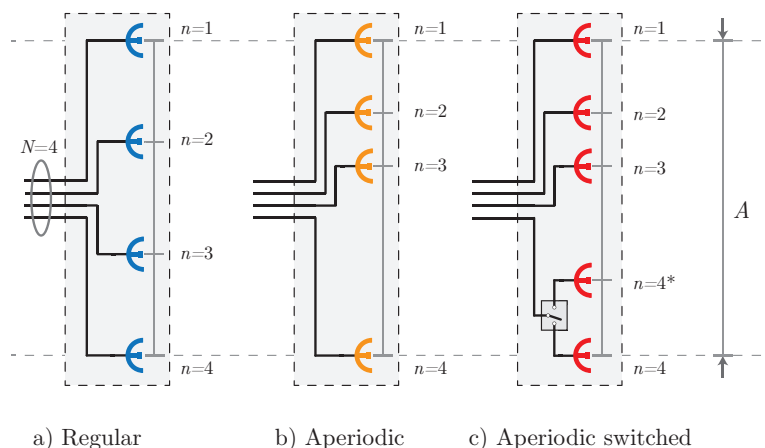
Figure 6.3: Illustration of the considered architectures.

link achieves the maximum capacity at the optimal distance R_{opt}, marked in green. Furthermore, as expected, as the distance R increases the channel converges to the farfield SISO case, shown in red. However, for $R < R_{\mathrm{opt}}$ an undesired oscillatory behavior with increasing frequency for smaller distances takes place. Some capacity dips reach as low as the SISO case, shown in yellow.

To explain this behavior, we can make use of a geometrical illustration of the link Fig. 6.2(top). It is worth noticing that the required extremely large inter-element spacings give rise to a large number of grating lobes, two of which are shown in lighter color. The Rayleigh distance (marked in green) is the smallest distance before the grating lobes interfere with the main beam. For a large distance (marked in red) the entire array is illuminated by a single beam and thus only SISO communication is possible. For shorter distances, capacity dips (shown in yellow) occur when the grating lobes suddenly illuminate the other antennas, thus creating coherent channels.

In practice, a limited capacity loss can be tolerated, which in turn reduces the usable distance intervals. Moreover, the uncontrolled deployment scenario, the position errors and a wide band make such an array issuable only for distances in the proximity of the optimal. Offering several specialized antennas, or mechanically tunable ones, would incur in considerable design, manufacturing and installation costs. It would thus be desirable to design a single flexible antenna readily deployable for a wide range of distances.

6.3   Results

Aperiodic arrays are ideal candidates for LoS systems, since the limited installation flexibility of regular arrays is related to the presence of grating
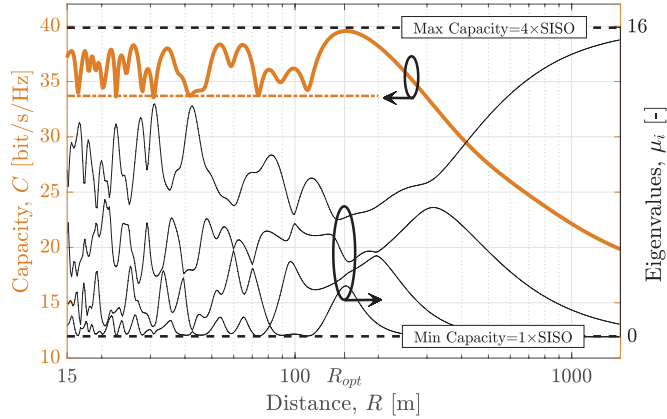
Figure 6.4: Capacity for aperiodic LoS MIMO array.
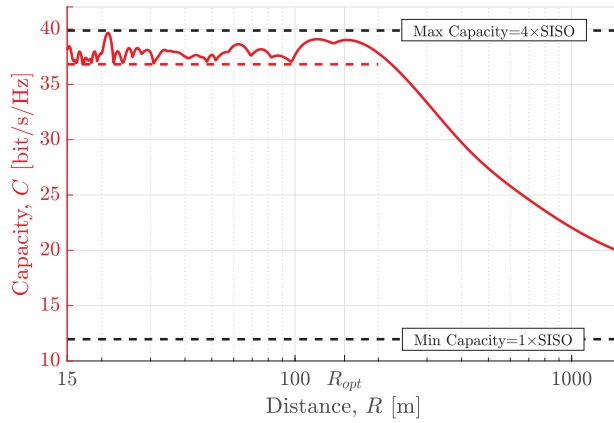
Figure 6.5: Capacity for aperiodic switched LoS-MIMO array.

lobes. Unlike regular arrays, aperiodic arrays manifest pseudo-grating lobes (see Section 3.2.1) and are thus immune to coherent signal interference. The array architectures considered in the following are cross-compared in Fig. 6.3.

LoS-MIMO systems typically employ a small number of antennas and thus an exhaustive search can still be a feasible synthesis approach. Keeping the aperture size constant, and thus with fixed positions for the two external elements, the two internal element positions have been swept to find the array with the highest minimum capacity over the range of interest, Fig. 6.3(b). In all cases, the receiving and transmitting antennas have the same layout, in order to allow the use of the same unit for both sides of the link. In Fig. 6.4 the capacity and the eigenvalues of the optimal aperiodic array are shown. As observed, the aperiodic array is very effective at removing the dips in the capacity which were experienced by the regular array. The minimum capacity is 33.7bit/s/Hz, or 84% of the maximum theoretical capacity. For

61

the conventional regular array, this is instead just 12bit/s/Hz or 30%.

An aperiodic switched design is also proposed to further increase the capacity with minimal additional complexity. As shown in Fig. 6.3(c), the array is equipped with a single switch and one auxiliary antenna so that one of the elements can be switched between two positions. The system is then capable of switching between three configurations (given by the combination of the trasmit and receive configuration) depending on which one provides the highest capacity for a given distance. The aperiodic switched array layout is optimized such that a combination of the three switched configurations has the highest minimum capacity over the range of interest. The resulting capacity is shown in Fig. 6.5. The minimum capacity is increased to 36.8bit/s/Hz, or 92% of the maximum theoretical capacity that the system can possibly achieve.

6.4   Summary and Conclusions

In this chapter we have discussed aperiodic arrays for Line-of-Sight (LoS) Multiple-Input-Multiple-Output (MIMO) backhauling. We have shown the poor flexibility of conventional regular array when it comes to distance between the terminals. Aperiodic arrays and aperiodic switched arrays have then been presented as a simple and effective solution to overcome this limitation. The synthesis is based upon a simple exhaustive search of all possible configurations due to the small number of elements involved.

Aperiodic arrays for LoS-MIMO systems are shown to be very effective in improving the minimum capacity over a wide range of distances between the terminals. For example, a 4×4 aperiodic linear array can guarantee a capacity better then 84% of the theoretical maximum. That represents a significant improvement over a conventional regular array's 30%. Moreover, by the addition of only a single switch and an auxiliary antenna it is possible to further increase the capacity. The aperiodic switched array is shown to provide capacity exceeding 92% of the theoretical maximum.

Chapter 7

Multi-User MIMO User Coverage

The predicted growth of the demand for mobile connectivity is calling for new multi-antenna concepts [70]. Some of the envisioned technologies are massive, Multi-User (MU) Multiple-Input-Multiple-Output (MIMO) systems at mm-wave frequencies [71]. Multiplexing typically requires the allocation of part of the system resources (time, frequency or code) to each of the users, thereby dividing the maximum capacity between the users [4, Chapter 14]. MU-MIMO instead supports Spatial Division Multiple Access (SDMA) which can distinguish the users based on their spatial signatures. The system can then transmit and receive with full resources to each user at the same time, thus considerably increasing the total capacity.

Contrary to prevailing understanding, the array layout affects the performance of MU-MIMO systems [72][xiv]. In particular, aperiodic arrays can be superior to their regular counterparts in terms of link quality, data rate and power efficiency, especially in large and crowded cells. To exploit this, we propose a novel statistical/density taper-based synthesis approach and discuss the results for different system sizes.

In this chapter we first introduce the application scenario and the most relevant figures of merit. We then discuss and explain intuitively why aperiodic arrays can be superior to regular ones. Subsequently we present a novel hybrid approach tailored for this application. Finally, results for different systems sizes and conclusion are presented. This chapter is based on Paper E and [xiv].

7.1   Application Scenario

Let us consider a $M \times K$ single cell narrowband Multi User (MU) Multiple-Input Multiple-Output (MIMO) system, as shown in Fig. 7.1. The Base Station (BS) is equipped with M antennas and serves a 120° sector where
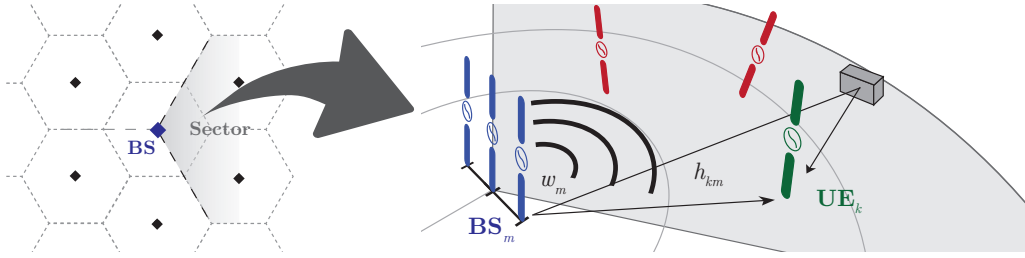
Figure 7.1: Illustration of a $M \times K$ MU-MIMO cell.

K single-antenna User Equipments (UEs) are arbitrarily located. We can distinguish two different regimes: in *uplink* the UEs transmit to the BS, while in *downlink* the BS transmits to the UEs; in both cases all users are served at the same time. Since the UEs operate individually and are equipped with a single antenna, the coding is performed on the BS side only, for both link directions. Although similar conclusions apply, we focus on the uplink scenario. For downlink please refer to Paper E.

The received signal $\mathbf{y} \in \mathbb{C}^{M \times 1}$ at the M BS antennas follows Eq. (2.7), here SNR is the *average* signal-to-noise-ratio [73]. For the channel model $\mathbf{H}$, we will here discuss only the Line-of-Sight (LoS) case, the most favorable for aperiodic array. Results for scattering environments are included in Paper E. The BS antennas are modeled as Huygens sources and the UEs are assumed randomly located and uniformly distributed in the sector [74]. Each UE is thus associated with a plane wave with a uniform random distribution in angle of arrival, amplitude, phase and polarization. This model is also referred to as Random Line-of-Sight. To obtain meaningful statistics from all the random variations, a large number of realizations are simulated.

To recover the original transmitted signal $\mathbf{x}$, the BS performs decoding on the received signal. We assume perfect channel state information at the BS, i.e., exact knowledge of $\mathbf{H}$. For linear de-coding, the reconstructed signals can be expressed as $\tilde{\mathbf{y}} = \mathbf{W}\mathbf{y}$, where $\mathbf{W}$ is the decoding matrix. Since in this scenario the interference between users is expected to be the limiting factor, we choose a beamforming algorithm that suppresses this. Zero Forcing (ZF) coding, i.e. $\mathbf{W} = (\mathbf{H}^H \mathbf{H})^{-1} \mathbf{H}^H$, accomplishes this.

The Signal-to-Interference-plus-Noise Ratio (SINR) for the kth UE is

$$\mathrm{SINR}_k \stackrel{\mathrm{ZF}}{=} \frac{\mathrm{SNR}}{(\mathbf{H}^H \mathbf{H})^{-1}_{k,k}}, \tag{7.1}$$

for ZF de-coding. The SINR is linearly dependent on the SNR and it is thus sufficient to show the results for one value of SNR (i.e. SNR=0dB) [75]. Moreover, for fixed $\mathbf{H}$, any improvement in the SINR translates directly to the SNR and vice versa.

Finally, the ergodic Sum Rate (SR) capacity, in a similar manner as in Eq.(2.9), can be written as [73]

$$\text{SR} = \sum_{k=1}^{K} \text{E}[\log_2 (1 + \text{SINR}_k)], \qquad (7.2)$$

which is the expected or average capacity over all possible random variations. To describe the statistics in more detail, we use instead the SINR Cumulative Distribution Function (CDF). In this regards, an important measure is the SINR evaluated at the 5% CDF level, $\text{SINR}|_{5\%}$. According to the above, this gives directly the required SNR, and thus the required transmitted power in order to provide a minimum target SINR to 95% of the users.

Another important aspect in MIMO systems is the effect of coding on the amplifiers' efficiency. The coding matrix **W** is changed adaptively depending on the channel **H**, thus it has a statical distribution itself. In practice, however, each antenna is connected to an amplifier which has a maximum output power and typically operates at maximum efficiency when saturated [76]. This is especially important when transmitting, i.e., in downlink, since power amplifiers are one of the most power demanding components. It is thus desirable to have all power amplifiers always operating at a fixed uniform power level, although the adaptivity of MIMO operates in the opposite direction. Consider the vector average power and variance for each antenna

$$\boldsymbol{\mu} = \text{E}[|\sum_{k=1}^{K} \mathbf{W}_{:,k}|^2]; \qquad \boldsymbol{\sigma}^2 = \text{Var}[|\sum_{k=1}^{K} \mathbf{W}_{:,k}|^2], \qquad (7.3)$$

where the fist should be uniform, and the second minimum. Moreover, to capture the overall array power range in a compact way, we define the power spread as

$$\text{PS} = \max(\boldsymbol{\mu} + \boldsymbol{\sigma}^2)/\min(\boldsymbol{\mu} - \boldsymbol{\sigma}^2), \qquad (7.4)$$

where 0dB represents the ideal constant and uniform power feeding. Larger values indicate instead an undesired tapering and/or variance.

7.2 Aperiodicity Effect

To demonstrate and explain the effect of an aperiodic layout on the system performance, we consider an 8×2 system [xiv], as illustrated in Fig. 7.2. We compare an aperiodic array to the reference regular array with the same aperture, as shown in Fig. 7.3(inset).
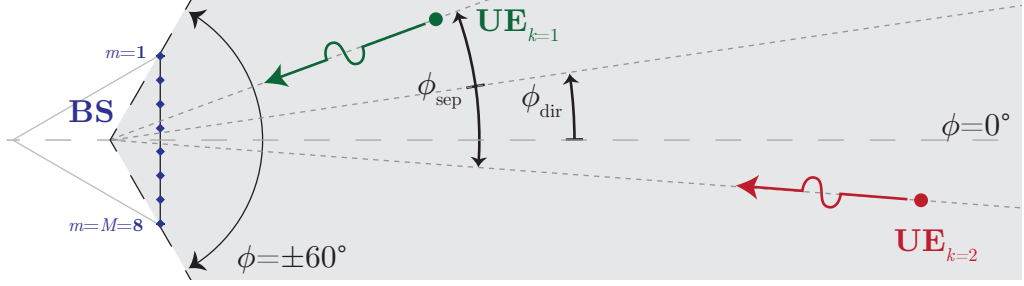
Figure 7.2: Illustration of a 8×2 MU-MIMO cell.
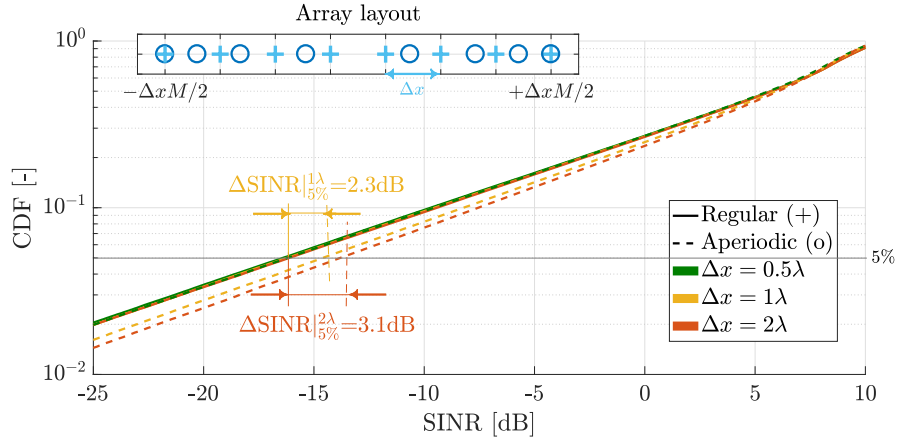
Figure 7.3: SINR CDFs for a 8×2 system with average element spacing of $\Delta x = 0.5, 1, 2\lambda$.

First, we consider the SINR CDF curves for both arrays with average element spacings of $\Delta x = 0.5, 1$ and 2λ, as shown in Fig. 7.3. Note that the rightmost curves are superior since higher powers are more probable. Clearly, the regular array (solid lines) is not affected by the spacing, whereas the aperiodic array is. Defining the aperiodic array SINR gain at 5% as

$$\text{SINRG} = \text{SINR}|_{5\%}^{\text{aperiodic}} / \text{SINR}|_{5\%}^{\text{regular}}, \qquad (7.5)$$

in the above cases we have a SINRG of 0.2, 2.3 and 3.1 dB respectively for different element spacings.

To better explain the origin of the aperiodic array gain, we focus on the $\Delta x = 1\lambda$ case and investigate the effect of the angle of arrival ϕ. In Fig. 7.4(left) we consider the SINRG for a variable angle of coverage: the two UEs are randomly located within a sector centered on ϕ_{dir} and ϕ_{sep} wide, cf. Fig. 7.2. The aperiodic array is always superior but from around $\phi_{\text{sep}} = 60°$ the SINRG rapidly increases to 2.3dB, which corresponds to the full-coverage . In Fig. 7.4(right), fixed scanning positions are instead investigated: UEs are now located only on the edges of the sector described

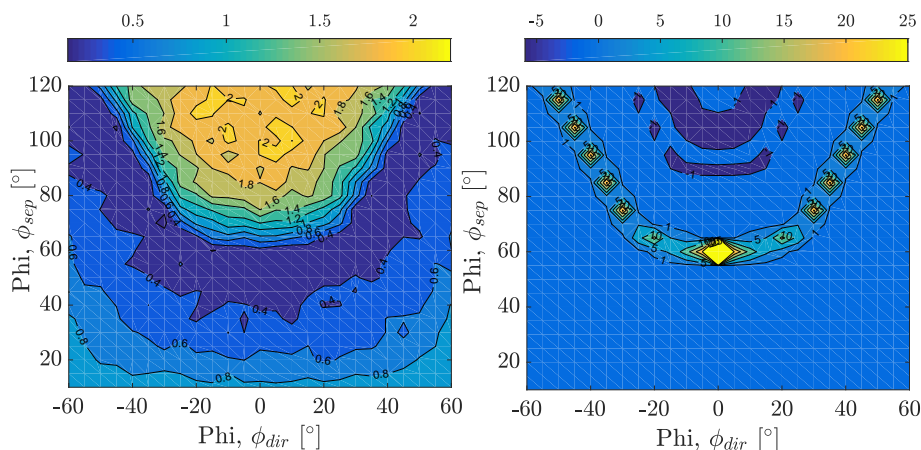Figure 7.4: SINRG in dB of the aperiodic array for a sector centered on ϕ_{dir} and ϕ_{sep} wide. In the left figure UEs are randomly located within the sector and in the right figure on the edge of coverage only.

before. Here the effect of grating lobes, and the immunity of the aperiodic array, are clearly visible with spot-like and high gain points. Also note how the transition to high SINRG and the grating lobes region coincide in the two figures.

The observations above support the idea that indeed the aperiodic array is superior to the regular one when grating lobes appear. To show this visually, let us consider a realization where the interfering UE is located in the proximity of the grating lobe for the regular array, as shown in Fig. 7.5. The irregular array allows for more accurate beamforming towards the intended user, while at the same time suppressing the interference signal more effectively too, as compared to the regular array counterpart. Clearly the pseudo-grating lobes of the aperiodic array allow for a higher interference suppression and better pattern control.

Finally, the non-uniform element density of the aperiodic array affects the power distribution among the antennas. In the next section we will show how a properly designed aperiodic array can obtain a more uniform power distribution and thus improve the amplifiers' efficiency. Similarly to the SINRG, we define also the Power Spread Compression (PSC)

$$\text{PSC} = \text{PS}^{\text{regular}}/\text{PS}^{\text{aperiodic}}. \tag{7.6}$$

Note that both the SINRG and PSC are positive when the aperiodic array is superior.
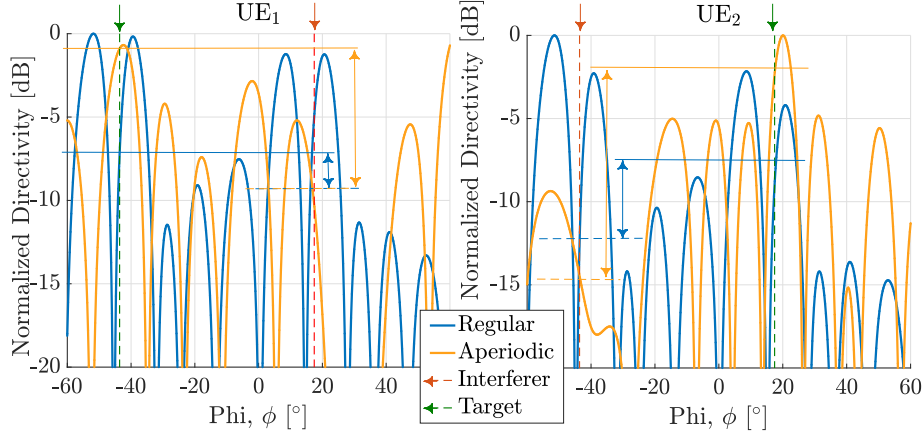
Figure 7.5: Example of radiation patterns of the regular and aperiodic arrays when the undesired UE is close to the grating lobe.

7.3   Synthesis

Current literature on aperiodic array design has mostly focused on conventional (fixed or switched beam) beamformers, where the desired beamshape is known a-priori. In MIMO applications, however, adaptive beamforming is employed. As such there is no pre-knowledge on the desired beamshape nor the excitations, since they are both entirely channel-dependent and continuously varying. For this reason most of the available methods for aperiodic array synthesis are not suitable or readily applicable to MIMO applications. The proposed aperiodic array synthesis method is based upon a new hybrid statistical-tapered approach, where the knowledge of the statistical distribution of the excitations is used to optimize the array layout. This approach is illustrated in Fig. 7.6. First, we perform a statistical analysis of the problem. To do so we densely sample the desired array aperture with fictitious antennas to achieve an accurate and almost continuous description of the available aperture. Then we simulate the array in the desired environment over a large number of realizations and take the resulting average power $\boldsymbol{\mu}$, see (7.3), as the reference distribution. In the second step, the layout is designed according to a density taper approach [77], i.e. by positioning elements with a density proportional to the reference distribution. Starting from $\mu(x) : [0, X]$, the auxiliary cumulative distribution $i(x) = \int_0^X w(\tau)\mathrm{d}\tau$ is introduced alongside its equipartition $\Delta I = i(X)/(M-1)$. The antennas' positions are then simply obtained as

$$x_m = i((m-1)\Delta I)^{-1} \quad m = 1 \dots M, \tag{7.7}$$

where i^{-1} denotes the inverse operation. As shown graphically in Fig. 7.6, starting from the reference distribution $\mu(x)$, the antenna positions are found
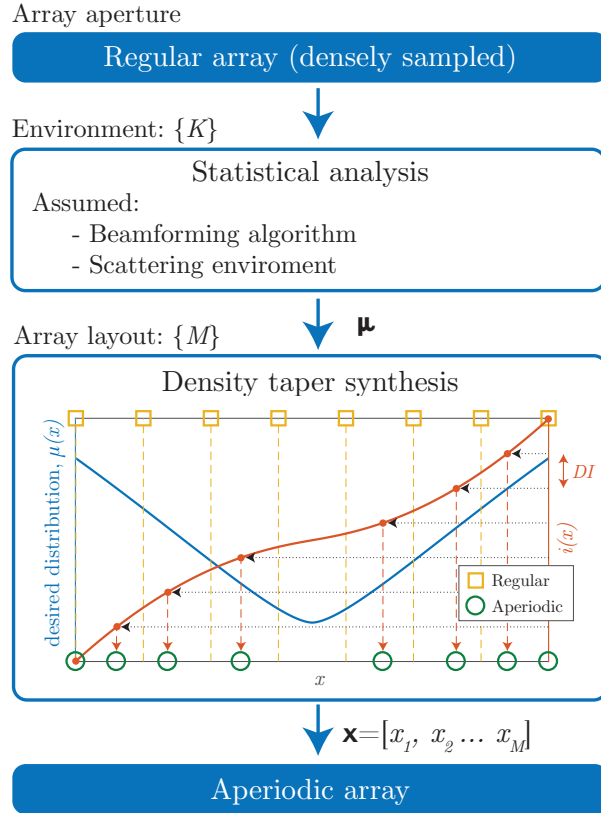
Figure 7.6: Illustration of the proposed aperiodic array design approach.

as the intersecting points between $i(x)$ and its equipartition.

7.4 Results

The proposed synthesis method has been applied to MU-MIMO systems of different sizes. As already shown, the aperiodic array can improve the SINR ratio, and thus the capacity too. In Fig. 7.7(a) we investigate the effect of the system size on the SINRG. Starting from the 8×2 system sizes as before (SINRG=2.3dB), if we double the number of BS antennas but keep the UEs fixed (16×2), the CDF improves as expected, however the SINRG now decreases to 1dB. Now if we also double the number of UEs (16×4), i.e., keeping the BS antenna to UEs ratio same as the first case, the CDFs stabilize between the two previous cases and the SINRG reaches 3.5dB. Finally, if the number of UEs is doubled (16×4), the SINRG exceeds 10dB. Note how the aperiodic 16×8 has approximately the same CDF as the 8×2 array, where the regular would instead lose 10dB at the 5% point. The SR capacity for the same set of systems sizes is instead shown in Fig. 7.7(b).

(a) Uplink CDFs of SINR at SNR=0dB.

(b) Uplink Sum Rate (SR) capacity.

(c) Amplifier's normalized average output power levels.

(d) Amplifier's power variance.

Figure 7.7: Aperiodicity effects for different MU-MIMO systems sizes.

Since this is the total system capacity, it increases both with the number of BS antennas and UEs. The aperiodic array is always superior to the regular and is increasingly so for larger and more crowded scenario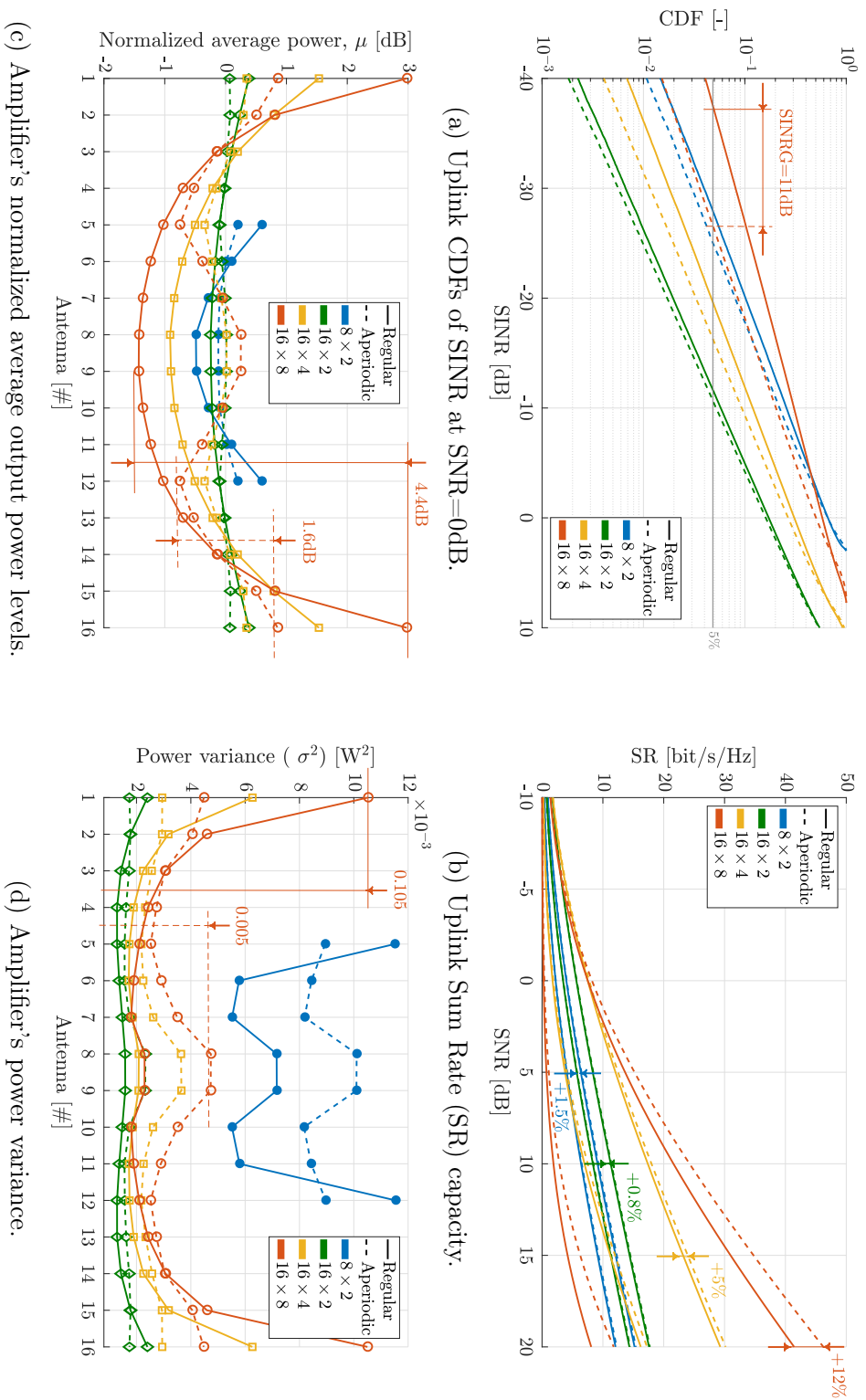s. Accordingly, the aperiodic array does not only improve the users's 5 percentile, and thus the minimum power budget, but also the capacity.

We now consider the effect of the element position on the power distribution among the antennas. In Fig. 7.7(c) the antenna's normalized average power is shown for the regular and aperiodic arrays for systems sizes as before. A similar behavior to the SINRG is observed: the regular array has an increase in power imbalance between the internal and external elements when increasing the number of BS antennas and the UEs to BS antennas ratio. The aperiodic array, on the other hand, exhibits a more uniform average power among elements. Again, a similar trend is also visible for the antenna's power variance, shown in Fig. 7.7(d). Here the aperiodic array reduces the maximum variance but is not beneficial for the inner element. Overall, the aperiodicity is mostly beneficial in ensuring a uniform average power allocation rather than substantially improving the variance.

As shown, both the link quality and amplifier power spread are strongly dependent on the system size. It is thus interesting to study the effects for massive MIMO architectures. Due to large number of system sizes considered, we will present only the compact metrics of the SINRG and PSC and not every CDF and power curves. Fig. 7.8(a) shows the SINRG as a function of number of BS antennas and cell crowdedness, i.e., number of UEs as percentage of BS antennas ($K/M * 100$). In Fig. 7.8(b) the PSC is also reported. In general the SINRG can be very substantial, especially in crowded cells and for larger number of BSs. The PSC, on the other hand, has more moderate gains and not a trend as easily identifiable. For example, a moderately large system with 64 BS antennas would benefit from a SINR increase of 3dB at 10% cell crowdedness and above 15dB at 30%, while also having a PSC between 1 to 3dB.

7.5 Summary and Conclusions

In this chapter, aperiodic arrays for Multi-User (MU) Multiple-Input-Multiple-Output (MIMO) systems have been discussed. Contrary to the prevailing understanding that the array layout has no effect on the performance, we have demonstrated and investigated the reason of the aperiodic array superiority. A novel hybrid statistical/density tapered synthesis approach is then proposed for the synthesis of optimal arrays in this application. Results for different system sizes are then presented and discussed.

Despite little work in the literature thus far, aperiodic arrays can offer
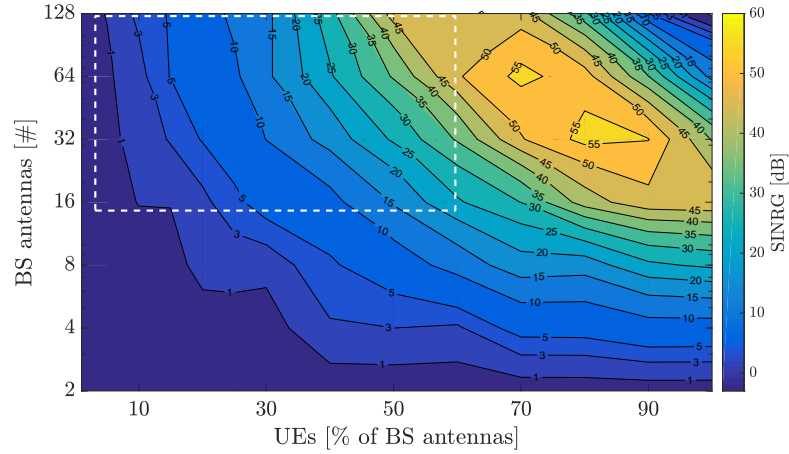
(a) Aperiodic array gain.
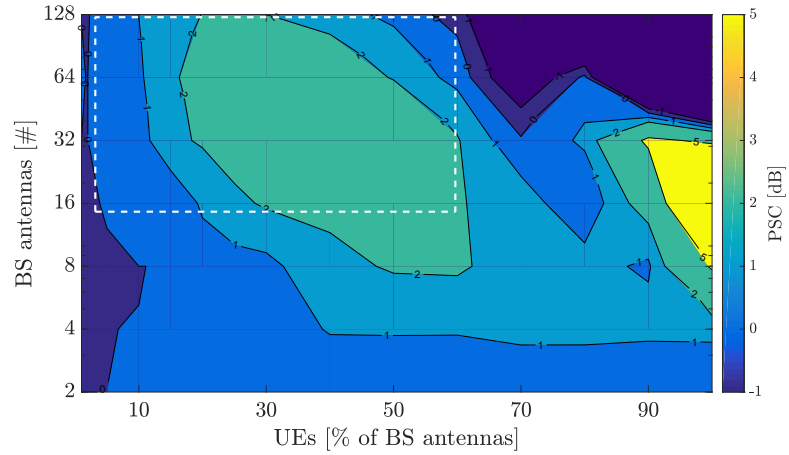
(b) Power spread compression

.

Figure 7.8: SINRG and PSC against BS antennas and cell crowdedness.

important performance improvements over regular arrays in MU-MIMO applications. These include increase in the signal-to-interference-plus-noise-ratio, the sum rate capacity and the amplifier power uniformity. These in turn result in a reduction of the power budget, an increase of the system capacity and an improvement of the power efficiency respectively. Even for a relatively small 16×8 MU-MIMO system, it is possible to achieve a 10dB power budget improvement, a 12% capacity increase and a 3dB reduction of the amplifiers power tapering reduction. Moreover, results show that the gains increase for large and crowded cells, thus of interest to future massive systems.

Chapter 8

Contributions and Recommendations for Future Work

Aperiodic array synthesis is a highly active research topic. Improving the performance and/or reducing the costs of array systems is certainly very attractive, however it is challenging too. In this thesis we have investigated the advantages of aperiodic arrays for both classical phased arrays and Muliple-Input-Multiple-Output (MIMO) systems. It also covers effective synthesis methods for aperiodic array designs. The considered application scenarios and the respective main contributions are:

- **Large sparse arrays for Satellite Communications (SATCOM)**
  In this scenario we have primarily focused on minimizing the number of antenna elements, and thus the costs associated with electronics and weight. To handle the massive antenna dimensions and the strict assorted requirements we have proposed a hybrid deterministic technique based on Compressive Sensing and fullwave analysis. The approach minimizes the number of elements, accounts for mutual coupling, and offers the flexibility to include several aspects. Several extensions have been investigated. Multi-element arrays can further reduce the number of elements. A modular or an isophoric architecture can lower the manufacturing costs. Reconfigurable arrays can offer multiple services with one single array. Electronics nonidealities in multi-beam systems can be modeled.

- **High efficiency arrays for Point-to-Point (PtP) backhauling**
  In backhauling systems, high directivity and strict interference limits are desired. We have successfully applied the synthesis method developed for SATCOM applications in the design of a dense isophoric

slotted waveguide for Ka band. The array is realized over three layers of aluminum and includes a feed network compensating for power and phase differences introduced by the aperiodicity. Simulation and measured results show wide impedance bandwidth, ETSI II compliant patterns and aperture efficiency above 80%.

- **Robust arrays for Line-of-Sight (LoS) MIMO backhauling**
  LoS-MIMO systems suffer from limited flexibility when it comes to the distance between the terminals. This implies significant costs for equipment manufacturer. However, aperiodic and switched aperiodic arrays are capable of substantially improving the minimum capacity over a desired distance interval. The capacity is guaranteed to always exceed 84% and 92% of the maximum possible capacity, for a large range of distances. A simple exhaustive search has been successfully adopted for the array synthesis, due to the small problem dimension.

- **Base station arrays for Multi User (MU) MIMO coverage**
  Aperiodic arrays for MU-MIMO can significantly improve the signal quality, the system capacity and the power efficiency of the base station. To include all the random variations introduced by the users we have developed a aperiodic array synthesis method based on a hybrid statistical/density taper-approach. The performance gains are shown to scale with the number of base station antennas and user equipments, making it attractive for upcoming massive MIMO systems.

8.1 Recommendations for Future Work

Aperiodic array synthesis still presents many open questions and possible directions for future work.

The array synthesis framework presented in this thesis is generic and flexible and therefore well-suited to be used also for other applications. However, while the adopted method proved to be very powerful, it suffers from some limitations. One of such limitations is the inability to rigorously avoid the collision of antenna elements, which can occur especially in dense layouts with strict pattern masks. Additionally, the method can be sensible to a series of indirect parameters which require tuning and complicate the design procedure.

In SATCOM applications, despite substantial work in the literature, few to none demonstrators have been manufactured so far. The associated costs are in fact extremely high. However, the possibility to measure a scaled version could be investigated. Also, measuring a prototype for less

demanding applications, such a lower orbit satellite, could represent an acceptable compromise.

In PtP communication systems, the increase in traffic will likely require a tightening of the interference limits. It would thus be interesting to push the limit of aperiodic isophoric arrays to stricter radiation pattern envelopes, such as ETSI class III and IV. Moreover, it would be interesting to investigate the applicability of different architectures and layouts.

In LoS-MIMO backhauling, the long term stability of the system with atmospheric variations is of key importance. However, to the author's knowledge, measurement campaigns have been performed only with regular arrays so far. It would thus be valuable to manufacture a prototype and perform long-term field measurements.

For MU-MIMO systems, aperiodic array have increasing performance advantages for larger and crowded systems. However, results show that the maximum gain is localized for a specific combination of number of base station antennas and user equipments. This might suggest that the proposed synthesis procedure could be further improved. Indeed, the work here presented is one of the very earliest on the topic and thus several questions are still open.

References

[1] P. Kildal, *Foundations of Antennas: A Unified Approach*, 2015. [Online]. Available: http://www.kildal.se/

[2] R. J. Mailloux, *Phased array antenna handbook*. Artech House antennas and propagation library, 2005.

[3] C. A. Balanis, *Antenna Theory: Analysis and Design*. Wiley-Interscience, 2005.

[4] A. Goldsmith, *Wireless Communications*. New York, NY, USA: Cambridge University Press, 2005.

[5] G. J. Foschini and M. J. Gans, "On limits of wireless communications in a fading environment when usingmultiple antennas," *Wirel. Pers. Commun.*, vol. 6, no. 3, pp. 311–335, Mar. 1998.

[6] D. Gesbert, M. Shafi, D. shan Shiu, P. J. Smith, and A. Naguib, "From theory to practice: an overview of mimo space-time coded wireless systems," *IEEE J. Sel. Areas Commun.*, vol. 21, no. 3, pp. 281–302, Apr 2003.

[7] C. Tepedelenlioglu, A. Abdi, and G. B. Giannakis, "The ricean k factor: estimation and performance analysis," *IEEE Trans. Wireless Commun.*, vol. 2, no. 4, pp. 799–810, July 2003.

[8] X. Chen, "Throughput modeling and measurement in an isotropic-scattering reverberation chamber," *IEEE Trans. Antennas Propag.*, vol. 62, no. 4, pp. 2130–2139, April 2014.

[9] E. Telatar, "Capacity of multi-antenna gaussian channels," *European transactions on telecommunications*, vol. 10, no. 6, pp. 585–595, 1999.

[10] A. Razavi and K. Forooraghi, "Thinned arrays using pattern search algorithms," *Progress In Electromagnetics Research*, vol. 78, pp. 61–71, 2008.

REFERENCES

[11] H. Unz, "Linear arrays with arbitrarily distributed elements," *Antennas and Propagation, IRE Transactions on*, vol. 8, no. 2, pp. 222–223, 1960.

[12] R. L. Haupt, "Thinned arrays using genetic algorithms," *IEEE Trans. Antennas Propag.*, vol. 42, no. 7, pp. 993–999, 1994.

[13] M. M. Khodier and C. G. Christodoulou, "Linear array geometry synthesis with minimum sidelobe level and null control using particle swarm optimization," *IEEE Trans. Antennas Propag.*, vol. 53, no. 8, pp. 2674–2679, 2005.

[14] E. Rajo-Iglesias and O. Quevedo-Teruel, "Linear array synthesis using an ant-colony-optimization-based algorithm," *IEEE Antennas Propag. Mag.*, vol. 49, no. 2, pp. 70–79, April 2007.

[15] G. G. Roy, S. Das, P. Chakraborty, and P. N. Suganthan, "Design of non-uniform circular antenna arrays using a modified invasive weed optimization algorithm," *IEEE Trans. Antennas Propag.*, vol. 59, no. 1, pp. 110–118, 2011.

[16] G. Oliveri, F. Caramanica, and A. Massa, "Hybrid ads-based techniques for radio astronomy array design," *IEEE Trans. Antennas Propag.*, vol. 59, no. 6, pp. 1817–1827, 2009.

[17] M. Andreasen, "Linear arrays with variable interelement spacings," *Antennas and Propagation, IRE Transactions on*, vol. 10, no. 2, pp. 137–143, 1962.

[18] A. Ishimaru, "Theory of unequally-spaced arrays," *Antennas and Propagation, IRE Transactions on*, vol. 10, no. 6, pp. 691–702, 1962.

[19] Y. Lo, "A mathematical theory of antenna arrays with randomly spaced elements," *IEEE Trans. Antennas Propag.*, vol. 12, no. 3, pp. 257–268, 1964.

[20] Y. Lo and S.-W. Lee, "A study of space-tapered arrays," *IEEE Trans. Antennas Propag.*, vol. 14, no. 1, pp. 22–30, 1966.

[21] B. Steinberg, "Comparison between the peak sidelobe of the random array and algorithmically designed aperiodic arrays," *IEEE Trans. Antennas Propag.*, vol. 21, no. 3, pp. 366–370, 1973.

[22] Y. Liu, Z. Nie, and Q.-H. Liu, "Reducing the number of elements in a linear antenna array by the matrix pencil method," *Antennas and Propagation, IEEE Transactions on*, vol. 56, no. 9, pp. 2955–2962, 2008.

[23] G. Oliveri, M. Donelli, and A. Massa, "Linear array thinning exploiting almost difference sets," *IEEE Trans. Antennas Propag.*, vol. 57, no. 12, pp. 3800–3812, 2009.

[24] D. Caratelli and M. Vigano, "A novel deterministic synthesis technique for constrained sparse array design problems," *IEEE Trans. Antennas Propag.*, vol. 59, no. 11, pp. 4085–4093, Nov 2011.

[25] A. Ishimaru, "Unequally spaced arrays based on the poisson sum formula," *IEEE Trans. Antennas Propag.*, vol. 62, no. 4, pp. 1549–1554, April 2014.

[26] W. P. M. N. Keizer, "Large planar array thinning using iterative fft techniques," *IEEE Trans. Antennas Propag.*, vol. 57, no. 10, pp. 3359–3362, Oct 2009.

[27] O. Bucci, S. Perna, and D. Pinchera, "Advances in the deterministic synthesis of uniform amplitude pencil beam concentric ring arrays," *IEEE Trans. Antennas Propag.*, vol. 60, no. 7, pp. 3504–3509, 2012.

[28] M. A. Davenport, M. F. Duarte, Y. C. Eldar, and G. Kutyniok, "Introduction to compressed sensing," *Preprint*, vol. 93, 2011.

[29] A. Massa, P. Rocca, and G. Oliveri, "Compressive sensing in electromagnetics-a review," *IEEE Antennas Propag. Mag.*, vol. 57, no. 1, pp. 224–238, 2015.

[30] G. Prisco and M. D'Urso, "Maximally sparse arrays via sequential convex optimizations," *IEEE Antennas Wireless Propag. Lett.*, vol. 11, pp. 192–195, 2012.

[31] S. E. Nai, W. Ser, Z.-L. Yu, and H. Chen, "Beampattern synthesis for linear and planar arrays with antenna selection by convex optimization," *IEEE Trans. Antennas Propag.*, vol. 58, no. 12, pp. 3923–3930, 2010.

[32] H. V. Bui, S. N. Jha, and C. Craeye, "Fast full-wave synthesis of printed antenna arrays including mutual coupling," *IEEE Trans. Antennas Propag.*, vol. 64, no. 12, pp. 5163–5171, Dec 2016.

[33] J. I. Echeveste, M. Ã. G. de Aza, J. Rubio, and C. Craeye, "Gradient-based aperiodic array synthesis of real arrays with uniform amplitude excitation including mutual coupling," *IEEE Trans. Antennas Propag.*, vol. 65, no. 2, pp. 541–551, Feb 2017.

[34] L. Cen, Z. L. Yu, and W. Ser, "Antenna array synthesis in presence of mutual coupling effect for low cost implementation," in *Integrated Circuits, ISIC '09. Proceedings of the 2009 12th International Symposium on*, Dec 2009, pp. 360–363.

[35] D. Pozar, "The active element pattern," *IEEE Trans. Antennas Propag.*, vol. 42, no. 8, pp. 1176–1178, Aug 1994.

[36] R. Maaskant, C. Bencivenni, and M. Ivashina, "Characteristic basis function analysis of large aperture-fed antenna arrays," in *Antennas and Propagation (EuCAP), 2014 8th European Conference on*, April 2014, pp. 2427–2431.

[37] R. Maaskant, "Analysis of large antenna systems," Ph.D. dissertation, Eindhoven University of Technology, Eindhoven, 2010. [Online]. Available: http://alexandria.tue.nl/extra2/201010409.pdf

[38] A. Ellgadt, L. Jonsson, M. Ivashina, R. Maaskant, M. Lanne, J. Carlert, P. Ingvarsson, B. Johassisson, P. Persson, L. Pettersson, and T. Boman, "Next generation arrays antennas," Chase Stage III Project Proposal, Sep. 2011.

[39] ESA/ESTEC, "Innovative architectures for reducing the number of controls of multiple beam telecommunications antennas," Tender AO/1-5598/08/NL/ST, Jan. 2008.

[40] P. Ingvarson and J. Zackrisson, "Swedish space antenna projects," in *EuCAP 2013*, April 2013, pp. 3161–3165.

[41] RUAG Space A.B., Personal discussion, 2014.

[42] A. Catalani, L. Russo, T. Isernia, O. M. Bucci, G. Toso, and P. Angeletti, "Ka-band active sparse arrays for satcom applications," in *Antennas and Propagation Society International Symposium (APSURSI), 2012 IEEE*, Jun. 2012, pp. 1–2.

[43] O. Bucci, T. Isernia, S. Perna, and D. Pinchera, "Isophoric sparse arrays ensuring global coverage in satellite communications," *IEEE Trans. Antennas Propag.*, vol. 62, no. 4, pp. 1607–1618, April 2014.

[44] M. Carlin, G. Oliveri, and A. Massa, "Hybrid bcs-deterministic approach for sparse concentric ring isophoric arrays," *IEEE Trans. Antennas Propag.*, vol. 63, no. 1, pp. 378–383, Jan. 2015.

[45] P. Angeletti and G. Toso, "Synthesis of circular and elliptical sparse arrays," *Electronics Letters*, vol. 47, no. 5, pp. 304–305, March 2011.

[46] M. Jaber, M. A. Imran, R. Tafazolli, and A. Tukmanov, "5g backhaul challenges and emerging research directions: A survey," *IEEE Access*, vol. 4, pp. 1743–1766, 2016.

[47] J. Hansen, A. A. Kishk, P. S. Kildal, and O. Dahlsjo, "High performance reflector hat antenna with very low sidelobes for radio-link applications," in *IEEE Antennas and Propagation Society International Symposium. 1995 Digest*, vol. 2, June 1995, pp. 893–896 vol.2.

[48] A. Vosoogh, P. S. Kildal, and V. Vassilev, "Wideband and high-gain corporate-fed gap waveguide slot array antenna with ETSI Class II radiation pattern in V-band," *IEEE Trans. Antennas Propag.*, vol. 65, no. 4, pp. 1823–1831, April 2017.

[49] *Fixed radio systems characteristics and requirements*, European Telecommunications Standards Institute (ETSI) Std. ETSI EN 302 217-4-2 V1.5.1 (2010-01), 2010. [Online]. Available: http://www.etsi.org/index.php

[50] K. V. Lemberg, O. A. Nazarov, V. S. Panko, and Y. P. Salomatov, "High gain substrate integrated waveguide slot antenna array," in *2015 International Siberian Conference on Control and Communications (SIBCON)*, May 2015, pp. 1–3.

[51] D. Y. Kim, W. Chung, C. Park, S. Lee, and S. Nam, "Design of a 45°-inclined SIW resonant series slot array antenna for Ka-band," *IEEE Antennas Wireless Propag. Lett.*, vol. 10, pp. 318–321, 2011.

[52] P. S. Kildal, E. Alfonso, A. Valero-Nogueira, and E. Rajo-Iglesias, "Local metamaterial-based waveguides in gaps between parallel metal plates," *IEEE Antennas Wireless Propag. Lett.*, vol. 8, pp. 84–87, 2009.

[53] M. Ando, J. Hirokawa, T. Yamamoto, A. Akiyama, Y. Kimura, and N. Goto, "Novel single-layer waveguides for high-efficiency millimeter-wave arrays," *IEEE Trans. Microw. Theory Tech.*, vol. 46, no. 6, pp. 792–799, Jun 1998.

[54] D. Y. Kim and R. S. Elliott, "A design procedure for slot arrays fed by single-ridge waveguide," *IEEE Trans. Antennas Propag.*, vol. 36, no. 11, pp. 1531–1536, Nov 1988.

[55] W. Wang, S.-S. Zhong, Y.-M. Zhang, and X.-L. Liang, "A broadband slotted ridge waveguide antenna array," *IEEE Trans. Antennas Propag.*, vol. 54, no. 8, pp. 2416–2420, Aug 2006.

REFERENCES

[56] Sakakibara, Y. Kimura, A. Akiyama, J. Hirokawa, M. Ando, and N. Goto, "Alternating phase-fed waveguide slot arrays with a single-layer multiple-way power divider," *IEE Proc. - Microw., Antennas and Propag.*, vol. 144, no. 6, pp. 425–430, Dec 1997.

[57] T. Li, H. Meng, and W. Dou, "Design and implementation of dual-frequency dual-polarization slotted waveguide antenna array for Ka-band application," *IEEE Antennas Wireless Propag. Lett.*, vol. 13, pp. 1317–1320, 2014.

[58] S. S. Oh, J. W. Lee, M. S. Song, and Y. S. Kim, "Two-layer slotted-waveguide antenna array with broad reflection/gain bandwidth at millimetre-wave frequencies," *IEE Proc. - Microw., Antennas and Propag.*, vol. 151, no. 5, pp. 393–398, Oct 2004.

[59] G. L. Huang, S. G. Zhou, T. H. Chio, H. T. Hui, and T. S. Yeo, "A low profile and low sidelobe wideband slot antenna array feb by an amplitude-tapering waveguide feed-network," *IEEE Trans. Antennas Propag.*, vol. 63, no. 1, pp. 419–423, Jan 2015.

[60] P. Kumar, A. Kedar, and A. K. Singh, "Design and development of low-cost low sidelobe level slotted waveguide antenna array in X-band," *IEEE Trans. Antennas Propag.*, vol. 63, no. 11, pp. 4723–4731, Nov 2015.

[61] D. Y. Kim and R. S. Elliott, "A design procedure for slot arrays fed by single-ridge waveguide," *IEEE Trans. Antennas Propag.*, vol. 36, no. 11, pp. 1531–1536, Nov 1988.

[62] J. Joubert and S. R. Rengarajan, "Design of unequal H-plane waveguide-power dividers for array applications," in *Proc. IEEE AP-S International Symposium*, vol. 3, July 1996, pp. 1636–1639.

[63] L. Hansryd and J. Edstam, "Microwave capacity evolution," *Ericsson Review*, 2011.

[64] L. Reggiani, B. Baccetti, and L. Dossi, "The role of adaptivity in mimo line-of-sight systems for high capacity backhauling," *Wireless Personal Communications*, vol. 74, no. 2, pp. 373–389, 2014.

[65] L. Liu, W. Hong, H. Wang, G. Yang, N. Zhang, H. Zhao, J. Chang, C. Yu, X. Yu, H. Tang, H. Zhu, and L. Tian, "Characterization of line-of-sight mimo channel for fixed wireless communications," *IEEE Trans. Antennas Propag.*, vol. 6, pp. 36–39, 2007.

[66] A. Razavi, A. A. Glazunov, P. S. Kildal, and J. Yang, "Characterizing polarization-mimo antennas in random-los propagation channels," *IEEE Access*, vol. 4, pp. 10 067–10 075, 2016.

[67] F. Bohagen, P. Orten, and G. E. Oien, "Design of optimal high-rank line-of-sight mimo channels," *IEEE Transactions on Wireless Communications*, vol. 6, no. 4, pp. 1420–1425, April 2007.

[68] X. Huang, Y. J. Guo, A. Zhang, and V. Dyadyuk, "A multi-gigabit microwave backhaul," *IEEE Commun. Mag.*, vol. 50, no. 3, pp. 122–129, March 2012.

[69] D. Gesbert, H. Bolcskei, D. A. Gore, and A. J. Paulraj, "Outdoor mimo wireless channels: models and performance prediction," *IEEE Trans. Commun.*, vol. 50, no. 12, pp. 1926–1934, Dec 2002.

[70] A. Osseiran, J. F. Monserrat, and P. Marsch, Eds., *5G Mobile and Wireless Communications Technology*. Cambridge, England: Cambridge University Press, 2016.

[71] F. Boccardi, R. W. Heath, A. Lozano, T. L. Marzetta, and P. Popovski, "Five disruptive technology directions for 5G," *IEEE Commun. Mag.*, vol. 52, no. 2, pp. 74–80, Feb 2014.

[72] X. Ge, R. Zi, H. Wang, J. Zhang, and M. Jo, "Multi-user massive MIMO communication systems based on irregular antenna arrays," *IEEE Trans. Wireless Commun.*, vol. 15, no. 8, pp. 5287–5301, Aug 2016.

[73] A. A. Glazunov, "Downlink massive MIMO performance of a vertically polarized uniform linear array in random line-of-sight," in *European Conference on Antennas and Propagation (EuCAP)*, April 2016, pp. 1–4.

[74] U. Carlberg, J. Carlsson, A. Hussain, and P. S. Kildal, "Ray based multipath simulation tool for studying convergence and estimating ergodic capacity and diversity gain for antennas with given far-field functions," in *ICECom, 2010 Conference Proceedings*, Sep 2010, pp. 1–4.

[75] H. Q. Ngo, Ed., *Massive MIMO: Fundamentals and System Designs*. Linkoping, Sweden: Linkoping University Electronic Press, 2015.

[76] D. Persson, T. Eriksson, and E. G. Larsson, "Amplifier-aware multiple-input single-output capacity," *IEEE Trans. Commun.*, vol. 62, no. 3, pp. 913–919, Mar 2014.

References

[77] P. Angeletti and G. Toso, "Array antennas with jointly optimized elements positions and dimensions part I: Linear arrays," *IEEE Trans. Antennas Propag.*, vol. 62, no. 4, pp. 1619–1626, April 2014.